ARCHIVES OF ACOUSTICS
26, 4, 271–276 (2001)

GAP DETECTION THRESHOLDS IN YOUNG MUSICIANS WITH NORMAL HEARING AND WITH VERY HIGH FREQUENCY SLOPING HEARING LOSS IN 1/3-OCTAVE WHITE NOISE CENTERED AT 4 kHz

A. JAROSZEWSKI, A. JAROSZEWSKA and P. ROGOWSKI

Frederic Chopin Academy of Music
(00-368 Warszawa, ul. Okólnik 2, Poland)
e-mail: pro@chopin.edu.pl

Gap detection thresholds in 1/3-octave white noise centred at 4 kHz were determined in young musicians with normal hearing preserved and with very high frequency sloping hearing loss. The thresholds were determined in the control group of 20 with normal hearing, i.e. flat audiogram up to 16 kHz, and in the experimental group of 15 with high frequency sloping hearing loss exceeding 30 dB at 12 kHz or at 16 kHz, the so called peculiar hearing loss. A group of 7 older subjects exhibiting also peculiar hearing loss was included for comparison. The results show gap detection thresholds in the normal hearing subjects ranging from 1 ms to 6 ms, which are in good agreement with the earlier data from the present authors. However, few examples of higher gap detection thresholds (11, 26 ms) in normal hearing were also observed. For the experimental group with high frequency sloping hearing loss at 12 kHz or at 16 kHz, the gap detection thresholds found were on the average significantly higher ranging from 6 ms to 26 ms. In the group of older subjects gap detection thresholds were on the average still significantly higher.

1. Introduction

Temporal acuity or temporal resolution of the hearing system provides ability to follow rapid changes of the signal with time. Simple and quite often used measure of temporal resolution is the gap detection threshold in continuous stimulus or between two bounding stimuli. This measure was introduced by Penner, see PENNER [13], for the determination of the decay time of auditory sensation.

Numerous investigations show that the gap detection threshold is larger in the subjects with sensorineural hearing loss i.e. these subjects can detect only larger gaps, e.g. TYLER *et al.* [17], BUUS and FLORENTINE [1], GLASBERG *et al.* [2], IRWIN and MCAULAY [4], JAROSZEWSKI *et al.* [5]. However, it was also reported that the gap detection thresholds are almost identical in normal hearing and hearing-impaired, at least for the gaps in the sinusoidal stimulus, e.g. MOORE and GLASBERG [9], MOORE *et al.* [10].

Gap detection threshold is larger in elderly subjects as reported by for example SCHNEIDER *et al.* [15], SCHNEIDER and HAMSTRA [14], NING-JI HE *et al.* [12] and

SNELL [16]. However, also in that respect controversial data were reported, e.g. MOORE *et al.* [11]. Typical gap detection thresholds in noise in normal hearing subjects and for presentation level above 30 dB SL amount from 2 to 3 ms up to approximately 10 ms, e.g. MOORE [8], GREEN [3], GLASBERG *et al.* [2]. In cases of hearing loss of 30–70 dB the gap detection thresholds are usually but not always larger and fall in the range from approximately 10 to 30 ms, e.g. GLASBERG *et al.* [2], JAROSZEWSKI *et al.* [7].

In the present report gap detection thresholds in noise, found in the subjects with normal hearing and with very high frequency rapidly sloping hearing loss (the so called peculiar hearing loss) are presented. This work was undertaken to find out if the peculiar hearing loss present in some young musicians (largely playing percussion and brass wind instruments, e.g. JAROSZEWSKI [5], ROGOWSKI *et al.* [6], JAROSZEWSKI *et al.* [7]), affects temporal acuity of the hearing system. No data referring to this particular question could be found in the literature.

2. Procedure and equipment

Hearing thresholds were determined with the use of the clinical audiometer Interacoustics AC 40 in the mode of tonal audiometry. The intermittent signal 250/250 ms was used at 11 standard audiometric frequencies i.e. 0.125, 0.250, 0.5, 0.75, 1.0, 1.5, 2.0, 3.0, 4.0, 6.0, and 8.0 Hz and at two frequencies above this band i.e. 12.0 and 16.0 kHz. Signal level was adjusted manually with the use of an electronic attenuator set at 1 dB step. In the range of low (standard) frequencies Telephonics TDH 39P headphones with MX41/AR cushions were used, while in the range of high frequencies (12 and 16 kHz) Koss HV PRO with circumaural cushions were used. Data acquisition, its preliminary processing and storage were executed by IBM PC and IABASE 95 program.

Simple closed block two alternative forced choice (2AFC) procedure was used to determine gap detection thresholds. The paradigm consisted of two observation intervals lasting 2 s each, separated by 500 ms interstimulus interval. After presentation of one pair of stimuli an answer interval of the duration of 2 s followed. Such sequence of the stimuli was repeated endlessly until listener indicated the interval containing the gap. The closed block of stimuli consisted of 20 repetitions of 5 pairs containing different gap durations i.e. of 100 pairs. Each of the five pairs containing the gap was presented 10 times in the first and 10 times in the second observation interval. The succession of the pairs containing different gaps and the occurrence of gaps in the successive test trials was random. Gap detection threshold was determined for each subject from individual psychometric function as the gap duration corresponding to 75 percent correct.

The filtered 1/3-octave band noise centered at 4 kHz was used to determine gap detection thresholds. A sample of noise was transferred into digital form and linear onset and decay functions were introduced at the beginning and at the end. The onset and the decay duration were 20 ms and 1 ms correspondingly. By reversing time succession and phase a second signal was obtained with onset time 1 ms and decay time 20 ms. Each trial consisted thus of two samples of noise separated by a gap of the duration of 2, 4, 8, 16 or 32 ms. The samples of noise were so organised that the onset

time of the first and the decay of the second were 20 ms each while flanks of the gap measured 1 ms.

The stimuli were presented to subjects binaurally through the Beyer Dynamic DT 911 headphones at a level of 15 dB SL. The hearing threshold of each subject was determined with the use of signal of analogical construction as the test signals. The generation of the stimuli, their time organisation, data acquisition and its preliminary processing were performed by an IBM PC running under control of the GAPDET program. A 16-bit MultiSound Fiji TurtleBeach transducer was used for digital to analog signal conversion.

Since the level of signal presentation was low, the spectral components resulting from the presence of the gap in the test signal were below the threshold of hearing of the subjects, did not affect their timbre and had no influence on the results.

3. Subjects

A group of 42 subjects participated in the experiment. 35 of them were young active musicians playing various instruments and these were aged 18 to 29, while the remaining 7 subjects were either musicians or not musicians and were aged from 28 to 69. In the group of 35 young musicians 15 were playing percussion or brass wind instruments and were so selected purposely on the grounds of the data from the earlier experiments, e.g. JAROSZEWSKI [5], JAROSZEWSKI *et al.* [7], ROGOWSKI *et al.* [6]. The remaining twenty musicians were less exposed.

Twenty young musicians of the test group were qualified as normal hearing and fifteen young musicians as hearing-impaired, on the grounds of the data from audiometric examination. As a criterion the value of hearing loss at frequencies of 12 kHz and 16 kHz only was used in selection (flat audiogram up to 16 kHz and hearing loss exceeding 30 dB at 12 kHz or at 16 kHz correspondingly). Hearing loss at these frequencies, called peculiar hearing loss earlier, is characterised by large values and very steep sloping between the range where normal hearing was preserved and the range of loss. The group of elder hearing-impaired subjects with the peculiar hearing loss was included to enable comparison of gap detection thresholds between subjects with the same hearing loss but of the different age.

4. Results and discussion

The examples of gap detection threshold psychometric functions for some subjects, selected from the three groups of subjects i.e. young normal hearing, young hearing-impaired and elder hearing-impaired are presented in Fig. 1. The results of the gap detection thresholds in 1/3-octave noise centered at 4 kHz are presented in Fig. 2 and in Fig. 3 as scatter diagrams. The gap detection thresholds related to the value of hearing loss at 16 kHz are given in Fig. 2, while the same data related to the hearing loss at 12 kHz are shown in Fig. 3. The value of hearing loss in the figures pertains always to the ear with larger loss.

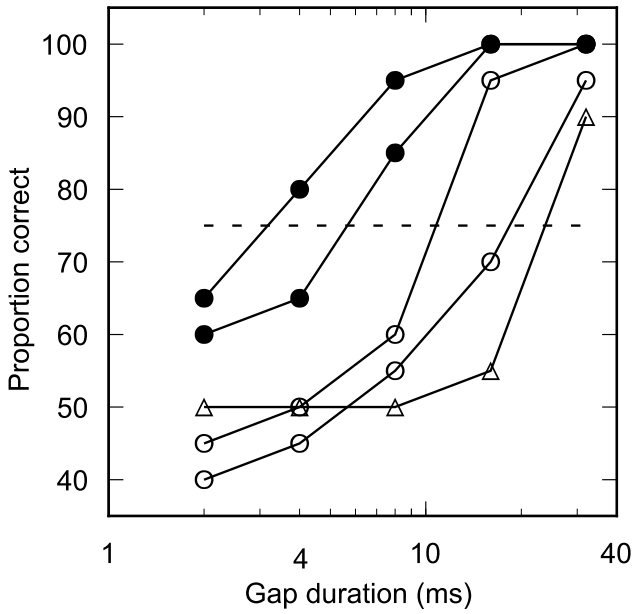

Fig. 1. The examples of gap detection threshold psychometric functions for some subjects selected from the three groups of subjects: young normal hearing (•), young hearing-impaired (○) and elder hearing-impaired (△).

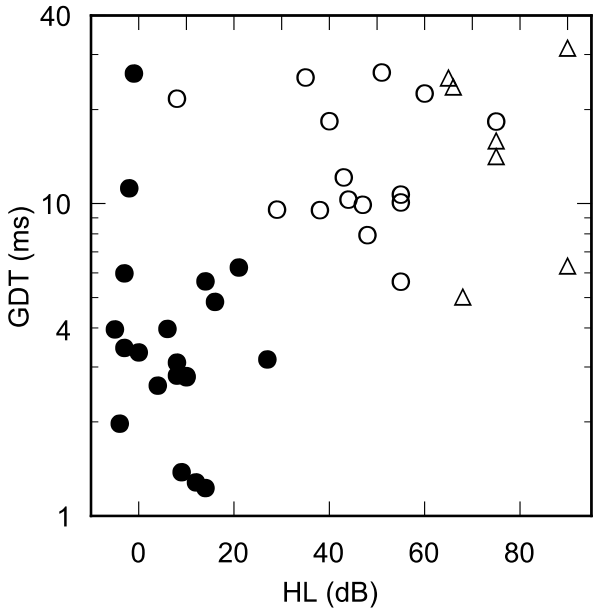

Fig. 2. The gap detection thresholds related to the value of hearing loss at 16 kHz in the better ear for the control group (•), experimental group (○) and the group of elder hearing-impaired subjects (△).

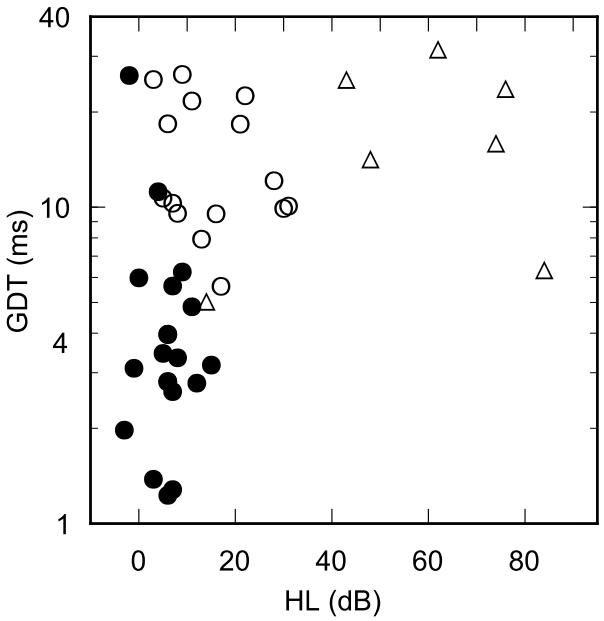

Fig. 3. The gap detection thresholds related to the value of hearing loss at 12 kHz in the better ear for the control group (•), experimental group (○) and the group of elder hearing-impaired subjects (△).

In both groups of young musicians tested a rather strong relation is observed between the values of the peculiar hearing loss at 12 and at 16 kHz and the gap detection thresholds. While the gap detection thresholds in normal hearing young musicians fall in the range from 1.3 to 6.2 ms, in hearing-impaired with peculiar hearing loss the gap detection thresholds amount from 5.6 to 26.3 ms. Large gap detection thresholds, but comparable to those observed in hearing-impaired young musicians was observed in the group of elder subjects with peculiar hearing loss (5.0 – 31.5 ms).

The results of the present investigation indicate, that the peculiar hearing loss which pertains to frequencies outside of the range of the standard routine audiometric testing (from 125 Hz to 8 kHz), significantly affects operation of the hearing system in time domain, decreasing its ability to follow rapid changes of the signal with time. It should be noted that the earlier published data on the relation between gap detection thresholds and hearing loss pertained exclusively to the wide band hearing loss, mostly in excess of $1\,^1/_2$ octave and in the range below 8 kHz.

Acknowledgements

This work was supported by grant KBN T 07B 051 15 from the State Committee for the Scientific Research. A body of this paper was presented to OSA 2000, XLVIII Open Seminar on Acoustics, Rzeszów 18 – 22 Sept. 2000.

References

[1] S. Buus and S. Florentine, *Gap detection in normal and impaired listeners: The effect of level and frequency*, [in:] Time Resolution in Auditory Systems, A. Michelsen [Ed.], Springer, 1985, 159–179.

[2] B.R. Glasberg, B.C.J. Moore and S.P. Bacon, *Gap detection and masking in hearing impaired and normal hearing subjects*, J. Acoust. Soc. Am., **81**, 1546–1556 (1987).

[3] D.M. Green, *Temporal factors in psychoacoustics*, [in:] Time Resolution in Auditory Systems, A. Michelsen [Ed.], Springer, 1985, 122–140.

[4] R.J. Irwin and S.F. McAuley, *Relations among temporal acuity, hearing loss, and the perception of speech distorted by noise and reverberation*, J. Acoust. Soc. Am., **81**, 1557–1565 (1987).

[5] A. Jaroszewski, *Wysokoczęstotliwościowe, osobliwe, trwałe i czasowe ubytki słuchu u młodych muzyków grających na instrumentach dętych blaszanych*, Prace XLVI Otwartego Seminarium z Akustyki, Poznań – Kiekrz, 1518.IX.1998, vol. I, 265–276 (1998).

[6] P. Rogowski, A. Rakowski and A. Jaroszewski, *High frequency hearing loss in percussion players*, Archives of Acoustics, **24**, 119–128 (1999).

[7] A. Jaroszewski, T. Fidecki and P. Rogowski, *Hearing damage from exposures to music*, Archives of Acoustics, **23**, 331 (1998).

[8] B.C.J. Moore, *Temporal analysis in normal and impaired hearing*, New York Academy of Sciences, June 1993, 682, 119–136.

[9] B.C.J. Moore and B.R. Glasberg, *Gap detection with sinusoids and noise in normal, impaired and electrically stimulated ears*, J. Acoust. Soc. Am., **83**, 1039–1101 (1988).

[10] B.C.J. Moore, B.R. Glasberg, E. Donaldson, T. McPherson and C.J. Plack, *Detection of temporal gaps in sinusoids by normally hearing and hearing impaired subjects*, J. Acoust. Soc. Am., **85**, 1266–1275 (1989).

[11] B.C.J. Moore, R.W. Peters and B.R. Glasberg, *Detection of temporal gaps in sinusoids by elderly subjects with and without hearing loss*, J. Acoust. Soc. Am., **92**, 1923–1932 (1992).

[12] He Ning-Ji, A.R. Horwitz, J.R. Dubno and J.H. Mills, *Psychometric functions for gap detection in noise measured from young and aged subjects*, J. Acoust. Soc. Am., **106**, 966–978 (1999).

[13] M.J. Penner, *Detection of temporal gaps in noise as a measure of the decay of auditory sensation*, J. Acoust. Soc. Am., **61**, 552–557 (1977).

[14] B.A. Schneider and S.J. Hamstra, *Gap detection thresholds as a function of tonal duration for younger and older listeners*, J. Acoust. Soc. Am., **106**, 371–380 (1999).

[15] B.A. Schneider, M.K. Pichora–Fuller, D. Kowalchuk and M. Lamb, *Gap detection and the precedence effect in young and old adults*, J. Acoust. Soc. Am., **95**, 980–991 (1994).

[16] K.B. Snell, *Age-related changes in temporal gap detection*, J. Acoust. Soc. Am., **101**, 2214–2220 (1997).

[17] R.S. Tyler, Q. Summerfield, E.J. Wood and M.A. Fernandes, *Psychoacoustic and phonetic temporal processing in normal and hearing impaired listeners*, J. Acoust. Soc. Am., **72**, 740–752 (1982).

ARCHIVES OF ACOUSTICS
26, 4, 277–291 (2001)

APPLICATION OF THE NARMAX METHOD TO THE MODELLING OF THE NONLINEARITY OF DYNAMIC LOUDSPEAKERS

A.B. DOBRUCKI and P. PRUCHNICKI

Institute of Telecommunications and Acoustics,
Wrocław University of Technology
(50-370 Wrocław, Wybrzeże S. Wyspiańskiego 27, Poland)
e-mail: ado@zakus.ita.pwr.wroc.pl, misio@zakus.ita.pwr.wroc.pl

The application of the NARMAX method to the modelling of the nonlinearity of dynamic loudspeakers is described. The principle of creating a polynomial representation of a model, the problems stemming from a too large number of model coefficients and the method of optimizing the model are presented. The method was tested on data from actual loudspeaker measurements. Different models are compared as regards their accuracy depending on the modelling parameters. Finally, the model characteristics are compared with the results of loudspeaker measurements performed by classical methods.

1. Introduction

Loudspeaker nonlinearity can be modelled by various methods such as Volterra series [7, 12], nonlinear analogous equivalent circuits [9], nonlinear differential equations [6] and so on. One of the methods is NARMAX (**N**on-linear **A**uto**R**egressive **M**oving **A**verage with e**X**ogenous input). The NARMAX model was proposed by LEONTARITIS and BILLINGS in 1985 [11, 12]. In this model, the output signal values are computed using both the input signal values and the previous output signal values. This greatly reduces the number of coefficients.

The NARMAX model is then analogous to IIR (Infinite Impulse Response) digital filters similarly as the Volterra series model is analogous to FIR (Finite Impulse Response) digital filters. FIR-filters use only input signal samples and require a large number of coefficients. IIR-filters use both input and output signal samples and require a much smaller number of coefficients. The above terminology is used in this paper.

The polynomial NARMAX model for the dynamic loudspeaker is described in the paper. It has been proved that the direct model can be unstable. In order to stabilize the model, the optimization procedure is necessary. The optimization causes also significant reduction of the number of coefficients. The modeling of an actual loudspeaker has been done, and the results of the modeling and measurements are compared.

2. Polynomial representation of the NARMAX model

The most general NARMAX model of a system with one input and one output can be expressed by the following equation:

$$y(t) = F[y(t-1), ..., y(t-n_y),\, x(t-d), ..., x(t-d-n_x),\, e(t-1), ..., e(t-n_e)] + e(t), \tag{1}$$

where $F[\cdot]$ — an unknown nonlinear function, t — the discrete time, $x(t)$ — the excitation, $y(t)$ — the system response, $e(t)$ — the prediction error, n_x — the order of the input signal, n_y — the order of the output signal, n_e — the order of the noise, d — the delay of the system.

If it is assumed that the system does not produce any noise, a simplified form of the NARMAX model can be developed. The latter can be described by the following general equation [1, 4]:

$$y(t) = F\left[y(t-1), \ldots, y(t-n_y),\, x(t-d), \ldots, x(t-d-n_x)\right] + e(t). \tag{2}$$

Polynomial functions are most commonly applied as the F functions, although other functions, e.g. rational or radial ones, can also be used [2, 4]. The polynomial representation of the NARMAX model is as follows:

$$y(t) = \sum_{i_1=0}^{n} \theta_{i_1} u_{i_1}(t) + \sum_{i_1=0}^{n} \sum_{i_2=i_1}^{n} \theta_{i_1 i_2} u_{i_1}(t) u_{i_2}(t) + \sum_{i_1=0}^{n} \sum_{i_2=i_1}^{n} \sum_{i_3=i_2}^{n} \theta_{i_1 i_2 i_3} u_{i_1}(t) u_{i_2}(t) u_{i_3}(t) + \ldots + e(t), \tag{3}$$

where $n = n_y + n_x$, $u_1(t) = y(t-1)$, $u_2(t) = y(t-2)$, ..., $u_{ny}(t) = y(t-n_y)$, $u_{ny+1}(t) = x(t-d)$, ..., $u_n(t) = x(t-d-n_x)$, θ — model coefficients.

Equation (3) can be written as:

$$y(t) = \sum_{m=1}^{M} \theta_m p_m(t) + e(t), \tag{4}$$

where M — the number of polynomial coefficients, $p_m(t)$ — the monomials of elements $u_i(t)$ of degree l at the most.

For example, for $n_y = n_x = l = 2$ there are $M = 20$ polynomials and they are as follows:

$$\begin{aligned}
p_1(t) &= y(t-1), & p_2(t) &= y(t-2),\\
p_3(t) &= x(t-d), & p_4(t) &= x(t-d-1),\\
p_5(t) &= x(t-d-2), & p_6(t) &= y^2(t-1),\\
p_7(t) &= y^2(t-2), & p_8(t) &= x^2(t-d),\\
p_9(t) &= x^2(t-d-1), & p_{10}(t) &= x^2(t-d-2),\\
p_{11}(t) &= y(t-1)\cdot y(t-2), & p_{12}(t) &= y(t-1)\cdot x(t-d),\\
p_{13}(t) &= y(t-1)\cdot x(t-d-1), & p_{14}(t) &= y(t-1)\cdot x(t-d-2),\\
p_{15}(t) &= y(t-2)\cdot x(t-d), & p_{16}(t) &= y(t-2)\cdot x(t-d-1),\\
p_{17}(t) &= y(t-2)\cdot x(t-d-2), & p_{18}(t) &= x(t-d)\cdot x(t-d-1),\\
p_{19}(t) &= x(t-d)\cdot x(t-d-2), & p_{20}(t) &= x(t-d-1)\cdot x(t-d-2).
\end{aligned}$$

If we have N input and output signal samples obtained from measurements, from Eq. (4) we can develop a system of equations which can be expressed in following matrix form [4, 5]:

$$\begin{bmatrix} y(1) \\ y(2) \\ \vdots \\ y(N) \end{bmatrix} = \begin{bmatrix} p_1(1) & p_2(1) & \dots & p_M(1) \\ p_1(2) & p_2(2) & \dots & p_M(2) \\ \dots & \dots & \dots & \dots \\ p_1(N) & p_2(N) & \dots & p_M(N) \end{bmatrix} \cdot \begin{bmatrix} \theta_1 \\ \theta_2 \\ \vdots \\ \theta_M \end{bmatrix} + \begin{bmatrix} e(1) \\ e(2) \\ \vdots \\ e(N) \end{bmatrix} \tag{5}$$

and in this simpler form:

$$\mathbf{Y} = \mathbf{P}\boldsymbol{\theta} + \mathbf{e}. \tag{6}$$

System (6) is a linear equation system since the terms of regression matrix $\mathbf{P}$ are numbers calculated from the measured data. The model is identified by the solution of system (6), where coefficients θ_1 ... θ_m are unknown. Prediction error vector $\mathbf{e}$ is assumed to be equal to 0.

There are various methods of solving a linear equation system, e.g. Gauss elimination or iterative methods [8]. System (6) is often ill-conditioned and therefore matrix $\mathbf{P}$ should be orthogonalized [1, 5] using, for example, the Gram-Schmidt method, the Givens rotations or the Householder transformation [8]. In this paper the classical Gram-Schmidt (CGS) orthogonalization is applied since it can be easily implemented in numerical computations.

The orthogonalization algorithm is based on the decomposition of the prediction matrix into two matrices [1, 5].

$$\mathbf{P} = \mathbf{W}\,\mathbf{A}, \tag{7}$$

where $\mathbf{W}$ is columnwise orthonormal, i.e. $\mathbf{W}^T\mathbf{W} = \mathbf{I}$, $\mathbf{I}$ is a unit matrix, $\mathbf{A}$ is a triangular upper matrix.

After orthogonalization, vector $\mathbf{g}$ is determined.

$$\mathbf{g} = \mathbf{W}^T\mathbf{Y}. \tag{8}$$

Then taking advantage of the fact that matrix $\mathbf{A}$ is triangular, reverse substitution is applied to determine coefficients θ:

$$\mathbf{A}\boldsymbol{\theta} = \mathbf{g}. \tag{9}$$

The main drawback of polynomial representation is that a very large number of parameters must be determined. The number of coefficients (M) in the polynomial which describes the model depends on the lag of the input and output signals and that of the noise and on the particular order of the polynomial (order of nonlinearity — l). The number can be determined from this recurrence formula [2, 14]:

$$M = \sum_{i=1}^{l} n_i\,, \qquad n_i = [n_{i-1}(n_y + n_x + n_e + i)]/i, \quad n_0 = 1. \tag{10}$$

For example for $n_y = n_x = n_e = 10$ and $l = 3$ the number of coefficients is as high as $M = 5983$ and the number of terms in matrix $\mathbf{P}$ is equal to $M \cdot N$ where $N \geq M$ (most often $N > M$).

In order to compare various models, the following measure of accuracy is assumed:

$$\varepsilon = \frac{\|e\|^2}{\|Y_r\|^2} = \frac{\sum (y_r - y_m)^2}{\sum y_r^2} \cdot 100\%, \tag{11}$$

where $\mathbf{Y}_r$ — the vector of the response of an actual loudspeaker — $\mathbf{Y}_r = \mathbf{P}\theta + \mathbf{e}$, $\mathbf{Y}_m$ — the vector of the response of the model — $\mathbf{Y}_m = \mathbf{P}\theta$, $\|a\| = \sqrt{\sum_i a_i^2}$ — Euclid's norm of the vector, ε is a ratio of the prediction error energy to the energy of the response.

3. Optimization of the model

Since the number of coefficients to be calculated is very large (due to the fact that the structure of the nonlinearity of the modelled actual system is unknown), the usefulness of such a model is rather small. There are also difficulties in the correct interpretation of the model. In addition, the unoptimized model is unstable in most cases.

In order to optimize the model, it is necessary to reject the insignificant coefficients, i.e. to identify the structure of the system.

The optimizing procedure has been built into the orthogonalization algorithm (CGS) for regression matrix $\mathbf{P}$. It is based on the choice of subset M_s ($M_s < M$) of columns from all possible columns M of matrix $\mathbf{P}$ (Fig. 1). This yields new regression matrix $\mathbf{P}_s$ with a lower number of coefficients. The columns of $\mathbf{P}_s$ are selected using this error reduction ratio [1, 5]:

$$[\mathrm{err}]_i = \frac{g_i^2}{\langle y, y \rangle}, \tag{12}$$

where $\langle \cdot, \cdot \rangle$ denotes the inner product, that is:

$$\langle y, y \rangle = \sum_{k=1}^{N} y_k^2(t) \tag{13}$$

and g_i is i-th term of vector $\mathbf{g}$.

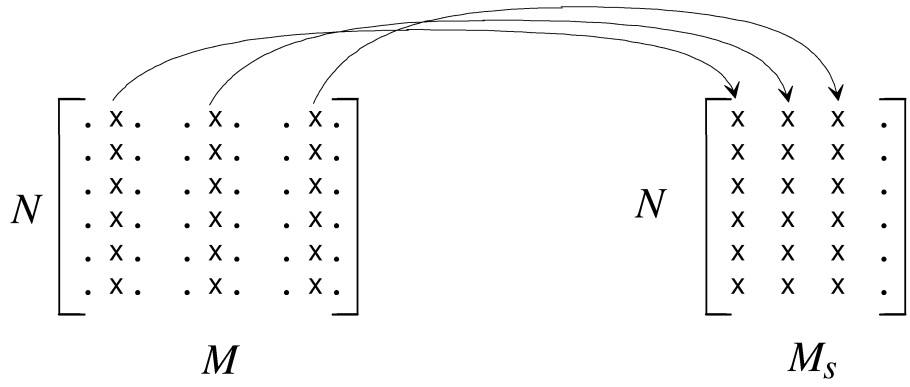

Fig. 1. Selection of most significant columns of regression matrix.

The value of $[\mathrm{err}]_i$ represents a decrease in the prediction error energy for coefficient θ_i expressed by column $\mathbf{p}_i$.

The optimizing procedure performs the following functions in every step of orthogonalization:

— the computation of error reduction ratio $[\mathrm{err}]_i$ for every coefficient,

— the choice of a coefficient with the maximum value of $[\mathrm{err}]_i$.

Now the size of matrix $\mathbf{P}_s$, i.e. the number of coefficients θ_i, remains to be determined. The accuracy of the model: ρ $(0 < \rho \leq 1)$ is often assumed as the optimization-end criterion [14]. The coefficients are selected as long as Eq. (14) is not fulfilled.

$$1 - \sum_{i=1}^{M_s} [\mathrm{err}]_i < \rho. \tag{14}$$

This criterion has a disadvantage. When a high model accuracy (a low value of ρ) is assumed, too many coefficients (often all of them $(M_s = M)$) may be taken into account. Akaike's information criterion (15) gives better results [1, 5, 14].

$$\mathrm{AIC}(\phi) = N \log \sigma_e^2 + M_s \phi, \tag{15}$$

where $\sigma_e^2 = \dfrac{1}{N} \sum\limits_{i=1}^{N} e_i^2$ — prediction error variance.

This criterion represents a compromise between the accuracy of the model (σ_e^2) and its compliance (M_s). The NARMAX model structure is usually defined by means of $\phi = 4$ (AIC(4)) [13]. The formation of $\mathbf{P}_s$ is stopped when AIC(4) reaches the minimal value.

4. High-order model

Because of the long loudspeaker impulse response, a satisfactory accuracy can be obtained only if the order of the model is sufficiently high but this entails a large number of coefficients. For example, to obtain a NARMAX model of the 30th order, a matrix consisting of about 50 000 columns must be orthogonalized. It is practically impossible to handle this amount of data — prediction matrix $\mathbf{P}$ would use about 20 GB of memory. Therefore a way had to be found to overcome this problem.

The fact that the number of coefficients can be reduced many times through the optimization procedure was exploited. The model is built in steps which are graphically represented in Fig. 2. First a low-order model with M_i: (300 – 500) coefficients is created and optimized. As a result, a model with maximally a few dozen coefficients is obtained. Then the model is supplemented with the next M_i coefficients due to its increased order. After the next optimization, again a few dozen coefficients (not necessarily the same as in the first step) are obtained. This procedure is repeated many times until all the coefficients associated with the assumed order of the model have been analyzed.

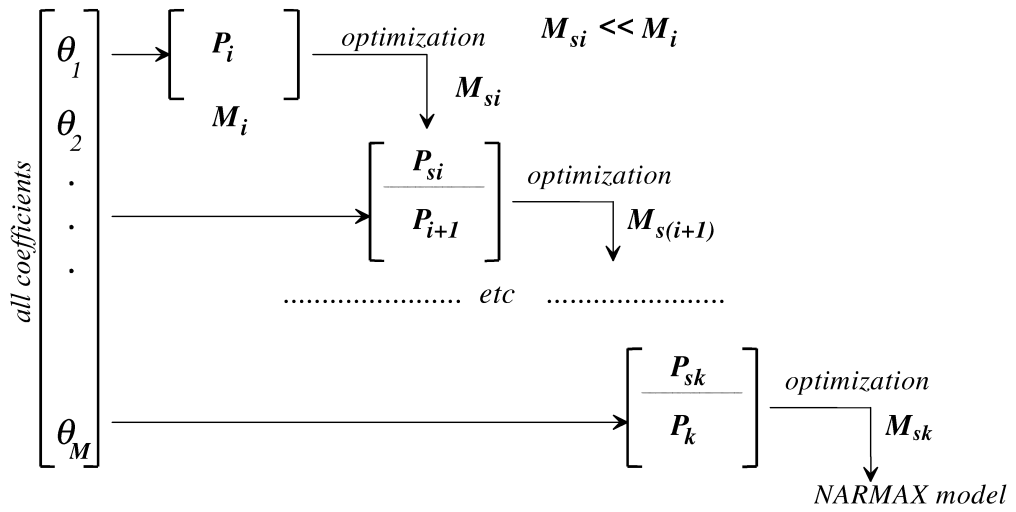

Fig. 2. Steps in creation of high-order NARMAX model.

5. Comparison of the results of measurements and modelling

5.1. Measurements

In order to obtain data (excitation $x(t)$ and response $y(t)$ values) for the creation of the model, measurements of a low-frequency loudspeaker were performed in the anechoic chamber of the Institute of Telecommunications and Acoustics. The loudspeaker (Tonsil GDN 20/35/1) was set in a closed box and digitally generated noise with uniform probability distribution and an amplitude of 15 V RMS (28 W) (2/3 of the loudspeaker's nominal power) was used as the input signal [3]. The loudspeaker response was recorded via a microphone and converted to a digital domain. In order to eliminate random noise, the response was averaged 100 times. The measurement setup is shown in Fig. 3.

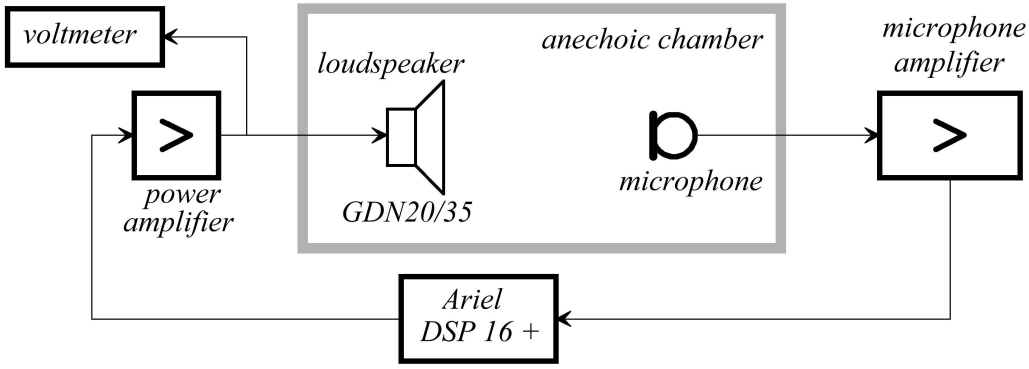

Fig. 3. Measurement setup.

5.2. Unoptimized NARMAX model

A linear FIR-type model of the 50-th order was investigated first. The impulse response of the model was compared with that of the loudspeaker — see Fig. 4. The accuracy was quite good, particularly in the initial part of the response.

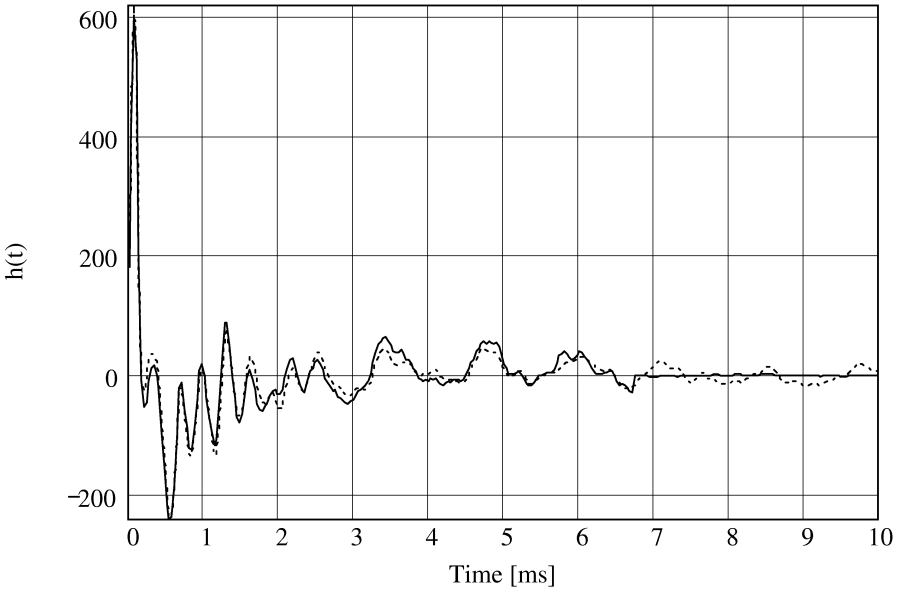

Fig. 4. Loudspeaker impulse response obtained from measurement (dashed line) and from model (solid line).

Then two IIR-type linear models of the 20-th and 50-th order were identified. Finally, FIR-type nonlinear models of the 8-th and 12-th order and IIR-type (i.e. NARMAX) models of the 4-th and 6-th order were studied. In all the nonlinear models, the order of nonlinearity was limited to $l = 3$.

The IIR-type models (which use also delayed system response samples) proved to be unstable. The number of coefficients and error ε for all the considered models are given in Table 1.

Table 1. Comparison of different loudspeaker models.

Model (structure)	ε [%]	No of coeff.
$l = 1$, $n_x = 50$, $n_y = 0$, (FIR)	8.65	51
$l = 1$, $n_x = 200$, $n_y = 0$, (FIR)	5.18	201
$l = 1$, $n_x = 20$, $n_y = 20$, (IIR)	–	41
$l = 1$, $n_x = 50$, $n_y = 50$, (IIR)	–	101
$l = 3$, $n_x = 8$, $n_y = 0$, (nonlinear FIR)	53.7	165
$l = 3$, $n_x = 12$, $n_y = 0$, (nonlinear FIR)	111.6	560
$l = 3$, $n_x = 4$, $n_y = 4$, (nonlinear IIR)	–	165
$l = 3$, $n_x = 6$, $n_y = 6$, (nonlinear IIR)	–	680

5.3. Optimized model

The results of the loudspeaker measurements described in Subsec. 5.1 were used to check the optimization procedure. Models with different structure (identical as in Subsec. 5.2) were considered. The optimization results are presented in Table 2.

Table 2. Comparison of various loudspeaker models (after optimization).

Model (structure)	ε [%]	No of coeff.
$l = 1$, $n_x = 50$, $n_y = 0$, (FIR)	8.43	30
$l = 1$, $n_x = 200$, $n_y = 0$, (FIR)	6.44	52
$l = 1$, $n_x = 20$, $n_y = 20$, (IIR)	10.57	26
$l = 1$, $n_x = 50$, $n_y = 50$, (IIR)	6.12	43
$l = 3$, $n_x = 8$, $n_y = 0$, (nonlinear FIR)	34.03	6
$l = 3$, $n_x = 12$, $n_y = 0$, (nonlinear FIR)	35.19	8
$l = 3$, $n_x = 4$, $n_y = 4$, (nonlinear IIR)	37.61	9
$l = 3$, $n_x = 6$, $n_y = 6$, (nonlinear IIR)	36.54	10

The characteristic feature of all the optimized models is their stability. For a similar or higher accuracy than that of the unoptimized models they require a much lower number of coefficients.

An illustrative impulse response of the 4-th order NARMAX model is shown in Fig. 5. The response is very short, which means that the order of the model is too low.

A comparison of the plots for the loudspeaker and the model excited by the same signal (Fig. 6) shows that the model has a tendency to reduce the maximum amplitude values.

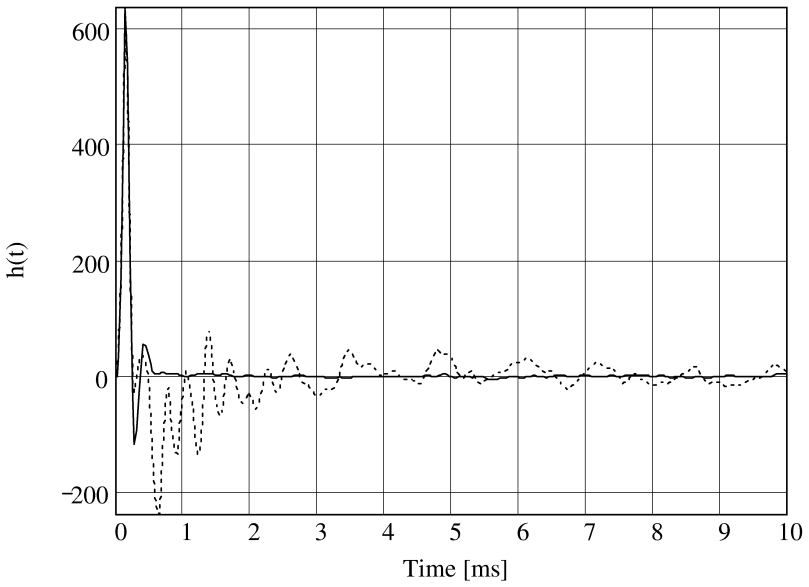

Fig. 5. Loudspeaker impulse response obtained from measurement (dashed line) and from 4-th order, 10-coefficient NARMAX model (solid line).

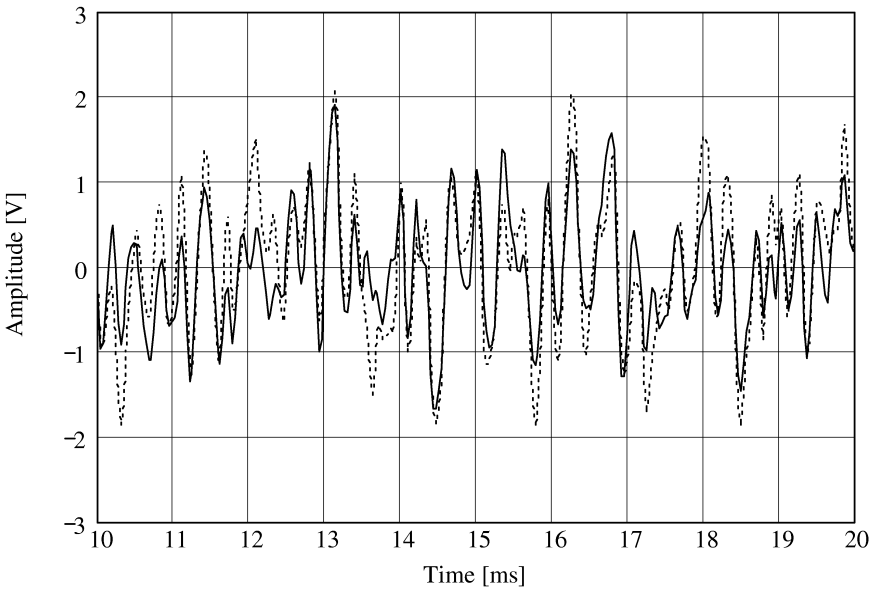

Fig. 6. Signal at loudspeaker output (dashed line) and from 4-th order, 10-coefficient NARMAX model (solid line).

The four coefficients which if included in the model ensure the highest error reduction values [err] are given in Table 3. They have the most decisive effect on the accuracy of the model and are selected as the first ones by the optimization procedure. The coefficients are linear since the loudspeaker nonlinearities were slight.

Table 3. Coefficients ensuring highest [err] values.

Model structure	1		2		3		4	
	term	[err]	term	[err]	term	[err]	term	[err]
FIR and NFIR	$x(t-2)$	0.20	$x(t-3)$	0.22	$x(t-1)$	0.14	$x(t-4)$	0.05
IIR and NIIR	$y(t-1)$	0.82	$y(t-2)$	0.10	$y(t-3)$	0.04	$x(t-1)$	0.01

To gain a picture of the relationship between model accuracy and the number of coefficients, a group of models was built. All the models were developed for the same signal and parameters:

— the order of nonlinearity — $l = 3$,

— the order of the model — $n_x = n_y = 16$,

— the criterion for the choice of coefficients — error reduction ratio [err],

— the criterion for ending model development — ρ.

Only the value of ρ was changed to obtain models with different numbers of coefficients. Also modelling for the termination criterion based on AIC(4) was performed to find out when the selection of coefficients will end.

The relationship between the modelling error and the number of coefficients is illustrated in Table 4 and Fig. 7.

Table 4. Relationship between modelling error and number of coefficients.

M_s (No of coeff.)	ε [%]	ρ [%]
7	44.56	2.00
9	24.14	1.00
11	15.22	0.70
13	13.41	0.60
15	14.53	0.50
16	17.26	0.45
18	17.39	0.40
20	14.33	0.37
21	17.63	0.35
24	15.19	0.33
27	13.51	0.30
28	13.19	0.28
29	11.27	AIC(4)
32	12.60	0.26
34	12.77	0.25

Fig. 7. Relationship between modelling error and number of coefficients for NARMAX model.

5.4. High-order model

A NARMAX model was built according to the algorithm described in Sec. 4 for the following modelling parameters:

— the order of nonlinearity — $l = 3$,

— the order of the model — $n_x = n_y = 33$,

— the number of rows in matrix $\mathbf{P}$ — $N = 700$,
— the number of coefficients determined in one step — $M_i = 400$,
— the number of samples for model testing — $N_f = 8192$,
— the criterion for the selection of coefficients — error reduction ratio [err],
— the criterion for ending the creation of the model — AIC(4).

The modelling resulted in a 64-coefficient NARMAX model characterized by error $\varepsilon = 13.9\%$.

The response of the model and that of the actual loudspeaker to the same excitation are shown in Fig. 8; the impulse responses and the frequency characteristics are shown respectively in Figs. 9 and 10.

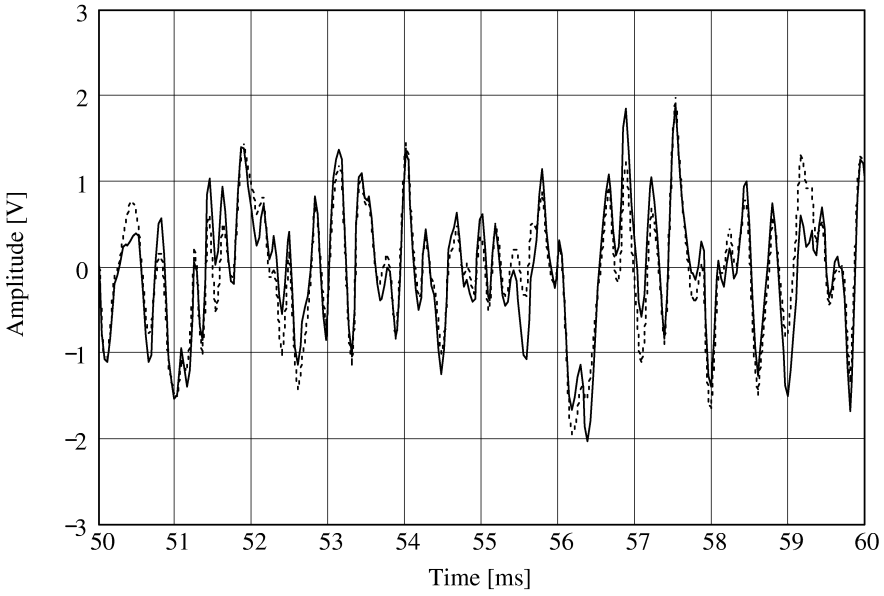

Fig. 8. Model response (solid line) and actual loudspeaker response (dashed line).

By comparing the impulse responses and the frequency characteristics we can assess only the linear properties of the model. To check how the model copes with nonlinearities, THD (a coefficient commonly used for assessing nonlinear distortions) was employed. To obtain the data needed for the calculation of THD, sinusoidal excitations with different frequencies were fed at the loudspeakers input and a spectral analysis of the loudspeaker responses was carried out, yielding the levels of the particular harmonics. The same excitation signals were fed at the input of the model and the latter's response was analyzed. Spectra of the response to the 300 Hz sinusoidal signal excitation are shown in Fig. 11. To see them better, the two spectra are shifted slightly relative to each other on the frequency axis. No components higher than the third harmonic occur in the model response spectrum (the left spectral lines) — due to the fact that the model nonlinearity was limited to the 3rd order.

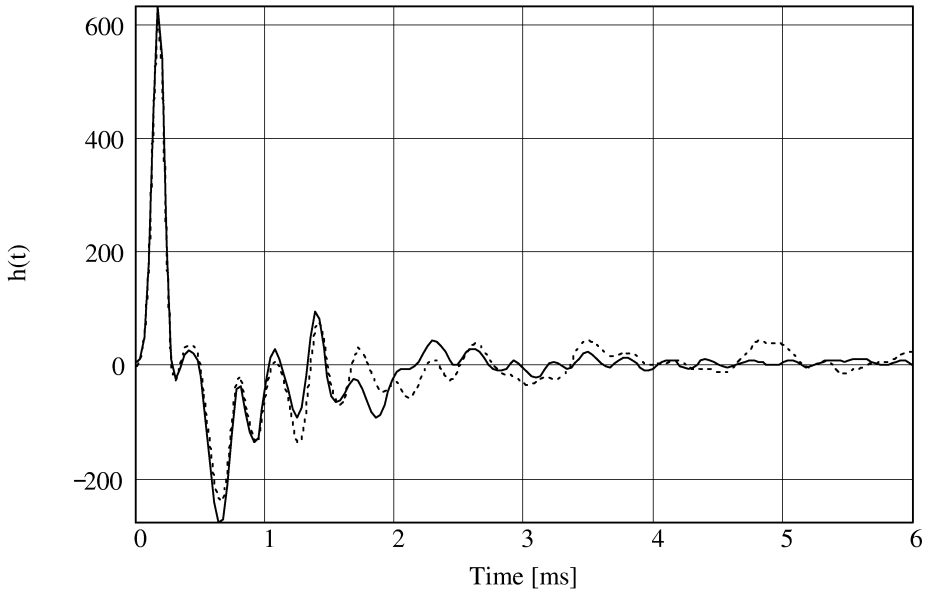

Fig. 9. Model impulse response (solid line) and actual loudspeaker impulse response (dashed line).

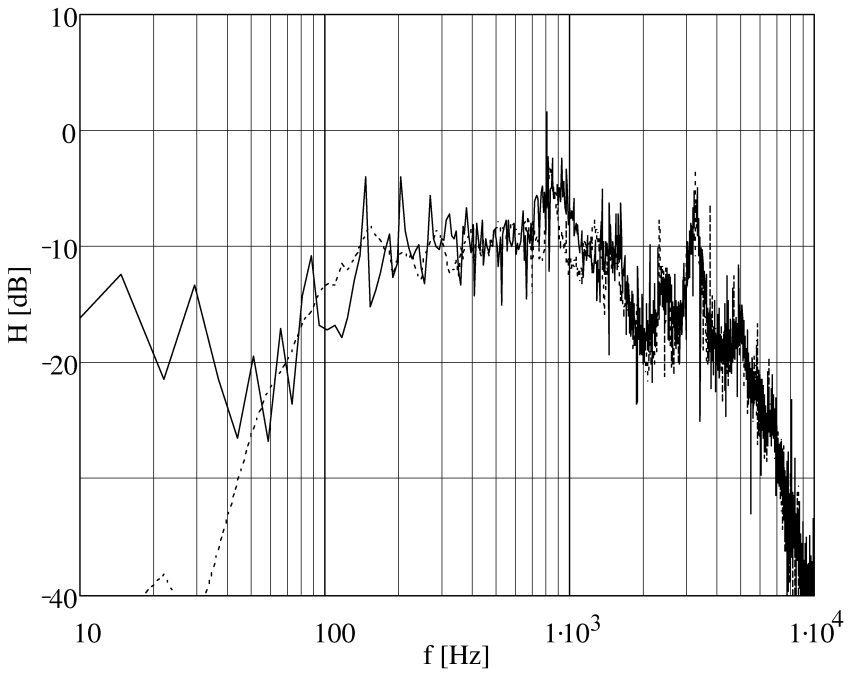

Fig. 10. Model frequency characteristic (solid line) and actual loudspeaker frequency characteristic (dashed line).

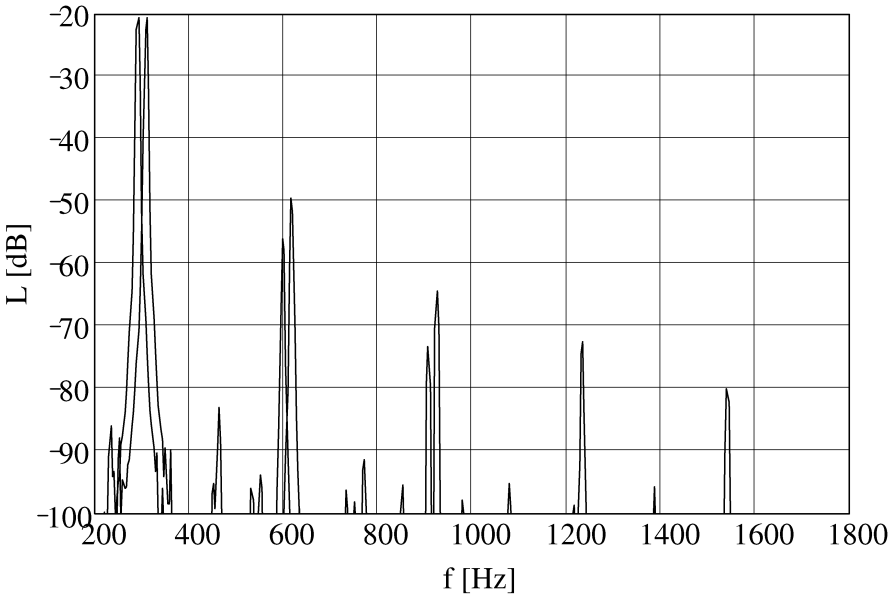

Fig. 11. Spectra of loudspeaker response (right spectral lines) and model response (left spectral lines) to 300 Hz sinusoidal signal excitation.

The THD (dB) for the first three harmonics was calculated from the following formula:

$$L_{\mathrm{THD}} = 10\log(10^{L_2/10} + 10^{L_3/10}) - L_1 \quad [\mathrm{dB}]. \tag{16}$$

The results are given in Table 5.

Table 5. THD for actual loudspeaker and model responses.

Frequency [Hz]	Loudspeaker THD [dB]	Model THD [dB]
100	−21.9	−39.1
150	−25.9	−48.2
200	−25.5	−33.2
300	−28.9	−35.1
500	−30.7	−35.6
700	−38.5	−44.0
1000	−37.8	−49.3
2000	−33.1	−51.8
4000	−49.5	−73.6

6. Conclusions

The simulations and the measurements have shown that to model a dynamic loudspeaker correctly it is necessary to use a high-order NARMAX model. A polynomial representation of such a model requires a very large number of coefficients. Besides the obvious computational and interpretational problems associated with operations on such

a large set of data, it is also difficult to obtain stability. All the unoptimized NARMAX models proved to be unstable (Table 1).

Therefore an optimization procedure was applied and as a result the number of coefficients was reduced considerably whereby the stability of the model improved (Table 2).

It follows from Table 3 that the chosen criterion (based on AIC(4)) for ending the selection of model coefficients ensured the highest accuracy of the model in the analyzed range of numbers of coefficients.

An analysis of the higher-order model showed a close similarity between the model linear characteristics and the actual loudspeaker linear characteristics. Some differences can be observed between the frequency characteristics — the model one is more jagged and irregular.

The model response has smaller linear distortions owing to the fact that no terms with higher orders of nonlinearity occur in the model: their presence would result in the appearance of higher harmonics and increase the level of the second and third harmonic.

Acknowledgments

The work was supported by the Polish State Committee for Scientific Research under grant 8 T11D 026 15.

References

[1] S.A. Billings and S. Chen, *Extended model set, global data and threshold model identification of severely non-linear systems*, Int. J. of Control, **50**, 1897–1923 (1989).

[2] S.A. Billings and S. Chen, *Identification of non-linear rational systems using a prediction-error estimation algorithm*, Int. J. of Systems Sci., **20**, 467–494 (1989).

[3] S.A. Billings and W.S.F. Voon, *Least squares parameter estimation algorithms for non-linear systems*, Int. J. of Systems Sci., **15**, 601–615 (1984).

[4] S. Chen and S.A. Billings, *Representations of non-linear systems: the NARMAX model*, Int. J. of Control, **89**, 1013–1032 (1989).

[5] S. Chen, S.A. Billings and W. Luo, *Orthogonal least squares methods and their application to non-linear system identification*, Int. J. of Control, **50**, 1873–1896 (1989).

[6] A.B. Dobrucki, *Nontypical effects in an electrodynamic loudspeaker with a non-homogeneous magnetic field in the air gap and nonlinear suspensions*, J. of the Audio Eng. Soc., **42**, 565–576 (1994).

[7] A.J. Kaiser, *Modeling of the nonlinear response of an electrodynamic loudspeaker by a Volterra series expansion*, J. Audio Eng. Soc., **35**, 421–433 (1987).

[8] A. Kiełbasiński and H. Schwetlick, *Numerical linear algebra* [in Polish], WNT, Warsaw 1992.

[9] W. Klippel, *The mirror filter — a new basis for reducing nonlinear distortion and equalizing response in woofer systems*, J. Audio Eng. Soc., **40**, 675–691 (1992).

[10] M. Korenberg, S.A. Billings, Y.P. Liu and P.J. Mcilroy, *Orthogonal parameter estimation algorithm for non-linear stochastic systems*, Int. J. of Control, **48**, 193–210 (1988).

[11] I.J. Leontaritis and S.A. Billings, *Model selection and validation methods for non-linear systems*, Int. J. of Control, **45**, 311–341 (1987).

[12] I.J. Leontaritis and S.A. Billings, *Input-output parametric models for non-linear systems, Part I: Deterministic non-linear systems*, Int. J. of Control, **41**, 303–328 (1985).

[13] I.J. Leontaritis and S.A. Billings, *Input-output parametric models for non-linear systems, Part II: Stochastic non-linear systems*, Int. J. of Control, **41**, 329–344 (1985).

[14] S.M. Potirakis, G.E. Alexakis, M.C. Tsilis and P.J. Xenitidis, *Time-domain nonlinear modeling of practical electroacoustic transducers*, J. of the Audio Eng. Soc., **47**, 447–468 (1999).

ARCHIVES OF ACOUSTICS
26, 4, 293–304 (2001)

SOME NOISE CANCELLATION AND PREDICTION METHODS ON THE RESPONSE PROBABILITY DISTRIBUTION FORM FOR COMPLICATED SOUND WALL SYSTEMS WITH BACKGROUND NOISE

M. OHTA

Emeritus Professor of Hiroshima University
(732-0824 Hiroshima City, 1106, Matoba 1-7-10, Minami-ku, Japan)

N. TAKAKI

Department of Electronics Eng.,
Faculty of Eng., Hiroshima Kokusai Gakuin University
(6-20-1, Nakano, Aki-ku, Hiroshima City, 739-0321 Japan)

In the actual situation of measuring an environmental noise, it is very often that only the resultant stochastic fluctuation contaminated by an additional noise of arbitrary distribution type can be observed. In this paper at first a noise cancellation for reasonably removing the effect of the above additional noise, especially in a whole probability distribution form, is derived theoretically in order to estimate only the undisturbed objective output response. Next, for the purpose of predicting a whole expression form of the output response probability of an acoustic system excited by an arbitrary stochastic input with the additional noise, a new stochastic signal processing method, reflecting the effect of the additional noise fluctuation, is proposed in a whole probability distribution form. The effectiveness of the proposed theoretical methods is experimentally confirmed too by applying them to the actual data measured in the complicated sound wall systems.

1. Introduction

In the actual measurement of environmental noise, the desired signal is usually contaminated by an additional noise of an arbitrary distribution type and it is only the resultant signal that can be observed [1].

In this paper, at first, a new practical trial of estimating (especially in a whole probability distribution form) the uncontaminated output response probability of sound wall systems with background noise is derived without using any artificial error criterion like the least-squares method. More concretely, a mathematical model of arbitrary sound environmental systems is introduced by using a physical law of additive principle on the energy scale [2] in a form of a linear system on the intensity scale. At first, after introducing a probability expression form of the resultant output response contaminated

by the background noise, a noise cancellation method in a whole probability distribution form is developed by which only the uncontaminated output response probability function form for the above sound environmental systems can be detected from the data contaminated by the background noise. Next, for the purpose of predicting the output response probability excited by an arbitrary stochastic input with background noise, a new signal processing method of probabilistically reflecting the effect of the background noise is proposed. More specifically, a relationship between two kinds of the probability density function (abbr. p.d.f.) and the cumulative distribution function (abbr. c.d.f.) forms on the system output excited by a specific stochastic input of reference type and an arbitrary random input without the additional noise for an arbitrary environmental systems is discussed in the form on an intensity scale. Then, a relationship between two kinds of p.d.f.s of the system outputs excited by an arbitrary stochastic input in the absence and in the presence of background noise is also derived in the form on an intensity scale. Based on these relationships, a new prediction method on a whole p.d.f. and/or c.d.f. forms of the system output for the arbitrary environmental systems with the background noise is proposed especially by the use of the observed data excited by the specific stochastic input of reference type with the background noise. Finally, the effectiveness of the proposed methods is confirmed experimentally too by applying them to the actual type sound wall systems.

2. Theoretical consideration

2.1. Noise cancellation on a whole probability form

The observed data are usually given in a sound level form (dB scale) based on the logarithmic type non-linear transformation of the sound pressure. Therefore, for the purpose of determining the uncontaminated output response, it is necessary to find a method of reasonably removing the effect of the background noise and that of the observation mechanism based on the above non-linear transformation.

Based on the additive principle of sound energy, the arbitrary sound environmental systems on an intensity scale can be described in a simplified form of the following linear system:

$$\xi = \sum_{i=0}^{N} a_i \cdot x_i \,, \tag{1}$$

where ξ and x_i are the system output and input, respectively. Here, the acoustic system order N and the system parameters a_i $(a_{N+1} = 1)$ have been found in advance in the previous paper [3]. Let us consider the observation mechanism based on the linear and/or non-linear transformations as following equations:

$$y = f(\xi), \tag{2}$$

$$z = f\left(\xi + \sum_{i=0}^{N+1} a_i \cdot v_i\right). \tag{3}$$

Hereupon, $f(\cdot)$ denotes the mechanism of the linear and/or non-linear transformation measurement. Also, z and y are two kinds of observed data with and without the background noise. And, v_i $(i = 1, 2, ..., N)$ and v_i $(i = N + 1)$ show the sound intensities of background noises added on the input and output sides, respectively.

Let us derive a synthetic probability density function of the stochastic sound environmental system with background noise, after the linear and/or non-linear transformations in Eqs. (2) and (3). If employing this synthetic probability expression into an inverse direction of analysis, it becomes possible to estimate reasonably a p.d.f. of the output response uncontaminated by the background noise without introducing any artificial error criterion like the well-known least-squares method. More concretely, we introduce an arbitrary function $\psi(z)$ which plays the role of a certain kind of the catalytic like operation in the decomposition of the above synthetic expression for the p.d.f. Here, let us write the expectation value of this arbitrary function under consideration, as a certain catalytic function of analysis, as follows:

$$I \equiv \langle \psi(z) \rangle = \int_{-\infty}^{\infty} \psi(z) p_z(z)\, dz, \tag{4}$$

where $p_z(z)$ is a p.d.f. of z and $\langle * \rangle$ denotes an expectation operation with respect to the variable $*$. Here, it seems to be natural to assume that the i-th $(i = 0, 1, 2, ...)$ successive derivatives of $\psi(z)$ and/or $p_z(z)$ tend to zero at the boundary region $z \to \pm\infty$. After substituting Eq. (3) into $\psi(z)$ and expanding it in a Taylor's expansion series form under the above natural boundary condition, $\psi(z)$ can be rewritten as follows:

$$\psi(z) = \sum_{n=0}^{\infty} \left[\left(\sum_{i=0}^{N+1} a_i \cdot v_i \right)^n \Big/ n! \right] \cdot (d/d\xi)^n \cdot \psi(f(\xi)). \tag{5}$$

Accordingly, after substituting Eq. (5) into Eq. (4) and successively integrating by parts, the expectation I of the arbitrary function $\psi(z)$ can be concretely expanded under the above natural boundary condition as follows:

$$I = \int_{-\infty}^{\infty} \psi(y) \cdot \left\{ \sum_{n=0}^{\infty} (-1)^n \Big/ n! \cdot A^n \cdot \left[\langle B^n \mid f^{-1}(y) \rangle \cdot p_y(y) \right] \right\} dy, \tag{6}$$

where

$$A = \left(\frac{1}{\dfrac{df^{-1}(y)}{dy}} \frac{d}{dy} \right), \qquad B = \left(\sum_{i=0}^{N+1} a_i \cdot v_i \right).$$

After replacing y with z owing to the property of the definite integral operation in Eq. (6) and comparing the definition of the expectation of the arbitrary function in Eq. (4) with Eq. (6), the above p.d.f. $p_z(z)$ of z can be derived as the following equations:

$$p_z(z) = p_y(z) + \sum_{n=1}^{\infty} (-1)^n \Big/ n! \cdot A^n \cdot \left[\langle B^n \mid f^{-1}(z) \rangle \cdot p_y(z) \right], \tag{7}$$

or

$$p_y(z) = p_z(z) - \sum_{n=1}^{\infty}(-1)^n \Big/ n! \cdot A^n \cdot \left[\langle B^n \mid f^{-1}(z)\rangle \cdot p_y(z)\right], \tag{8}$$

Here, we must notice the fact that $p_y(z)$ means to replace only a stochastic variable y with z in the p.d.f. expression $p_y(y)$ of y itself. Based on the above synthetic probability expression Eq. (8), it is possible to estimate reasonably only the undisturbed p.d.f. $p_y(y)$ of the objective output y without the background noise for arbitrary sound environmental systems. That is, after substituting $p_y(z)$ in the expansion series expression on the right hand side of Eq. (8) by the whole right side of this equation and successively repeating the same procedure, the following expression of $p_y(y)$ can be derived:

$$\begin{aligned} p_y(y) = p_z(y) &- \sum_{n_1=1}^{\infty} A_{n_1} \cdot A^{n_1} \cdot \left[\langle B^{n_1} \mid f^{-1}(y)\rangle\right] \cdot p_z(y) + \cdots \\ &+ (-1)^s \sum_{n_1=1}^{\infty}\sum_{n_2=1}^{\infty} \ldots \sum_{n_s=1}^{\infty}\prod_{k=1}^{s} A_{n_s} \cdot A^{n_k} \cdot \left[\langle B^{n_k} \mid f^{-1}(y)\rangle\right] \cdot p_z(y) + \cdots, \end{aligned} \tag{9}$$

where

$$A_{n_k} = (-1)^{n_k}/n_k!.$$

Therefore, the p.d.f. expression for the output response of sound environmental systems after noise cancellation can be explicitly estimated from the observed actual data obtained by the logarithmic type non-linear transformation of the data including background noise.

2.2. Prediction of the system response probability with background noise and arbitrary input

First, we derive, both on the intensity scale and in the parameter differential form, the relationship between two p.d.f.s of the system outputs excited by a reference stochastic input and an arbitrary input without additional noise. Let a system output without additional noise change from y_0 to y:

$$y = y_0(1 + \gamma/s_0), \tag{10}$$

where y_0 and y denote two system outputs emitted by a specific stochastic input of reference type and an arbitrary random input without additional noise in the form of the intensity scale, respectively. The γ/s_0 shows some ratio of a dimensionless deviation from a standard distribution type and is statistically independent of y_0. We can express a relationship between two p.d.f.s of acoustic system responses excited by a specific input of reference type and an arbitrary input without additional noise in the expression form of p.d.f. as follows [4]:

$$p_y(y) = \sum_{l=0}^{\infty}(-1)^l/l! \cdot (d/dy)^l \left[\left\langle (\gamma \cdot y/s_0)^l \mid y\right\rangle \cdot p_{y_0}(y)\right]. \tag{11}$$

Here, we must notice the fact that only a random variable is changed from the original y_0 to y in the proper p.d.f. expression $p_{y_0}(*)$ of y_0. Also, the conditional moment can be directly obtained as:

$$\left\langle (\gamma \cdot y/s_0)^l \,|\, y \right\rangle = y^l/s_0^l \cdot \langle \gamma^l \rangle. \tag{12}$$

Accordingly, after substituting Eq. (12) into Eq. (11), the latter can be easily rewritten as follows:

$$\begin{aligned} p_{y(y)} &= \sum_{l=0}^{\infty} (-1)^l/l! \cdot (d/dy)^l \left[y^l/s_0^l \cdot \langle \gamma^l \rangle \cdot p_{y_0}(y) \right] \\ &= \sum_{l=0}^{\infty} (-1)^l/l! \cdot \langle \gamma^l \rangle (d/dy)^l \left[p_{y_0}(y) \cdot y^l/s_0^l \right]. \end{aligned} \tag{13}$$

Paying our attention to the fact that the system output on an intensity scale, y always fluctuates in a non-negative region. The probability density function for the system output can be expressed in advance especially in the general form of a statistical Laguerre expansion series [5] as:

$$p_{y_0}(y) = \left\{ 1 + \sum_{n=1}^{\infty} C_n \cdot L_n^{(m_0-1)}(y/s_0^l) \right\} p_{\Gamma}(y; m_0, s_0), \tag{14}$$

where

$$m_0 = \langle y \rangle^2 \Big/ \left\langle (y - \langle y \rangle)^2 \right\rangle, \qquad s_0 = \left\langle (y - \langle y \rangle)^2 \right\rangle \Big/ \langle y \rangle, \tag{15}$$

$$p_{\Gamma}(y; m_0, s_0) = y^{m_0 - 1} \cdot e^{-y/s_0} / \left(\Gamma(m_0) \cdot s_0^{m_0} \right) \tag{16}$$

and

$$C_n = \Gamma(m_0) \cdot n!/\Gamma(m_0 + n) \cdot \left\langle L_n^{(m_0-1)}(y/s_0) \right\rangle, \tag{17}$$

where $L_n^{(m_0-1)}(*)$ is a Laguerre polynomial of the n-th order, and C_n is the expansion coefficient reflecting hierarchically the lower and higher order statistics of the output intensity fluctuation. Furthermore, Eq. (14) can be transformed into a parameter differential type series expansion expression taking a gamma distribution function as the first expansion term:

$$p_{y_0}(y) = \left\{ 1 + \sum_{n=1}^{\infty} C_n'(\partial/\partial s_0)^n \right\} p_{\Gamma}(y; m_0, s_0), \tag{18}$$

where

$$C_n' = \Gamma(m_0) \cdot (-s_0)^n \Big/ \Gamma(m_0 + n) \cdot \left\langle L_n^{(m_0-1)}(y_0/s_0) \right\rangle. \tag{19}$$

After some complicated calculation procedures, the following relationship between the variable differential and the parameter differential can be derived as:

$$(\partial/\partial y)^l \left[p_{y_0}(y) \cdot y^l/s_0^l \right] = (-1)^l (\partial/\partial s_0)^l p_{y_0}(y). \tag{20}$$

Consequently, by employing Eq. (20), Eq. (13) can be rewritten as follows:

$$p_y(y) = \sum_{l=0}^{\infty} 1/l! \cdot \langle \gamma^l \rangle \cdot (\partial/\partial s_0)^l p_{y_0}(y). \tag{21}$$

Next, the relationship between the two kind p.d.f.s of the system output emitted by the arbitrary stochastic input with and without additional noise is also introduced by the expression of the parameter differential form on an intensity scale. Based on these relationships, we derive a new prediction method being able of evaluating the acoustic system output excited by the arbitrary stochastic input in the presence of additional noise. The output fluctuation on the intensity scale for the arbitrary sound environmental system can be written in the following linear form:

$$z = y + \sum_{i=0}^{N+1} a_i v_i \,, \tag{22}$$

where z and y denote the system outputs with and without additional noise in the form of an intensity scale. Here, N and a_i are the system order and system parameter. Also, v_i $(i = 1, 2, ..., N)$ and v_i $(i = N + 1)$ denote the intensities of additional noises on the input and output sides, respectively. The following expression can be simply deduced from Eq. (7) taking into consideration that $df^{-1}(z)/dz = 1$ for the system output given by Eq. (22) and $\langle B^n | f^{-1}(z) \rangle = \langle B^n \rangle$ when the system output y and the additional noise are statistically independent:

$$p_z(z) = \sum_{n=0}^{\infty} (-1)^n / n! \cdot \left\langle \left(\sum_{i=0}^{N+1} a_i v_i \right)^n \right\rangle \cdot (d/dz)^n p_y(z). \tag{23}$$

After substituting Eq. (21) into Eq. (23) under the above condition, it is possible to rewrite Eq. (23) as:

$$\begin{aligned} p_z(z) &= \sum_{n=0}^{\infty} (-1)^n / n! \cdot \left\langle \left(\sum_{i=0}^{N+1} a_i v_i \right)^n \right\rangle \cdot (d/dz)^n \left\{ \sum_{l=0}^{\infty} 1/l! \cdot \langle \gamma^l \rangle \cdot (\partial/\partial s_0)^l p_{y_0}(z) \right\} \\ &= \sum_{n=0}^{\infty} (-1)^n / l! \cdot (\partial/\partial s_0)^l \left\{ \sum_{n=0}^{\infty} (-1)^n \Big/ n! \cdot \left\langle \left(\sum_{i=0}^{N+1} a_i v_i \right)^n \right\rangle \cdot (d/dz)^n p_{y_0}(z) \right\}. \end{aligned} \tag{24}$$

Consequently, after taking into consideration a p.d.f. $p_{y_0}(z)$ of z corresponding only to y_0 (instead of y) expressed in the same form as Eq. (23), we directly have:

$$p_z(z) = \sum_{l=0}^{\infty} 1/l! \cdot \langle \gamma^l \rangle \cdot (\partial/\partial s_0)^l p_{z_0}(z). \tag{25}$$

Thus, we can predict theoretically the response p.d.f. for an actual sound environmental system with an arbitrary stochastic input in the presence of additional noise, especially by employing the information on the system output p.d.f. for the same system with a specific reference input in the presence of an additional noise knowing its statistics.

3. Experimental consideration

3.1. Experimental arrangement

Figure 1 shows a block diagram of the experimental arrangement in two reverberation rooms. The speaker excites the transmission room and two microphones receive the input

and output intensity fluctuations of the sound insulation system respectively. Table 1 shows values of the system parameters for the sound insulating structures considered in the experiment (the system order $N = 2$). We have employed the actual road traffic noise measured in Hiroshima City and the white noise as the stochastic input and the background noise, respectively. The aperture of the wall between the transmission and the reception has an area of $1.74\,\mathrm{m} \times 0.84\,\mathrm{m}$.

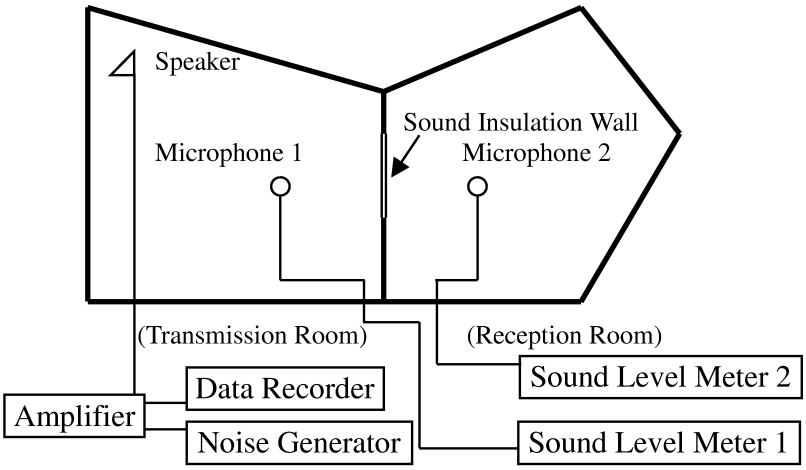

Fig. 1. Block diagram of experimental arrangement.

Table 1. Values of the system parameters.

	a_0	a_1	a_2
Single wall	2.43×10^{-3}	2.10×10^{-3}	1.95×10^{-3}
Non-parallel double wall	9.28×10^{-3}	6.08×10^{-3}	5.53×10^{-3}
Double wall with sound bridge	5.52×10^{-3}	4.18×10^{-3}	3.37×10^{-3}

The proposed methods are applied to three types of the sound insulation wall systems, a) a single wall — an aluminum panel (surface density : $3.22\,\mathrm{kg/m^2}$, thickness : $1.2\,\mathrm{mm}$), b) a non-parallel wall — composed of aluminum (at an angle 9 degrees each other), and c) a double wall with sound bridge — composed of aluminum with a sound bridge (air gap thickness : $50\,\mathrm{mm}$).

3.2. Experimental results

3.2.1. Noise cancellation on a whole probability form. The results of the c.d.f. for the estimation of the output response probability after the background noise cancellation in cases of the double wall with sound bridge and the non-parallel double wall are shown in Fig. 2. The good agreement between the theoretically calculated values and experi-

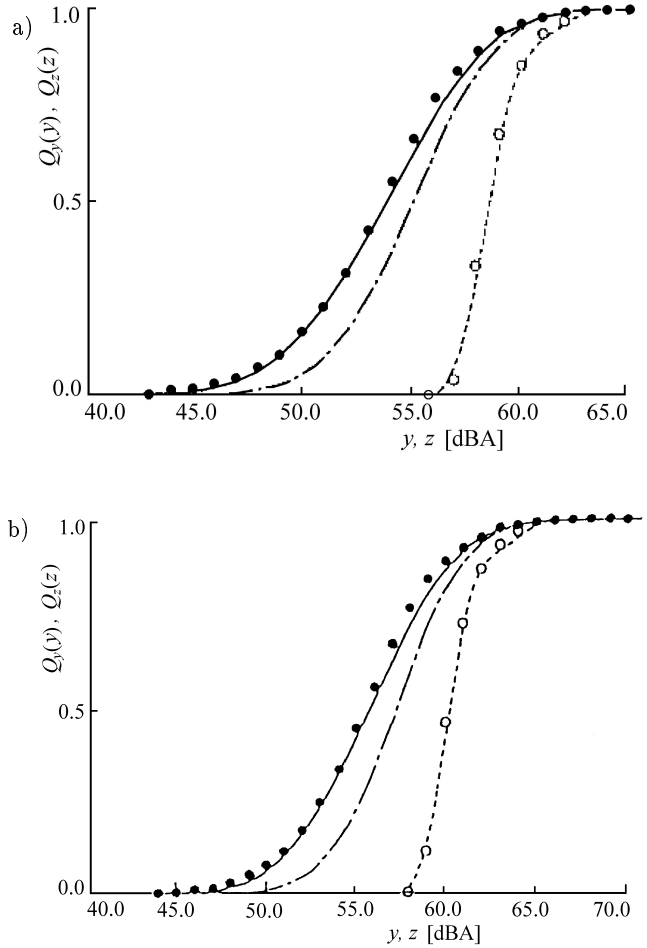

Fig. 2. Comparison between theoretically estimated curves and experimentally sampled values for cumulative distribution function; a) a double wall with sound bridge, b) a non-parallel double wall. The observed and fitted curve for $Q_z(z)$ are shown as (○) and (· · ·). The true and estimated curves for $Q_y(y)$ are shown as (●), (– · –): 1st approx. and (—): 2nd approx.

mentally observed data is recognized in Fig. 2 by employing only the first few expansion terms in the proposed theoretically expansion expression.

3.2.2. Prediction of the system response probability with background noise and an arbitrary input. The results of the c.d.f. for the prediction of the system output are shown in Fig. 3 in cases of the single wall and the non-parallel double wall, respectively. Here, the 1st, 2nd or 3rd approximations correspond to the cases of employing the 1st, 2nd or 3rd terms in the above theoretical expansion expression, respectively. In the inverse problem of infinite series expression, there is generally some risk of series divergency even if its original series expression is convergent. So, some reasonable countermeasure of divergent error seem fairly important. For the purpose of reasonably minimizing this

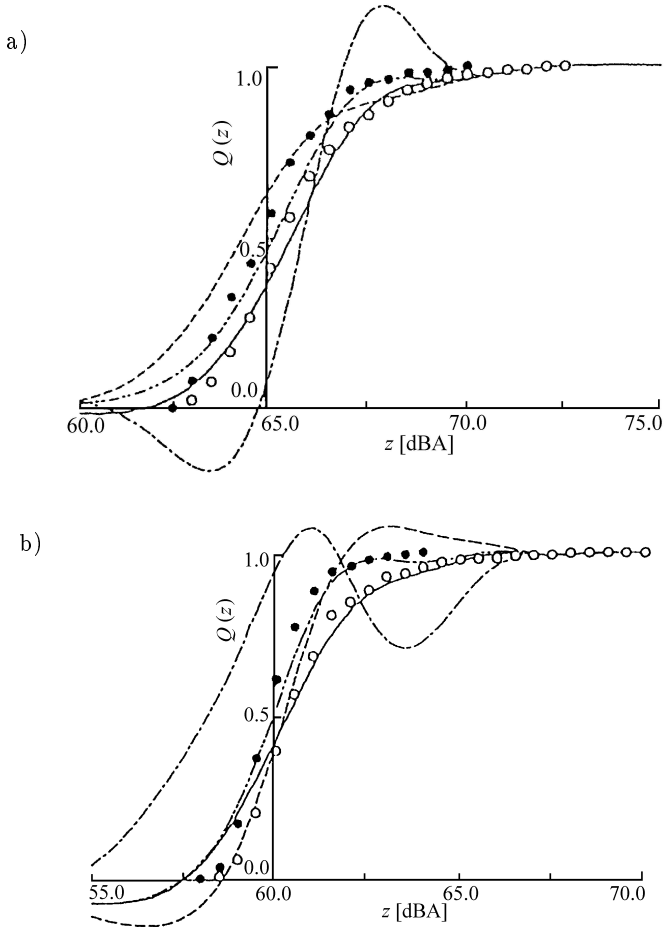

Fig. 3. Comparison between theoretically predicted curves and experimentally sampled values for cumulative distribution function; a) a single wall, b) a non-parallel double wall. Experimentally sampled values in cases of the arbitrary input and the reference input are marked by (•) and (○), respectively. Theoretically predicted curves are shown by (—): 1st approx., (···): 2nd approx., (– · –): 3rd approx. and (– ·· –): averaging method.

divergency error caused by employing only the first finite terms in the above infinite series expansion expression, some averaging evaluation procedure can be derived theoretically as follows:

$$Q(z) = Q_0(z) + (b+c)/(a+b+c) \cdot Q_1(z) + c/(a+b+c) \cdot Q_2(z) \\ +1/(a+b+c) \cdot (a \cdot \varepsilon_0 + b \cdot \varepsilon_1 + c_2 \cdot \varepsilon_2), \qquad (26)$$

where $Q_i(z)$'s $(i = 0, 1, 2)$ are respectively the c.d.f. in the special cases taking the 1st, 2nd or 3rd terms in the above infinite series type theoretical p.d.f. expansion expression, and a, b and c are the arbitrary constants. Also, the ε_i's $(i = 0, 1, 2)$ denote the errors caused by use of the finite expansion terms in the cases of $Q_i(z)$ $(i = 0, 1, 2)$, respectively.

From Fig. 3, it seems that the 1st, 2nd and 3rd approximation curves do not show any agreement with the experimentally sampled points owing to the above error. The averaging method in Eq. (26), however, shows a better agreement with the experimentally sampled points compared with the other curves.

4. Conclusion

In this paper, we have proposed two stochastic signal processing methods on a whole probability distribution form without introducing in advance any artificial error criterion. That is, for the arbitrary sound environmental system under the existence of background noise, we have developed the method of estimating the output response probability after noise cancellation and that of predicting the system output emitted by an arbitrary input with background noise by employing the information on the system output p.d.f. for the same system excited only by a specific reference input in the presence of the background noise knowing its statistics.

Finally, the practical effectiveness of the proposed methods have been experimentally confirmed too by applying them to the actually observed response data in the reverberation room.

Since the present methods are at an earlier stage of study, there still remain some kinds of future problems, for example, to apply them to many other actual systems and to find more simplified methods for practical use through some approximation of the proposed methods.

Appendix A

A.1. Simplified determination method of the order for an arbitrary sound insulation system based on time series model

An arbitrary sound insulation system can be described by the following discrete-time type:

$$z_k = f(X_k; A) \qquad X_k \equiv (x_k, x_{k-1}, ..., x_{k-l}), \tag{A.1}$$

where x_k and z_k are the system input and output at the discrete-time k, and $f(\ )$ denotes the linear and/or non-linear mechanisms of the system. Furthermore, a vector $A \equiv (a_1, a_2, ..., a_N)^T$ show system parameters.

We introduce a somewhat more simplified method rather than such methods as the well-known AIC method or the FPE method for determining the system order on the time series model. When the white noise is adopted on trial as a test input of the system described by Eq. (A.1), the relationship between the test input $(= u_k)$ and the system output $(= y_k)$ can be written in the following form:

$$y_k = f(U_k; A) \qquad U_k \equiv (u_k, u_{k-1}, ..., u_{k-l}). \tag{A.2}$$

Because the statistical independence property originally does not change, even in an arbitrary nonlinear transformation of the systems, the statistical independence for the arbitrary random signal y_k can be evaluated in terms of the following measure $\varepsilon(y_k, y_{k+j})$:

$$\varepsilon(y_k, y_{k+j}) = \frac{\langle y_k y_{k+j} \rangle}{\langle y_k \rangle \langle y_{k+j} \rangle} - 1, \tag{A.3}$$

where $\langle * \rangle$ denotes the expected value of $*$ and $\varepsilon(y_k, y_{k+j}) = 0$ when y_k and y_{k+j} are statistically independent. Then, it is surely reasonable that we adapt the system order as $l = j - 1$, in the case when the value of $\varepsilon(y_k, y_{k+j})$ is saturated downward the neighborhood of zero at j.

Figure 4 shows the result of the system order determined by Eq. (A.3). From this figure, it can be found that the system order is approximately 2 because the value of $\varepsilon(y_k, y_{k+j})$ is close to zero at $j = 3$.

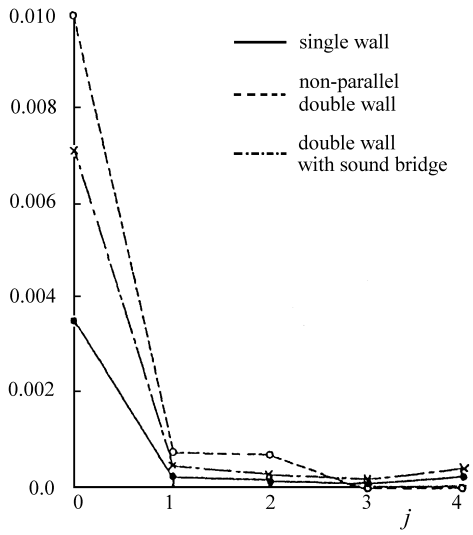

Fig. 4. Identification results for the order of time series model based on the criterion function of independency; $\varepsilon(j) = \langle y_k, y_{k+j} \rangle / \langle y_k \rangle \cdot \langle y_{k+j} \rangle - 1$.

A.2. Prediction of output probability distribution

Equation (A.1) can be rewritten as the following linear system on an intensity scale supported by the well-known statistical energy analysis method:

$$z_k = \sum_{i=0}^{2} a_i x_{k-i} \,. \tag{A.4}$$

By use of Eq. (A.4), the prediction of the output probability distribution can be obtained for the sound insulation system excited by random input contaminated by background noise.

Acknowledgements

The authors would like to express our cordial thanks to Prof. K. HATAKEYAMA, Prof. A. IKUTA, Mr. K. NISHIHARA and Mr. N. HANADA for their helpful assistance.

References

[1] A. LONDON, *Transmission of reverberant sound through double walls*, J. Acoust. Soc. Am., **22**, 270–279 (1950).

[2] M.J. CROCKER and A.J. PRICE, *Sound transmission using statistical energy analysis*, J. Sound Vib., **9**, 469–486 (1969).

[3] M. OHTA and H. YAMADA, *A simple method for predicting the output energy distribution of an arbitrary sound insulation system by use of the least-squares method* [in Japanese], J. Acoust. Soc. Jpn., **(J)39**, 756–765 (1983).

[4] M. OHTA and N. TAKAKI, *A practical estimation and prediction method of response probability distribution for arbitrary sound environmental systems with background noise and its application to the sound wall system*, J. Acoust. Soc. Jpn. **(E)17**, 3, 121–126 (1996).

[5] M. OHTA and T. KOIZUMI, *General statistical treatment of the response of a nonlinear rectifying device to a stationary random input*, IEEE Trans. Inf. Theory, IT-14, 595–598 (1969).

ARCHIVES OF ACOUSTICS
26, 4, 305–329 (2001)

EVALUATION OF MATERIAL PARAMETERS, TEXTURE AND STRESS OF A PRESTRESSED POLYCRYSTALLINE AGGREGATE FROM ULTRASONIC MEASUREMENTS

J. LEWANDOWSKI

Polish Academy of Sciences
Institute of Fundamental Technological Research
(00-049 Warszawa, Świętokrzyska 21, Poland)

The propagation of ultrasonic plane waves in a polycrystalline aggregate (steel) is considered for a bulk sample of the material with plane initial (residual) stress, the material being made of cubic crystals of the highest symmetry. Some effective stiffness moduli of the bulk sample and the components of the initial stress are found as functions of the propagation velocities of the respective ultrasonic plane waves. Moreover, the use is made of Jaynes' principle of maximum Shannon entropy and the averaging procedure proposed by Voigt. In this way, the probability density function of the crystallite orientation (texture) and the effective stiffness moduli of a single crystallite of the polycrystalline aggregate are evaluated numerically for the initial plane stress increasing from zero up to about 300 MPa (in the range of elasticity). The numerical analysis shows that while the effect of the initial stress on the results of these calculations increases with increasing initial stress, the changes in the texture and effective stiffness moduli of a single crystallite are inconsiderable in the region of the values of the initial stress taken in to account.

Keywords: Polycrystalline aggregate, texture, initial (residual) stress, ultrasonic waves, elastic moduli.

1. Introduction

Polycrystalline metals are of the form of polycrystalline aggregate of numerous grains, each grain being a crystallite (monocrystal) with a single crystal symmetry of its structure and elastic properties. In general, in a macroscopic sample of the polycrystalline aggregate, which is free of initial stress and is in the so-called natural state with respect to its plastic deformation history (i.e., is in the state before its first plastic deformation), the grains are randomly oriented resulting in isotropic symmetry of the overall (effective) elastic properties of the sample. Anisotropy of the effective elastic properties and residual stress in bodies, however, usually arises from forming processes being accompanied by plastic and often nonuniform deformation. Such processes leave the crystallites in certain preferred orientations called the texture and subjects the body to a state of residual stress. The texture and residual stress induce anisotropy of the effective elastic properties, and consequently, cause variations in the speeds at which ultrasonic waves propagate through the sample, the variations depending on the directions of wave propagation and

polarization. In this context, it is natural to define the effective elastic coefficients (e.g., stiffness moduli) of a such prestressed inhomogeneous body in a well-known manner as coefficients in linearized equations of motion governing the propagation of small-amplitude elastic waves in this body, the governing equations being assumed to be of the same mathematical form as the equations governing the propagation of the waves in a bulk prestressed monocrystal with the same symmetry of the elastic properties as that of the inhomogeneous polycrystalline body under consideration. Making use of this definition, we arrive at the acoustoelastic dependencies which raise the possibility of using ultrasonics as a nondestructive technique for measurements of residual stress and evaluating some effective stiffness moduli of the bulk sample as well as for estimating the texture and the effective stiffness moduli of a single crystallite in the body. In this context, the probability density function of the crystallite orientation in such a body with non randomly oriented grains, which describes the texture, is called herein also the texture. The aim of the paper is to present the proposal of a procedure which allows us to evaluate initial (residual) stress and some effective stiffness moduli of the bulk sample as well as enable us to estimate the texture and the effective stiffness moduli of the single crystallite from the variations of the velocity of ultrasonic waves propagating through a bulk sample of a prestressed polycrystalline aggregate, which has been plasticly deformed.

The rudiments of the acoustoelastic theory, which is employed in constructing the procedure, have been developed in Refs. [1, 2]. Many practical suggestions utilized in the present paper have arisen from studying Refs. [3–5] or have their origin in these works. Proceeding in this direction, we become able to evaluate both effective stiffness moduli of the prestressed sample of the polycrystalline aggregate under consideration and the initial plane stress in that from measurements of the propagation velocities of ultrasonic waves. The second part of the problem to be solved is preparing a procedure of estimating from the same ultrasonic measurements both the texture and the effective stiffness moduli of a single crystallite in the body under consideration. The rudiments of an information theory approach are developed in this work within the framework of inversion of the VOIGT [6] concept of evaluating the effective stiffness moduli of a polycrystalline aggregate. It is well known that the essential step of utilizing the Voigt averaging procedure is calculation of the orientational volume average of functions of single crystal elastic stiffness moduli. Here the calculation of the orientational volume average denotes averaging over all crystallites in the bulk sample through the probability density function of the crystallite orientation (i.e., weighting by the probability density function). Therefore, the assumption that the Voigt concept of evaluating the effective stiffness moduli of the polycrystalline aggregate under consideration is equivalent to that based on the propagation equations and measurements of ultrasonic velocities, raises the possibility of formulating a set of integral equations with the probability density function of the crystallite orientation as an unknown function. In this context, the inversion of the Voigt procedure of evaluating the effective stiffness moduli of a prestressed polycrystalline aggregate we define as seeking the answer to the following question: for what probability density function of the crystallite orientation (texture) and for what values of the effective stiffness moduli of a single crystallite do the velocities of plane

ultrasonic waves propagating in the polycrystalline aggregate take the measured values? Formulated in such a way, the problem is ambiguous and is insoluble by using deterministic formalism. To overcome these difficulties, we make use of the probability density function of the crystallite orientation in the form implied by JAYNES [7] principle of minimum prejudice and make choice of the values of the effective stiffness moduli of a single crystallite in accordance with the minimum difference criterion, following Refs. [8, 9], respectively.

The paper is organized in the following manner. Within the framework of the formulation of the problem, basic equations, definitions, notations and concepts on acoustoelasticity are introduced in Sec. 2, the scope of the compendium being limited to that needed for formulating and solving the problem for the cases of plane initial stress different from zero and equal to zero. In Sec. 3, the theory and relevant expressions for constructing algorithms for these two cases are summarized, together with pointing out the differences between the algorithms. Controlling on line the convergence of iteration procedures and checking the exactness of numerical calculations are described in Sec. 4. Finally, numerical results obtained for steel polycrystalline aggregate with texture approximating the orthorhombic one are discussed in Sec. 5.

2. Formulation of the problem

Now a brief outline is given of the theoretical preliminaries of the proposed ultrasonic method that enable us to determine simultaneously the texture, stress and material effective parameters of a textured and prestressed polycrystalline aggregate. The solid bulk samples are assumed to be composed of a large number of cubic crystallites with the highest symmetry. In this paper, only such orientation statistics of the crystallites is considered which contributes to the orthorhombic symmetry of the effective dynamic properties of a solid bulk specimen of the polycrystalline material under examination. To discuss the orientation of a crystallite and describe all the vector and tensor quantities involved in the problem under analysis, we introduce two orthogonal reference systems. A Euler orthogonal reference system $0x_1x_2x_3$ with the axes $0x_1$, $0x_2$, and $0x_3$ is supposed to be suitably chosen, for example, in the case of a rolled plate, $0x_1$ could coincide with the rolling direction, the axes $0x_2$ and $0x_3$ being transverse to the rolling direction and normal to the rolling plane, respectively. Then the planes x_1x_2, x_2x_3 and x_3x_1 are the planes of mirror symmetry connected with the orthorhombic symmetry of the solid bulk sample. The unit vectors along the directions of the axes $0x_1$, $0x_2$, and $0x_3$ are denoted by $\mathbf{e}_1$, $\mathbf{e}_2$ and $\mathbf{e}_3$, respectively. The other orthogonal reference system $0X_1X_2X_3$ with the axes $0X_1$, $0X_2$, and $0X_3$ is supposed to be suitably chosen for a single cubic crystallite, the axes being chosen in the crystallographic directions [100], [010] and [001], respectively. The unit vectors along the directions of the axes $0X_1$, $0X_2$, and $0X_3$ are denoted by $\mathbf{E}_1$, $\mathbf{E}_2$ and $\mathbf{E}_3$, respectively. In the subsequent considerations, the orientation of a crystallite within the polycrystalline sample is described by giving the values of three Eulerian angles, θ, φ and ϕ, of the OX_1, OX_2, and OX_3 axes relative to the sample axes, Ox_1, Ox_2, and Ox_3. The notations θ ($\theta = \cos^{-1}(\mathbf{E}_3 \cdot \mathbf{e}_3)$), φ and ϕ stand for the

angle of nutation, precession and proper rotation respectively. The texture will be described by the probability density function of the crystallite orientation, $p(\xi, \varphi, \phi)$, where $\xi = \cos(\theta)$. Then $p(\xi, \varphi, \phi)\, d\xi\, d\varphi\, d\phi$ expresses the probability of a crystallite having an orientation described by the Euler angles θ $(= \cos^{-1}\xi)$, φ and ϕ, lying in the intervals $\langle \cos^{-1}\xi, \cos^{-1}(\xi + d\xi)\rangle$, $\langle \varphi, \varphi + d\varphi\rangle$ and $\langle \phi, \phi + d\phi\rangle$, respectively. The following considerations are concerned with orthorhombic bulk samples that are under applied or residual constant plane stress called the initial stress, σ^0_{ij} $(i, j = 1, 2, 3)$. It is assumed that the two principal axes of the initial plane stress, σ^0_{ij}, coincide with symmetry axes $0x_1$ and $0x_2$ of the orthorhombic material. Then the initial stress, σ^0_{ij}, does not change the symmetry and the number of independent effective elastic constants of the bulk sample under consideration. Generally, when a stress tensor σ_{ij} is referred to the reference system with the axes Ox_1, Ox_2, and Ox_3 coinciding with the principal directions of the stress σ_{ij}, then the shear stress components $\sigma_{12} = \sigma_{21}$, $\sigma_{13} = \sigma_{31}$ and $\sigma_{23} = \sigma_{32}$ vanish. Then for plane stress analysis, where the shear stress components $\sigma^0_{12} = \sigma^0_{21}$, $\sigma_{23} = \sigma_{32}$, and $\sigma_{13} = \sigma_{31}$ as well as the component σ_{33} vanish or are negligible small as compared with $\{\sigma^0_{11}, \sigma^0_{22}\}$, the only components of the initial stress, σ^0_{ij}, present in the considerations are $\{\sigma^0_{11}, \sigma^0_{22}\}$.

To be enabled to determine simultaneously the texture and initial stress σ^0_{ij} of a polycrystalline aggregate from the measurements of the propagation velocities of ultrasonic waves in a sample of the material being acted on by an ultrasonic transducer, some effective material parameters [10] must be known for characterizing both overall and single-crystal effective elastic properties. The term *effective properties* of the bulk sample under study is used to describe both the physical properties of the so-called equivalent homogeneous medium that exhibits the same symmetry of the macroscopic mechanical properties as the sample, and the so-called effective displacement response, $\mathbf{u}$, of the equivalent medium to the transducer loading. The effective displacement response is the same as the averaged displacement response of the polycrystalline material to the same loading, the averaging being carried out over a statistical ensemble of the bulk samples [8], i.e. over all crystallites through the function $p(\xi, \varphi, \phi)$. The effective dynamic properties of the prestressed orthorhombic polycrystalline aggregate under study and its single cubic crystallite (monocrystalline grain) are defined by the tensors of the effective elastic stiffness moduli, C^{eff}_{ij} and c^{eff}_{ij}, respectively. Since it is assumed that the principal axes of the initial stress, σ^0_{ij}, coincide with the symmetry axes $0x_1$ and $0x_2$ of the orthorhombic material then the initial stress, σ^0_{ij}, does not change the symmetry and the number of independent effective elastic constants of the solid bulk sample. Therefore, the non-vanishing independent effective elastic stiffness moduli of the orthorhombic polycrystalline bulk sample under consideration as well as those of a single cubic crystallite of the macroscopic sample are $\{C^{\text{eff}}_{11}, C^{\text{eff}}_{22}, C^{\text{eff}}_{33}, C^{\text{eff}}_{44}, C^{\text{eff}}_{55}, C^{\text{eff}}_{66}, C^{\text{eff}}_{12}, C^{\text{eff}}_{13}, C^{\text{eff}}_{23}\}$ and $\{c^{\text{eff}}_{11}, c^{\text{eff}}_{12}, c^{\text{eff}}_{44}\}$, respectively.

Such residual plane stresses in steel may be induced by inhomogeneous plastic deformation in some technological processes, e.g., when the steel is uniaxially rolled in cold rolling process. Then, if the axis $0x_1$ of the reference system coincides with the rolling direction, while the other axes $0x_2$ and $0x_3$ of the reference system are transverse to

the rolling direction and normal to the rolling plane, respectively, the axes Ox_1 and Ox_2 coincide simultaneously with the principal directions of the residual stress. Consequently, if the tensor σ_{ij}^0 of the residual stress is referred to the reference system with axes Ox_1, Ox_2, and Ox_3, then the shear stress components $\sigma_{12}^0 = \sigma_{21}^0$, $\sigma_{13}^0 = \sigma_{31}^0$, $\sigma_{23}^0 = \sigma_{32}^0$ vanish and if moreover σ_{33}^0 also vanishes (or at least is negligible small), the residual stress is plane. Without going into detail, the process of inducing the residual stress in the steel uniaxially rolled in cold rolling process σ_{ij}^0 may be explained after [11] as follows: The friction between the plate surface and the rolls together with plastic flow result in a complex process with the dominant component in the form of material flow process similar to sausage filling. Namely, the surfaces of the plate act as a skin, and the interior of the plate is pressed in between towards the exit side of the roll gap, the interior being in the state of compression. The compression causes also transverse material flow in the roll gap, the transverse flow being much smaller than that in the rolling direction. In this way, in the cold rolling mill, the plate becomes longer and thinner due to the plastic flow. Since all volume elements of the plate are stuck together, these length changes are absorbed partially by elastic strains, which are accompanied by the residual stresses $\{\sigma_{11}^0, \sigma_{22}^0\}$. In turn, the residual stresses are stored in the material as dislocations in the atomic lattice. If the temperature is sufficiently high, the dislocations are free to move becoming able to release the residual stresses.

In the paper, for the sake of brevity and convenience, the following tensor quantities are defined:

$$\overline{c}_{ij} = \frac{c_{ij}^{\text{eff}}}{\rho}, \qquad \overline{C}_{ij} = \frac{C_{ij}^{\text{eff}}}{\rho}, \qquad \overline{\sigma}_{11}^0 = \frac{\sigma_{11}^0}{\rho}, \qquad \overline{\sigma}_{22}^0 = \frac{\sigma_{22}^0}{\rho}. \tag{1}$$

The quantities $\overline{C}_{ij}$ and $\overline{c}_{ij}$ are used in describing the effective dynamic properties of the polycrystalline aggregate under study and its single crystallite, respectively. ρ denotes the effective density which is assumed in this paper to be equal to the density averaged over the volume of a single bulk sample. In a prestressed solid, apart from the stress σ_{ij} accompanying the strain ε_{kl} due to, e.g., the propagation of ultrasonic waves, there exists an additional initial stress σ_{ij}^0 which is accompanied by the initial strain ε_{kl}^0, both the initial quantities being assumed to be independent of time. As was mentioned, the stress σ_{ij}^0 can be both applied and residual since there is no restriction that the resulting deformations are elastic. Every $\overline{C}_{ijkl}$ is highly dependent on both microstructure and the initial stress σ_{ij}^0. For a monocrystal $C_{ijkl}^{\text{eff}} = c_{ijkl}^{\text{eff}} = c_{ijkl}$, when $\sigma_{ij}^0 = 0$.

Similar to the effective (average) density, ρ, the effective elastic moduli C_{ijkl}^{eff} are also independent of the position vector $\mathbf{x}$ (space coordinates x_1, x_2, x_3), but they are dependent on the angular frequency ω of the loading ultrasonic transducer. In contrast, the average (effective) displacement field resulting from the dynamic load with the angular frequency ω is harmonically dependent on the position vector $\mathbf{x} = (x_1, x_2, x_3)$ and time t with the same frequency ω and, consequently, is also called the effective displacement wave $\mathbf{u}$.

In the Euler coordinate system $0x_1x_2x_3$, the equations of motion for small effective elastic displacement, $\mathbf{u}$, which accompanies the propagation of an ultrasonic displacement

wave in the prestressed solid under consideration, can be written in the following form:

$$\left(\overline{C}_{ijkl} + \overline{\sigma}^0_{jl}\delta_{ik}\right) \frac{\partial^2 u_k}{\partial x_j \partial x_l} = \frac{\partial^2 u_i}{\partial t^2}, \qquad i,j,k,l = 1,2,3, \tag{2}$$

where δ_{ik} is the Kronecker tensor. Equation (2) are written by utilizing some results of Refs. [1, 2, 4, 5] under the assumption that both the material properties $\overline{C}_{ijkl}$ and the initial stress $\overline{\sigma}^0_{ij}$ vary only slightly over distances of the wavelength.

In this paper, we are interested only in the average displacement field, $\mathbf{u} = (u_1, u_2, u_3)$, in the form of a plane ultrasonic wave propagating in the direction of the unit vector $\mathbf{n} = (n_1, n_2, n_3)$ and polarized in the direction of the unit vector $\mathbf{p} = (p_1, p_2, p_3)$. Through the remainder of the paper, all equations, relations and formulae are written with locating the vector and tensor quantities relative to the $0x_1x_2x_3$ reference system. Then, $x_i = \mathbf{x}\cdot\mathbf{e}_i$, $u_i = \mathbf{u}\cdot\mathbf{e}_i$, $n_i = \mathbf{n}\cdot\mathbf{e}_i \doteq \cos(\alpha_i)$ and $p_i = \mathbf{p}\cdot\mathbf{e}_i \doteq \cos(\beta_i)$, and the wave being of interest for us may be described by the following equation:

$$\mathbf{u} = \mathbf{p}u_0 \exp\left[ik_{np}(\mathbf{n}\cdot\mathbf{x} - V_{np}t)\right] \doteq \mathbf{p}u_0 \exp\left[ik_{np}(\mathbf{n}\cdot\mathbf{x} - \omega t)\right], \tag{3}$$

where V_{np} is the phase velocity of a wave propagating in the direction of the unit vector $\mathbf{n}$ and polarized in the direction of the unit vector $\mathbf{p}$, k_{np} stands for the wave number, $k_{np} = \omega/V_{np}$ and u_0 denotes the displacement wave amplitude. The two sets of angles, $\{\alpha_i\}$ and $\{\beta_i\}$, $i = 1,2,3$, define the directions of the wave propagation and polarization, respectively.

We seek a simple particular solution to Eqs. (2) in the form given by Eq. (3). On this basis, if we put the expression given by Eq. (3) in Eqs. (2), we can infer for each pair of the propagation and polarization directions ($\mathbf{n}$ and $\mathbf{p}$) that Eqs. (2) may be solved. Moreover, the satisfaction of Eqs. (2) not only requires that, for a given polarization direction $\mathbf{p}$, the phase velocity V_{np} depends on the propagation direction $\mathbf{n}$, material parameters $\overline{C}_{ijkl}$ and initial stress $\overline{\sigma}^0_{ij}$ but also determines the form taken by the function $V_{np} = V_{np}\left(\mathbf{n}, \overline{C}_{ijkl}, \overline{\sigma}^0_{ij}\right)$. Going into detail let us remind that on substituting the plane wave solution (3) into Eqs. (2), one obtains the so-called Christoffel equations for an anisotropic material under the initial plane stress $\overline{\sigma}^0_{ij}$. If the plane stress tensor $\overline{\sigma}^0_{ij}$ is referred to the orthogonal reference system $0x_1x_2x_3$ with axes Ox_1 and Ox_2 coinciding with the principal directions of the stress $\overline{\sigma}^0_{ij}$, then, for the case under consideration, the Christoffel equations referred to the same reference system $0x_1x_2x_3$ may be expressed in the following form:

$$\left[\overline{C}_{ijkl}n_in_l + \left(\overline{\sigma}^0_{il}n_in_l - V^2_{np}\right)\delta_{jk}\right]p_k = 0 \quad \Leftrightarrow \quad A_{jk}p_k = 0, \quad i,j,k,l = 1,2,3, \tag{4}$$

where

$$\begin{aligned}
A_{11} &= \left(\overline{C}_{11} + \overline{\sigma}^0_{11}\right)(n_1)^2 + \left(\overline{C}_{66} + \overline{\sigma}^0_{22}\right)(n_2)^2 + \overline{C}_{55}(n_3)^2 - V^2_{np}, \\
A_{22} &= \left(\overline{C}_{66} + \overline{\sigma}^0_{11}\right)(n_1)^2 + \left(\overline{C}_{22} + \overline{\sigma}^0_{22}\right)(n_2)^2 + \overline{C}_{44}(n_3)^2 - V^2_{np}, \\
A_{33} &= \left(\overline{C}_{55} + \overline{\sigma}^0_{11}\right)(n_1)^2 + \left(\overline{C}_{44} + \overline{\sigma}^0_{22}\right)(n_2)^2 + \overline{C}_{33}(n_3)^2 - V^2_{np}, \\
A_{12} &= A_{21} = \left(\overline{C}_{66} + \overline{C}_{12}\right)n_1n_2, \\
A_{13} &= A_{31} = \left(\overline{C}_{55} + \overline{C}_{13}\right)n_1n_3, \\
A_{23} &= A_{32} = \left(\overline{C}_{44} + \overline{C}_{23}\right)n_2n_3.
\end{aligned} \tag{5}$$

If the system of Eqs. (4) is to have a solution different from the trivial one: every $p_k = 0$, then, in accordance with Cramer's rule, the determinant constructed from the coefficients of the A_{ij} given by Eqs. (5) must vanish. Thus we arrived at the following secular equation:

$$|A_{ij}| = 0 \tag{6}$$

which enables us to establish the above mentioned dependence of the phase velocity V_{np} on $\mathbf{n}$, $\overline{C}_{ijkl}$, and $\overline{\sigma}^0_{ij}$. Equation (6) is an equation of the third degree in V_{np} and therefore has three roots. Therefore, for any pair of unit vectors $\mathbf{n} = (n_1, n_2, n_3)$ and $\mathbf{p} = (p_1, p_2, p_3)$ we arrive at the system of Eqs. (4) – (6) and obtain three functions $V_{np} = V_{np}\left(\mathbf{n}, \overline{C}_{ijkl}, \overline{\sigma}^0_{ij}\right)$, after utilizing Cardan's solution of the cubic equation. For an ultrasonic wave given by Eq. (3) and for a vector $\mathbf{p}$, each of the three relationships defines such a form of the dependence $V_{np} = V_{np}\left(\mathbf{n}, \overline{C}_{ijkl}, \overline{\sigma}^0_{ij}\right)$, which ensure that the wave given by Eq. (3) satisfies Eqs. (2).

It is obvious that the knowledge of the three relationships, $V_{np} = V_{np}\left(\mathbf{n}, \overline{C}_{ijkl}, \overline{\sigma}^0_{ij}\right)$, enables us to construct, in the first step, an algorithm for computing some moduli $\overline{C}_{ijkl}$ and initial stress components $\overline{\sigma}^0_{ij}$ from the measurements of phase velocities V_{np}. This step is based on finding the solution with respect to $\overline{C}_{ijkl}$ of the Christoffel equation (6) and consists in applying the method proposed and developed by A.D. DEGTYAR and S.I. ROKHLIN [5] for evaluating some C^{eff}_{ijkl} and σ^0_{ij} from the nondestructive measurements of the respective ultrasonic velocities V_{np} in the polycrystalline material under examination. On finding from V_{np} the respective C^{eff}_{ijkl} of an orthorhombic polycrystalline made of cubic crystals with the highest symmetry, we are able to estimate, in the second step, the texture (i. e., to find the estimate of the function $p(\xi, \varphi, \phi)$) and all the three independent effective stiffness moduli, $\overline{c}_{11}$, $\overline{c}_{12}$ and $\overline{c}_{44}$, of a cubic crystallite. This step consists in applying the approach proposed and developed by LEWANDOWSKI [8, 9] and is based on utilization an algorithm which can be constructed by inverting the VOIGT [6] scheme of calculating $\overline{C}_{ijkl}$. Here let us remind, that the Voigt scheme consists in averaging some functions of θ, φ, ϕ, $\overline{c}_{11}$, $\overline{c}_{12}$, and $\overline{c}_{44}$ with $p(\xi, \varphi, \phi)$ as the weight function to obtain the respective effective stiffness moduli, $\overline{C}_{ijkl}$. Therefore, in the situation where $\overline{C}_{ijkl}$ can be evaluated from the measurements of V_{np} by utilizing Eqs. (4), (6), the function $p(\xi, \varphi, \phi)$ may be estimated together with $\overline{c}_{11}$, $\overline{c}_{12}$, and $\overline{c}_{44}$, by inverting the VOIGT [6] scheme of calculating $\overline{C}_{ijkl}$. However, the problem formulated in such a way is not unambiguous and the lack of uniqueness must be overcome by employing a suitable additional condition. For this reason, LEWANDOWSKI [8, 9] proposed to introduce the JAYNES' [7] principle of the maximum prejudice as a suitable additional condition and, consequently, has developed the method of estimating the function $p(\xi, \varphi, \phi)$ by inverting in the maximum-entropy approximation the Voigt averaging procedure.

Although the method proposed and developed by A.D. DEGTYAR and S.I. ROKHLIN [5] seems to be the most promising nondestructive way of evaluating $\overline{C}_{ijkl}$ and $\overline{\sigma}^0_{ij}$, great difficulty is encountered in analysis when one wishes to utilize this method for a case described by Eqs. (4) – (6) in the full form. In consequence of that, in this case all the quantities, which are to be calculated from the ultrasonic measurements, are involved in an algorithm describing relationships between them, the relationships being nonlinear and

of great complexity. Evidently, when the initial stress, $\overline{\sigma}^0_{ij}$, is not plane and its principal axes do not coincide with the symmetry and reference axes $0x_1$, $0x_2$ and $0x_3$, to which is referred the tensor of the stress σ^0_{ij}, the situation is still more complex. However, in the situation where we confine ourselves to consider a case described by Eqs. (4) – (6) with respectively chosen V_{np}, Eqs. (4) – (6) are to be used in more or less reduced form inducing in this way simplification of the algorithm. An example is presented below of such choice of a set of ultrasonic velocities V_{np} which not only enables us to evaluate $\overline{\sigma}^0_{ij}$ as well as some of moduli $\overline{C}_{ijkl}$, $\overline{c}_{11}$, $\overline{c}_{12}$ and $\overline{c}_{44}$, but also gives the possibility of estimating the function $p(\xi, \varphi, \phi)$.

Throughout the remainder of this paper, the procedure is outlined, which enable us to evaluate some $\overline{C}_{ijkl}$, $\overline{\sigma}^0_{ij}$, $\overline{c}_{11}$, $\overline{c}_{12}$ and $\overline{c}_{44}$, and to estimate the function $p(\xi, \varphi, \phi)$ in the maximum-entropy approximation. In these considerations are involved ultrasonic plane- and linearly-polarized waves that propagate in polycrystalline aggregates with orthorhombic symmetry, the aggregates being composed of crystals of the cubic class with the highest symmetry. The experimental tools for the investigations discussed in this paper are confined to the measurements of the propagation velocities V_{ij} $(i = 1, 2, 3)$ of ultrasonic plane waves propagating and polarized in the directions of the Cartesian reference axes $0x_i$ and $0x_j$, respectively, the reference axes being simultaneously the axes of the symmetry of the material bulk sample and the principal axes of the initial plane stress σ^0_{ij}. Moreover, the bulk sample is made of steel by rolling and the axis $0x_1$ coincides with the rolling direction, the other axes $0x_2$ and $0x_3$ being transverse to the rolling direction and normal to the rolling plane, respectively. Then the axes Ox_1, Ox_2, and Ox_3 coincide both with the symmetry axes of the material bulk sample (plate) and with the principal directions of the plane initial stress σ^0_{ij}. Consequently, the shear components of the initial stress, $\sigma^0_{12} = v^0_{21}$, $\sigma^0_{13} = \sigma^0_{31}$ and $\sigma^0_{23} = \sigma^0_{32}$, vanish, and two principal stress components, σ^0_{11} and σ^0_{22}, are the only nonzero initial stress components.

3. Algorithm for numerical calculations

In accordance with the earlier assumption, let us insert into Eqs. (4), (5) the ultrasonic velocities only in the form of the propagation velocities V_{ij} $(i = 1, 2, 3)$ of ultrasonic plane waves propagating and polarized in the directions of the Cartesian reference axes $0x_i$ and $0x_j$, respectively, the reference axes being simultaneously the axes of the symmetry of the orthorhombic material bulk sample and the principal axes of the initial plane stress σ^0_{ij}. This situation reduces Eqs. (4), (5) to the following simple relationships:

$$\begin{aligned} \overline{C}_{11} &= V^2_{11} - \overline{\sigma}^0_{11}\,, \qquad \overline{C}_{22} = V^2_{22} - \overline{\sigma}^0_{22}\,, \qquad \overline{C}_{33} = V^2_{33}\,, \\ \overline{C}_{44} &= V^2_{23} - \overline{\sigma}^0_{22} = V^2_{32}\,, \qquad \overline{C}_{55} = V^2_{13} - \overline{\sigma}^0_{11} = V^2_{31}\,, \qquad \overline{C}_{66} = V^2_{12} - \overline{\sigma}^0_{11}\,. \end{aligned} \tag{7}$$

Hence,

$$\overline{\sigma}^0_{22} = V^2_{23} - V^2_{32}\,, \qquad \overline{\sigma}^0_{11} = V^2_{13} - V^2_{31}\,, \qquad \overline{C}_{11} = V^2_{11} + V^2_{31} + V^2_{31} - V^2_{13}\,, \tag{8}$$

an so on.

Therefore, if the values of the eight ultrasonic velocities V_{11}, V_{22}, V_{33}, V_{12}, V_{13}, V_{23}, V_{31}, V_{32} (see Table 1) are known, the two principal stress components, σ^0_{11} and σ^0_{22}, as well as the effective material parameters $\overline{C}_{11}$, $\overline{C}_{22}$, $\overline{C}_{33}$, $\overline{C}_{44}$, $\overline{C}_{55}$, and $\overline{C}_{66}$ can be evaluated immediately from Eqs. (7), (8) but the values of the other effective material parameters ($\overline{C}_{12}, \overline{C}_{13}, \overline{C}_{23}, \overline{C}_{22}$ and $\overline{C}_{66}$) remain unattainable.

Table 1.

Input data [10^5 cm s^{-1}]								
N	V_{11}	V_{22}	V_{33}	V_{12}	V_{13}	V_{23}	V_{31}	V_{32}
1	5.93552	5.91855	5.87884	3.15212	3.22559	3.25662	3.22559	3.25662
2	5.93553	5.91855	5.87883	3.15214	3.22560	3.25661	3.22557	3.25659
3	5.93553	5.91855	5.87883	3.15217	3.22561	3.25659	3.22555	3.25656
4	5.93553	5.91857	5.87883	3.15237	3.22574	3.25644	3.22545	3.25630
5	5.93552	5.91860	5.87883	3.15262	3.22589	3.25624	3.22531	3.25596
6	5.93552	5.91862	5.87883	3.15288	3.22602	3.25605	3.22515	3.25563
7	5.93553	5.91864	5.87883	3.15312	3.22617	3.25586	3.22501	3.25530
8	5.93552	5.91877	5.87883	3.15465	3.22704	3.25472	3.22414	3.25332
9	5.93836	5.91999	5.87883	3.15796	3.23111	3.25280	3.22269	3.25000

Among the material parameters $\overline{C}_{11}$, $\overline{C}_{22}$, $\overline{C}_{33}$, $\overline{C}_{44}$, $\overline{C}_{55}$, and $\overline{C}_{66}$ involved in Eqs. (7), (8) only $\overline{C}_{33}$ can not be presented in the form of $\overline{C}_{ii} = V^2_{jk} - \overline{\sigma}^0_{mm}$ ($i = 1, 4, 5$; $j, k = 1, 2, 3$; $m = 1, 2$), but is of the form $\overline{C}_{ii} = V^2_{jk}$ only. Therefore, from all the material parameters $\overline{C}_{ii}$ involved in Eqs. (7) – (8) only $\overline{C}_{33}$ represents an entirely textural contribution to the material anisotropy, the other $\overline{C}_{ii}$ contributing to the material anisotropy due to the texture (preferred orientation of the grains) together with the initial stress σ^0_{ij}. However, in the situation where the initial stress is negligibly small or is absent, i.e., in the limiting case $\sigma^0_{ij} \to 0$, Eqs. (7) – (8) becomes a part of the system of equations describing the case when only the texture contributes considerably to the anisotropy of physical properties. This limiting case was discussed by LEWANDOWSKI in Ref. [9] where the full system of equations was outlined with utilizing some SAYERS's [3] results as well as some ultrasonic velocities were employed to predict either the texture $p(\xi, \varphi, \phi)$ in the maximum-entropy approximation and the values of some effective macroscopic parameters $\overline{C}_{ij}$ and the effective parameters $\overline{c}_{11}$, $\overline{c}_{12}$, and $\overline{c}_{44}$ of a single crystallite.

In the present paper similarly as in Ref. [9], we solve the problem of estimating the texture $p(\xi, \varphi, \phi)$ in the maximum-entropy approximation confining ourselves to inverting the averaging procedure of VOIGT [6] only. The Voigt procedure will be explained here as expressed by Eqs. (9), (10). The reason of confining ourselves in both papers to considering the case when the texture $p(\xi, \varphi, \phi)$ is estimated in the maximum-entropy approximation with using the Voigt averaging procedure only is as follows: Earlier in Ref. [8], LEWANDOWSKI compared the results of seeking the maximum-entropy estimate of the function $p(\xi, \varphi, \phi)$ for orthorhombic texture by employing in the long-wavelength approximation, the results being obtained with inverting successively the averaging procedures of VOIGT [6], REUSS [12] and HILL [13]. Moreover, the results were obtained under the assumptions that three respectively chosen velocities, V_{ij}, had been measured

and the single-crystal material parameters, c_{11}, c_{12}, c_{44} and ρ were known and did not vary (ideal polycrystalline aggregate approximation) with varying texture (due to plastic deformation). After finding the function $p(\xi, \varphi, \phi)$ from the three known ultrasonic velocities, the other six velocities, V_{ij} $(i = 1, 2, 3)$, were successively determined for each applied averaging procedure in the following two ways: from the orthorhombic symmetry conditions and by employing the maximum-entropy estimate of the function $p(\xi, \varphi, \phi)$. Next the results of calculating these velocities from both the symmetry conditions and the function $p(\xi, \varphi, \phi)$ were successively compared with each other in pairs, for each applied averaging procedure, to verify the proposed method of finding the maximum-entropy estimate of the function $p(\xi, \varphi, \phi)$ from the ultrasonic measurements. In these tests, only the velocities in each pair, in which one of the velocities was deduced from the analysis with inverting the Voigt averaging procedure, fitted the same values. This agreement in values in velocity pairs shows that the analysis with inverting the Voigt averaging procedure yields such a maximum-entropy function, $p(\xi, \varphi, \phi)$, which implies the same anisotropy of the dynamic (and propagation) properties of the polycrystalline aggregate under consideration as that deduced from the observed ultrasonic velocities by employing the othorhombic-symmetry rules. In other words, if the three respective velocities, V_{ij}, fit the measurements performed on an ideal polycrystalline aggregate with orthorhombic symmetry of the effective dynamic properties and if the maximum-entropy estimate of the function $p(\xi, \varphi, \phi)$ is deduced from this three V_{ij} by the analysis with inverting the Voigt averaging procedure, then the values of the other six velocities, V_{ij}, of ultrasonic waves propagating and polarized along the principal directions, which are calculated from the function $p(\xi, \varphi, \phi)$, also fit the respective measurements performed on the same material. As was mentioned above, in the present, paper similarly as in Ref. [9], this conclusion is the reason to confine ourselves to considering only the case when the maximum-entropy estimate of function $p(\xi, \varphi, \phi)$ is deduced by inverting the Voigt averaging procedure. In Ref. [9] was presented an approach which enables us to determine simultaneously for the limiting case $\sigma_{ij}^0 \to 0$ the effective stiffness dynamic moduli of a single grain in orthorhombically deformed steel, c_{11}^{eff}, c_{12}^{eff} and c_{44}^{eff}, some effective (overall) stiffness dynamic moduli, C_{ij}^{eff}, of the bulk sample under examination and its $p(\xi, \varphi, \phi)$, all the quantities being estimated from the measurements of ultrasonic velocities.

The algorithm of the presented numerical analysis starts with Eqs. (7), (8) which define some effective macroscopic parameters, $\overline{C}ij$, as functions of V_{ij} and $\overline{\sigma}_{i,j}^0$, c_{11}, c_{12}, c_{44}. Let us remind that, the Voigt procedure of averaging the single-crystal elastic moduli, c_{11}, c_{12}, c_{44}, enables us to evaluate the effective elastic moduli, C_{ij}^{eff}, of a bulk sample of the considered polycrystalline aggregate, the evaluation being performed under the assumption of the uniformity of strains ε_{ij} across the crystallite boundaries, i.e., under assumption that all grains are subjected to the same strain. This assumption arrives us at the following equations enabling us to calculate $\overline{C}_{ij} = c_{ij}^{\text{eff}}/\rho$:

$$\begin{aligned} \overline{C}_{ijkl} &= \langle T_{mnpq} \rangle (c_{mnpq}/\rho), \qquad T_{mnpq} = t_{im} t_{jn} t_{kp} t_{lq}\,, \\ \langle T_{mnpq} \rangle &= \int_{-1}^{1} d\xi \int_{0}^{2\pi} d\varphi \int_{0}^{2\pi} d\phi \; T_{mnpq} p(\xi, \varphi, \phi), \end{aligned} \tag{9}$$

where t_{im} denote components of the transformation matrix $\mathbf{t}(\xi, \varphi, \phi)$ which appears in the following rule of the coordinate transformation from X_j to x_i:

$$x_i = t_{ji} X_j \,. \tag{10}$$

The solutions of the Christoffel equations for an orthorhombically textured solid, which are obtained with applying the Voigt approximation (averaging procedure) to the calculation of the effective stiffness moduli of an ideal polycrystalline aggregate, are listed in Ref. [3] as formulae (10) – (21). It should perhaps be stressed that the values of the dynamic stiffness moduli c_{11}, c_{12}, c_{44} and density ρ of a single grain (crystal), were considered in [3, 8] for a deformed and textured steel as being equal to the values of c_{11}, c_{12}, c_{44} and ρ, which had been determined for a single-crystal of pure Fe with using a statical method. It is not to be expected that such an approximation, which can be called the long-wavelength and ideal Fe crystal approximation, would be always acceptable for steel, which is a polycrystalline aggregate of Fe with impurities and structure defects.

Herein is presented the next stage of the modification of seeking a complex solution to the problem of finding simultaneously c_{11}^{eff}, c_{12}^{eff} and c_{44}^{eff}, some effective stiffness dynamic moduli C_{ij}^{eff} of a prestressed orthorhombic polycrystalline aggregate, the initial stress σ_{ij}^0, and $p(\xi, \varphi, \phi)$ from the measurements of ultrasonic velocities. In the present paper, we are estimating numerically the solution to this problem in the situation where the stress σ_{ij}^0 increases from zero to a finite value. We do that in the two following ways: first, in the limiting case $\sigma_{ij}^0 \to 0$, by utilizing the approximation of small initial plane stress developed in Ref. [8, 9] and secondly, by making the use of Eqs. (7), (8) when σ_{ij}^0 is different from zero. While sketching out the main points of the enlarged numerical analysis of these problems, which is based on Eqs. (7), (8), only the concepts, definitions and equations required for following the considerations will be reiterated herein after [8, 9].

Therefore, analysing the first case when the initial stress $\sigma_{ij}^0 \to 0$, we utilize the approach proposed in Ref. [9] in seeking $p(\xi, \varphi, \phi)$ as well as c_{11}^{eff}, c_{12}^{eff}, c_{44}^{eff}, and some moduli C_{ij}^{eff}. Let us remind that in this approach [9], using [3, formulae (10) – (21)], which had been deduced from the definitions given by Eqs. (9), we arrived at the following equations [9, Eqs. (5) – (10)], after algebraic manipulation:

$$\langle r_1(\xi, \varphi, \phi) \rangle = \frac{1}{2\overline{c}} \left(\overline{c}_{11} - V_{11}^2 \right), \qquad \overline{c} = \overline{c}_{11} - \overline{c}_{12} - 2\overline{c}_{44} \,, \tag{11}$$

$$\langle r_2(\xi, \varphi, \phi) \rangle = \frac{1}{2\overline{c}} \left(\overline{c}_{11} - V_{22}^2 \right), \tag{12}$$

$$\langle r_3(\xi, \varphi, \phi) \rangle = \frac{1}{2\overline{c}} \left(\overline{c}_{11} - V_{33}^2 \right), \tag{13}$$

$$\langle r_4(\xi, \varphi, \phi) \rangle = \frac{1}{\overline{c}} \left(V_{23}^2 - \overline{c}_{44} \right), \tag{14}$$

$$\langle r_5(\xi, \varphi, \phi) \rangle = \frac{1}{\overline{c}} \left(V_{31}^2 - \overline{c}_{44} \right), \tag{15}$$

$$\langle r_6(\xi, \varphi, \phi) \rangle = \frac{1}{\overline{c}} \left(V_{12}^2 - \overline{c}_{44} \right), \tag{16}$$

where

$$r_4 = r_3 + r_2 - r_1 \,, \qquad r_5 = 2(r_1 - r_2) + r_4 \,, \qquad r_6 = 2r_1 - r_5 \,, \tag{17}$$

$$\begin{aligned} r_1 &= l_1^2 l_2^2 + l_1^2 l_3^2 + l_2^2 l_3^2\,, \qquad r_2 = m_1^2 m_2^2 + m_1^2 m_3^2 + m_2^2 m_3^2\,, \\ r_3 &= n_1^2 n_2^2 + n_1^2 n_3^2 + n_2^2 n_3^2\,, \\ l_i &= \mathbf{E}_i \cdot \mathbf{e}_1\,, \qquad m_i = \mathbf{E}_i \cdot \mathbf{e}_2\,, \qquad n_i = \mathbf{E}_i \cdot \mathbf{e}_3\,. \end{aligned} \tag{18}$$

The abbreviations $\langle r_q \rangle$, $q = 1, 2, ..., 6$, in Eqs. (11) – (16) denote averaging the functions $r_q(\theta, \varphi, \phi)$ of a single-crystal orientation defined earlier, the averaging being performed over all the crystallites in the sample, i.e. $\langle r_q(\theta, \varphi, \phi) \rangle$ is $r_q(\theta, \varphi, \phi)$ weighted by $p(\theta, \varphi, \phi)$:

$$\langle r_q(\xi, \varphi, \phi) \rangle = \int_0^{2\pi} \int_0^{2\pi} \int_{-1}^{1} r_q(\xi, \varphi, \phi) p(\xi, \varphi, \phi) d\xi \, d\varphi \, d\phi. \tag{19}$$

The probability density function $p(\xi, \varphi, \phi)$ fulfils the normalization condition

$$\langle p(\xi, \varphi, \phi) \rangle \doteq \int_0^{2\pi} \int_0^{2\pi} \int_{-1}^{1} p(\xi, \varphi, \phi) d\xi \, d\varphi \, d\phi = 1. \tag{20}$$

It should perhaps be emphasized that each left-hand side of the six equations (5) – (10) is of the form of an expectation value of one of the six known functions, $r_q(\xi, \varphi, \phi)$, of a single-crystal orientation. From these six functions, only three functions $r_q(\xi, \varphi, \phi)$ are linearly independent of each other. Each right-hand side of the six equations (5) – (10) is of the form of a known function of an ultrasonic velocity, V_{ij}, and single-crystal effective material parameters $\bar{c}_{11}$, $\bar{c}_{12}$, $\bar{c}_{44}$ defined by Eqs. (1). It can be easily seen from Eqs. (11) – (16) that each of such three velocities V_{ij}, which satisfies the rule that each of the numbers 1, 2 and 3 appear as subscripts i and/or j at no more than two velocities (e.g., V_{11}, V_{33}, and V_{31}) is involved in a formula determining the value of only one expectation value, $\langle r_q(\xi, \varphi, \phi) \rangle$, the three expectation values being linearly independent of each other. For this reason, the measurements of V_{11}, V_{33}, and V_{31} were in Ref. [8] sufficient for the probability density function $p(\xi, \varphi, \phi)$ to be *fully* estimated for aggregates with orthorhombic symmetry with known $\bar{c}_{11}$, $\bar{c}_{12}$, $\bar{c}_{44}$, and $\sigma_{ij}^0 = 0$. Essentially, then the probability density function $p(\xi, \varphi, \phi)$ implied by the JAYNES' [7] principle of maximum Shannon entropy is given in terms used in Eqs. (11) – (16) by the following expression:

$$p(\xi, \varphi, \phi) = \frac{1}{Z} \exp\left[-L_1 r_1(\xi, \varphi, \phi) - L_3 r_3(\xi, \varphi, \phi) - L_5 r_5(\xi, \varphi, \phi)\right], \tag{21}$$

where the partition function Z and the Lagrangian multipliers L_1, L_3 and L_5 are to be determined from Eqs. (11), (13), (15) and the normalization condition (20).

In Ref. [9], which concerns non-prestressed ($\sigma_{ij}^0 = 0$) aggregates with orthorhombic symmetry, the system of equations (11) – (18) was used for estimating in the maximum entropy approximation the probability density function $p(\xi, \varphi, \phi)$, unknown material parameters $\bar{c}_{11}$, $\bar{c}_{12}$, $\bar{c}_{44}$, and some $\overline{C}_{ij}$. The problem was solved in two steps for the case when the same three ultrasonic velocities V_{11}, V_{33}, V_{31} and additionally one of the velocities V_{22}, V_{23} and V_{12} are known. In the first step, the analytical form of the probability density function $p(\xi, \varphi, \phi)$ was deduced from the observables V_{11}, V_{33} and V_{31} by utilizing the JAYNES' [7] principle of maximum Shannon entropy. Consequently, the analytical

form of $p(\xi,\varphi,\phi)$ in [9] also is given by Eq. (21) but with the partition function Z and the Lagrangian multipliers L_1, L_3 and L_5, which are to be found in the second step together with the material parameters $\overline{c}_{11}$, $\overline{c}_{12}$ and $\overline{c}_{44}$, from the seven equations (11) – (16), (20) with employing the orthorhombic symmetry rules and the values of the ultrasonic velocities V_{11}, V_{33}, V_{31}, and an additional one, say, V_{23}. Since the system of equations (11) – (16), (20) for the quantities Z, L_1, L_3, L_5, $\overline{c}_{11}$, $\overline{c}_{12}$ and $\overline{c}_{44}$, which results from formulating the variational problem for the conditional maximum of missing information and inverting the Voigt averaging procedure, describes very complicated dependencies of these quantities on each other, a direct solution of the task is not available and a tedious numerical method is required to be used. A more detailed description of the operations of the program evaluating Z, L_1, L_3, L_5, $\overline{c}_{11}$, $\overline{c}_{12}$ and $\overline{c}_{44}$ was presented in Ref. [9]. To avoid making the paper even longer, any detailed description of the numerical method will not be reiterated herein after [9], although it should be stressed that the approach proposed in Ref. [9] is considered here as a suitable one only in the case when the initial stress, σ^0_{ij}, is small, i.e., in accordance with Eqs. (8), when

$$\mathrm{DABS}\left(\left(V^2_{ij}-V^2_{ji}\right)/\mathrm{DMIN}\,1\left(V^2_{ij},V^2_{ji}\right)\right)\ll 1, \qquad i,j=1,2,3, \quad i\neq j. \tag{22}$$

The nomenclature introduced in Eq. (22) is as follows: DABS denotes the FORTRAN 77 intrisinc function that returns the absolute value of its argument, DMIN1 is another FORTRAN 77 intrisinc function which returns the minimum value in the argument list. The smaller are the components of the initial stress, σ^0_{ij}, the better is the approximation of the texture of a prestressed polycrystalline obtained by using the approach proposed in Ref. [9].

In this paper, the proposed method of estimating the textural contribution to the orthorhombic acoustic anisotropy of prestressed polycrystalline aggregates ($\sigma^0_{ij}\neq 0$) is based on Eqs. (7), (8). On inserting Eqs. (9), (10) into Eqs. (7), (8), we arrive at the following system of equations, after employing [3, formulae (10) – (21)] and algebraic manipulation:

$$\langle r_1(\xi,\varphi,\phi)\rangle = \frac{1}{2\overline{c}}\left(\overline{c}_{11}-H_{11}\right), \qquad H_{11}=V^2_{11}+V^2_{31}-V^2_{13}, \tag{23}$$

$$\langle r_2(\xi,\varphi,\phi)\rangle = \frac{1}{2\overline{c}}\left(\overline{c}_{11}-H_{22}\right), \qquad H_{22}=V^2_{22}+V^2_{32}-V^2_{23}, \tag{24}$$

$$\langle r_3(\xi,\varphi,\phi)\rangle = \frac{1}{2\overline{c}}\left(\overline{c}_{11}-V^2_{33}\right), \tag{25}$$

$$\langle r_4(\xi,\varphi,\phi)\rangle = \frac{1}{\overline{c}}\left(V^2_{32}-\overline{c}_{44}\right), \tag{26}$$

$$\langle r_5(\xi,\varphi,\phi)\rangle = \frac{1}{\overline{c}}\left(V^2_{31}-\overline{c}_{44}\right), \tag{27}$$

$$\langle r_6(\xi,\varphi,\phi)\rangle = \frac{1}{\overline{c}}\left(H^2_{12}-\overline{c}_{44}\right), \qquad H_{12}=V^2_{12}+V^2_{31}-V^2_{13}. \tag{28}$$

Equations (23) – (28), (20) are the reliable basis for the maximum-entropy estimate of the orthorhombic texture of the prestressed polycrystalline aggregate from the measurements of the propagation velocities V_{ij} $(i,j=1,2,3)$ of the ultrasonic plane and linearly

polarized waves. This method consists in finding in two stages the maximum-entropy estimation of the probability density function $p(\xi, \varphi, \phi)$. Similarly to Eqs. (11) – (16), each left-hand side of Eqs. (23) – (28) is of the form of the expectation value of one of the functions $r_i(\xi, \varphi, \phi)$, $i = 1$ to 6, weighted with $p(\xi, \varphi, \phi)$, and each right-hand side of these equations is of the form of a known function of some quantities belonging to the set of the following five quantities: an ultrasonic velocity, V_{ij}, three material parameters $\bar{c}_{11}$, $\bar{c}_{12}$, $\bar{c}_{44}$ and the two (σ^0_{11} and σ^0_{22}) non vanishing components of the initial plane stress, σ^0_{ij}. From the system of Eqs. (23) – (28), (20), it can immediately be seen which of the nine ultrasonic velocities V_{ij} $(i, j = 1, 2, 3)$ should be known from the measurements for each situation under consideration. On performing the respective measurements, the two (σ^0_{11} and σ^0_{22}) non-vanishing components of the initial plane stress can be evaluated directly from Eqs. (8). The analytical form of the function $p(\xi, \varphi, \phi)$ can be determined from a system of three equations obtained by reducing the system of six equations (23) – (28) to that with three functions $r_i(\xi, \varphi, \phi)$, which are linearly independent of each other. Then the analytical form of $p(\xi, \varphi, \phi)$ can be determined from such a system of three equations by inverting in the maximum-entropy approximation the Voigt averaging procedure, which was assumed to be suitable for calculating the expectation values involved in Eqs. (23) – (28). For example, if $r_1(\xi, \varphi, \phi)$, $r_3(\xi, \varphi, \phi)$, and $r_5(\xi, \varphi, \phi)$ are chosen as the three independent of each other functions $r_i(\xi, \varphi, \phi)$, then the analytical form of the function $p(\xi, \varphi, \phi)$ is again given by Eq. (21). While the probability density function $p(\xi, \varphi, \phi)$ implied by the observables V_{11}, V_{33} and V_{31} and by the JAYNES' [7] principle of maximum Shannon entropy is also of the form given by Eq. (21) as in Ref. [9], now the partition function Z and the Lagrangian multipliers L_1, L_3 and L_5 are to be determined together with the unknown material parameters $\bar{c}_{11}$, $\bar{c}_{12}$ and $\bar{c}_{44}$ from Eqs. (23) – (28), (20), some of them being more complicated than their analogues in Ref. [9]. The increase in the complexity is due to the dependence of each of the seven unknown quantities Z, L_1, L_3, L_5, $\bar{c}_{11}$, $\bar{c}_{12}$ and $\bar{c}_{44}$ on both the texture $p(\xi, \varphi, \phi)$ and the initial plane stress $\sigma^0_{ij} = \{\sigma^0_{11}, \sigma^0_{22}\} \neq 0$.

4. Results of numerical analysis

In the subsequent numerical analysis, we seek the function $p(\xi, \varphi, \phi)$, material parameters $\bar{c}_{11}$, $\bar{c}_{12}$, $\bar{c}_{44}$, and some $\overline{C}_{ij}$ for a rolled steel plate. It is assumed that the values of the ultrasonic velocities presented in Table 1 were obtained from experiments. Moreover, it is assumed that the set of the values in each row was obtained in the same of the nine groups of measurements, each measurement of any group being performed on the same sample in the same state of the initial plane stress σ^0_{ij}. In accordance with Eqs. (7), (8), the values given in any row of Table 1 enable us to evaluate immediately the initial plane stress $\sigma^0_{ij} = \{\sigma^0_{11}, \sigma^0_{22}\} \neq 0$ and some material parameters, $\overline{C}_{11}$, $\overline{C}_{22}$, $\overline{C}_{33}$, $\overline{C}_{44}$, $\overline{C}_{55}$, and $\overline{C}_{66}$ of the prestressed body. After algebraic manipulation, the values given in any row of Table 1 lead us directly to that given in Table 2 in the row of the same number where the *Input data* are presented in the form suitable for inserting into Eqs. (23) – (28) in order to perform further calculations, with utilizing also Eq. (20). These calculations

are performed for the case when $r_1(\xi,\varphi,\phi)$, $r_3(\xi,\varphi,\phi)$, and $r_5(\xi,\varphi,\phi)$ are chosen as the three independent of each other functions $r_i(\xi,\varphi,\phi)$, i.e., when the analytical form of the function $p(\xi,\varphi,\phi)$ is given by Eq. (21). On inserting the values given in the respective row of Table 2 into Eqs. (23) – (28) and enclosing Eq. (20), we arrive at a system of nonlinear

Table 2.

Input data $[\mathrm{cm^2 s^{-2}}]$						
No	$H_{11}\cdot 10^{-11}$	$V_{33}^2\cdot 10^{-11}$	$V_{31}^2\cdot 10^{-11}$	$H_{22}\cdot 10^{-11}$	$V_{32}^2\cdot 10^{-11}$	$H_{12}\cdot 10^{-11}$
1	3.52304	3.45607	1.04044	3.50293	1.06056	0.993586
2	3.52303	3.45607	1.04043	3.50292	1.06054	0.993581
3	3.52301	3.45607	1.04042	3.50291	1.06052	0.993579
4	3.52286	3.45607	1.04035	3.50286	1.06035	0.993559
5	3.52267	3.45607	1.04026	3.50280	1.06013	0.993530
6	3.52248	3.45607	1.04016	3.50273	1.05991	0.993501
7	3.52230	3.45607	1.04007	3.50267	1.05970	0.993471
8	3.52117	3.45607	1.03951	3.50227	1.05841	0.993309
9	3.51930	3.45607	1.03857	3.50162	1.05625	0.993019

Table 3. Some results of numerical calculations.

No	L_1, L_3, L_5	$\overline{\sigma}_{11}\cdot 10^{-6}$ $[\mathrm{cm^2 s^{-2}}]$	$\overline{\sigma}_{22}/\overline{\sigma}_{11}$	Q_c	$q_{\min}\cdot 10^7$
1	$L_1 = -2.235763183772$ $L_3 = 1.0979886139440$ $L_5 = 0.5487668886877$	0.0	–	0.100859	3.184
2	$L_1 = -2.235960972127$ $L_3 = 1.0983295503730$ $L_5 = 0.5488253145014$	1.87084	0.4874	0.100992	4.879
3	$L_1 = -2.236795947828$ $L_3 = 1.0988891388090$ $L_5 = 0.5491093285845$	3.74168	0.4874	0.101234	4.879
4	$L_1 = -2.234641453048$ $L_3 = 1.1000725429550$ $L_5 = 0.5496786820460$	18.7084	0.4874	0.101991	4.892
5	$L_1 = -2.232686689108$ $L_3 = 1.1023022949130$ $L_5 = 0.5505769647418$	37.4169	0.4873	0.103102	2.746
6	$L_1 = -2.229401607267$ $L_3 = 1.1030163310740$ $L_5 = 0.5511099378546$	56.1252	0.4873	0.103932	4.894
7	$L_1 = -2.225893773403$ $L_3 = 1.1043245324470$ $L_5 = 0.5515539359085$	74.8337	0.4872	0.104756	4.871
8	$L_1 = -2.207377222687$ $L_3 = 1.111587495000$ $L_5 = 0.5551990370096$	187.84	0.4870	0.110156	4.875
9	$L_1 = -2.149780065096$ $L_3 = 1.104165497590$ $L_5 = 0.5570847777796$	374.168	0.4866	0.114811	4.880

equations of great complexity that are regarded by us as a reliable basis for evaluating numerically the partition function Z, the Lagrangian multipliers L_1, L_3, and L_5 together with the single-crystal effective material parameters $\overline{c}_{11}$, $\overline{c}_{12}$ and $\overline{c}_{44}$. Some of the results obtained by utilizing this algorithm are presented in Table 3, the others are presented in the forms of the diagrams in Figs. 1 – 10. All the numerical results are obtained for polycrystalline aggregate being under plane initial stress $\{\sigma^0_{11}, \sigma^0_{22}\}$ with the components $\sigma^0_{11} \geq 0$, $\sigma^0_{22} \simeq 0.487\sigma^0_{11}$ having successively the value of zero and eight different positive values.

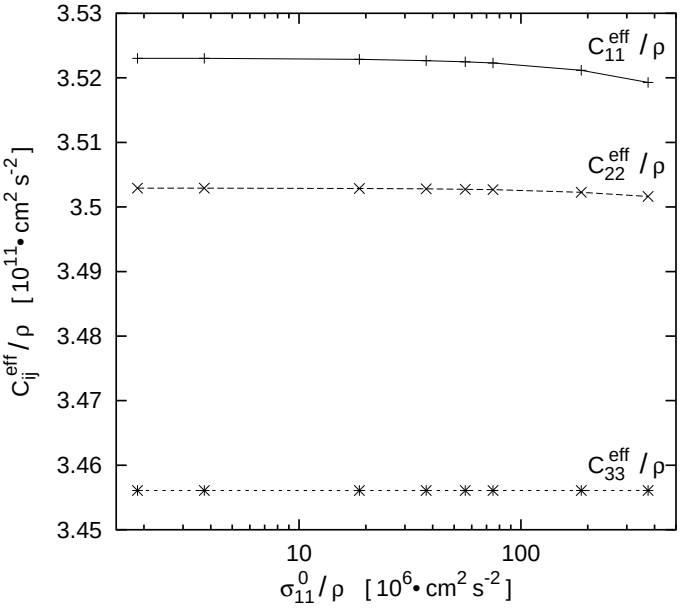

Fig. 1. C^{eff}_{11}/ρ, C^{eff}_{22}/ρ, and C^{eff}_{33}/ρ plotted against σ^0_{11}/ρ. On the horizontal (normalized initial stress σ^0_{11}/ρ) axis is set log scaling.

Solving the problem numerically, we have been encouraging in trying to do that by the implicit function theorem, which gives us only the hope, not certainty of satisfying seven nonlinear Eqs. (23) – (28), (20) in seven unknowns, Z, L_1, L_3, L_5, $\overline{c}_{11}$, $\overline{c}_{12}$ and $\overline{c}_{44}$, simultaneously. However, a set of nonlinear equations may have no (real) solutions at all or, contrariwise, it may have more than one solution, as it happens in each of the nine examples under consideration. In such nonlinear problems, solution finding invariably proceeds by iteration. Starting from some trial values of L_1, L_3, and L_5, a useful algorithm will improve the solution until some predetermined convergence criterions are satisfied, the solution being a set $\{Z, L_1, L_3, L_5, \overline{c}_{11}, \overline{c}_{12}, \overline{c}_{44}\}$. In order to have some check of the actual accuracy of calculation and the rate of convergence, a parameter Gm has been defined, the parameter Gm being a modification of that given in Ref. [9]:

$$Gm = \text{DMAX1}\,(G_{11}, G_{22}, G_{33}, G_{12}, G_{31}, G_{32}), \tag{29}$$

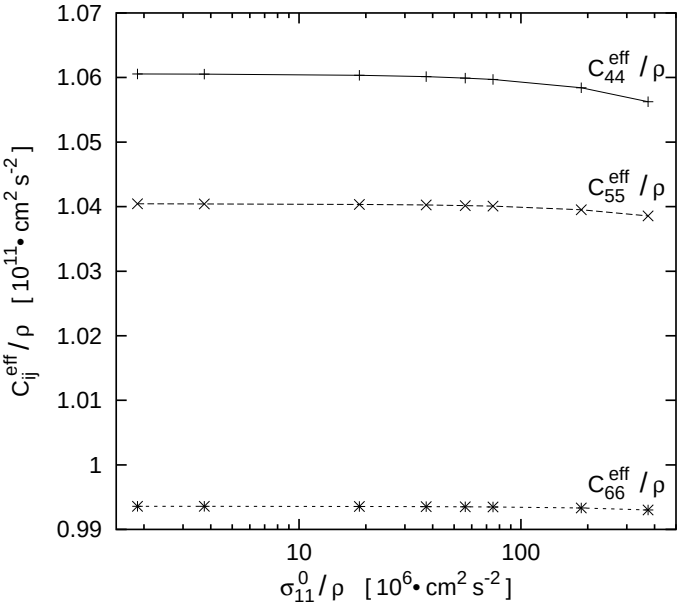

Fig. 2. C_{44}^{eff}/ρ, C_{55}^{eff}/ρ, and C_{66}^{eff}/ρ plotted against σ_{11}^0/ρ. On the horizontal (normalized initial stress σ_{11}^0/ρ) axis is set log scaling.

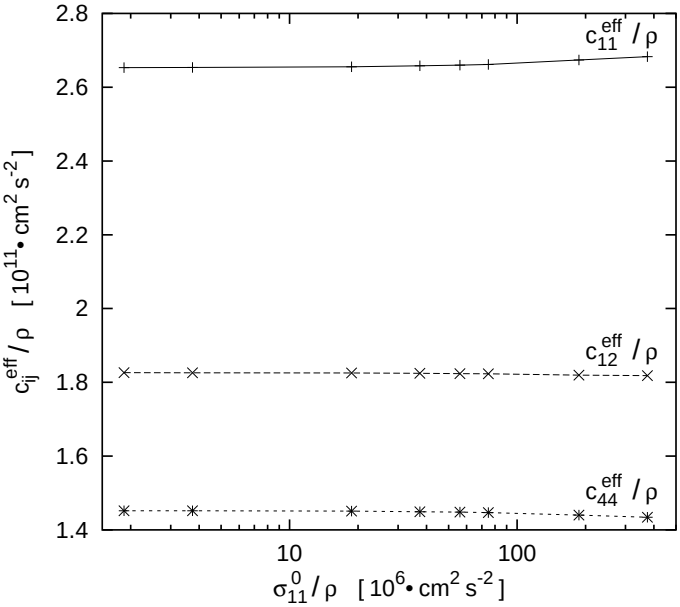

Fig. 3. c_{11}^{eff}/ρ, c_{12}^{eff}/ρ, and c_{44}^{eff}/ρ plotted against σ_{11}^0/ρ. On the horizontal (normalized initial stress σ_{11}^0/ρ) axis is set log scaling.

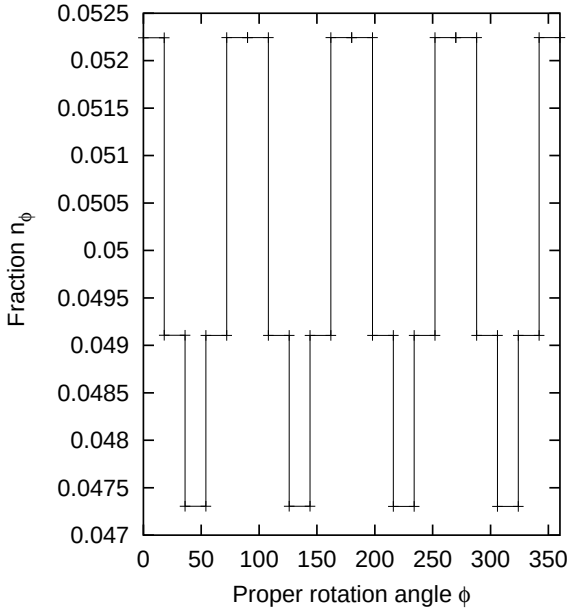

Fig. 4. Distribution of the particles $n_\phi(\phi_2, \phi_1)$ calculated from formula (34) for $\sigma^0_{11} = \sigma^0_{22} = 0$. The values of the angle of proper rotation (ϕ) are expressed in degrees.

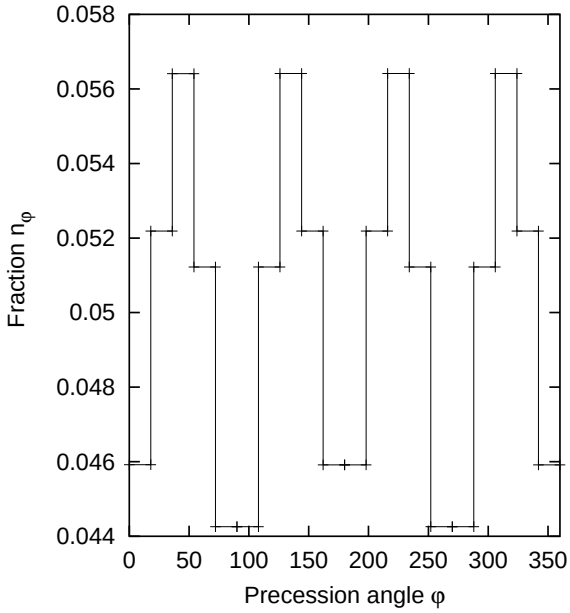

Fig. 5. Distribution of the particles $n_\varphi(\varphi_2, \varphi_1)$ calculated from formula (35) for $\sigma^0_{11} = \sigma^0_{22} = 0$. The values of the angle of precession (φ) are expressed in degrees.

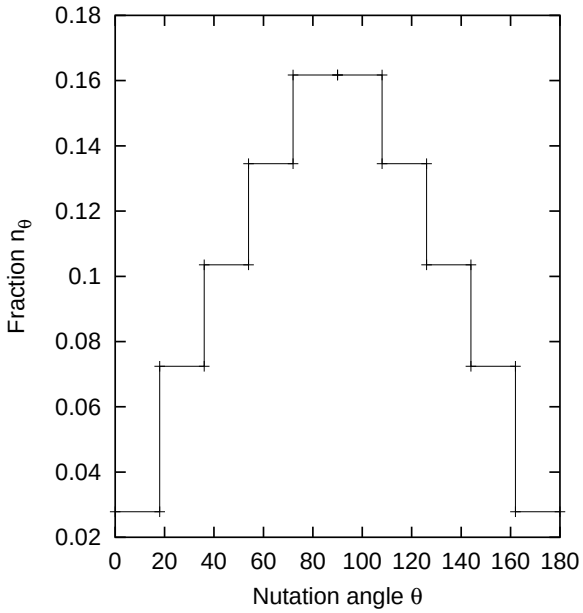

Fig. 6. Distribution of the particles $n_\theta(\theta_2, \theta_1)$ calculated from formula (36) for $\sigma^0_{11} = \sigma^0_{22} = 0$. The values of the angle of nutation (θ) are expressed in degrees.

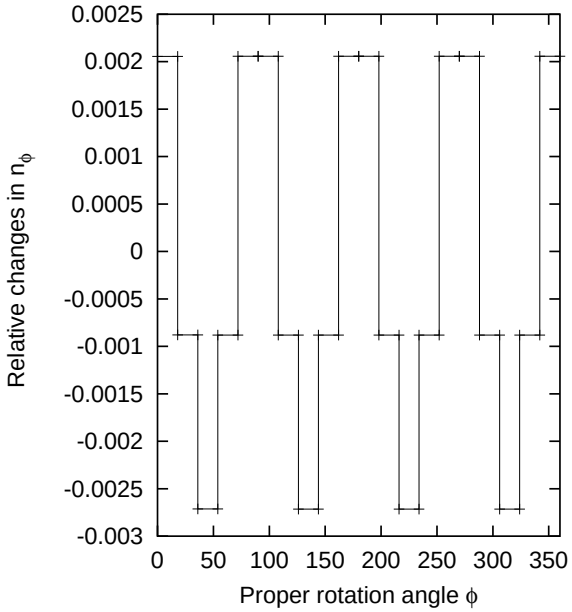

Fig. 7. The relative discrepancies between two histograms drawn for $n_\phi(\phi_2, \phi_1)$ at the limiting stresses: $\sigma^0_{11} = \sigma^0_{22} = 0$ and $\sigma^0_{11} = 3.74 \cdot 10^8\,\mathrm{cm^2 s^{-2}}$, $\sigma^0_{22} \simeq 0.487 \cdot \sigma^0_{11}$, the discrepancies being divided by the respective values of the histogram for $n_\phi(\phi_2, \phi_1)$ at $\sigma^0_{11} = \sigma^0_{22} = 0$. The values of the angle of nutation (ϕ) are expressed in degrees.

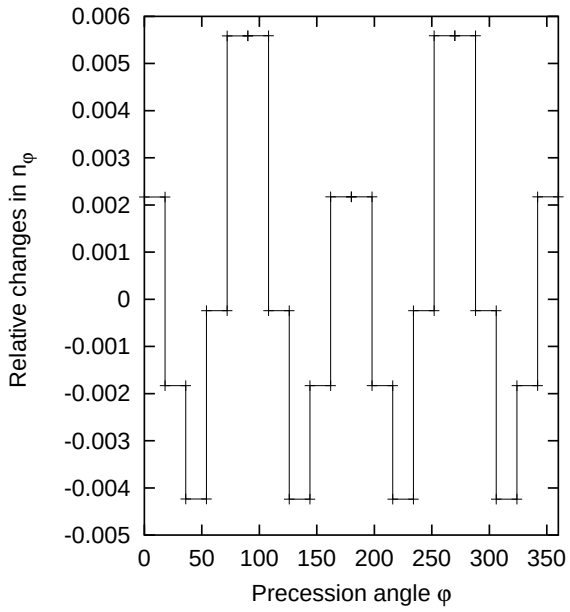

Fig. 8. The relative discrepancies between two histograms drawn for $n_{\varphi}(\varphi_2, \varphi_1)$ at the limiting stresses: $\sigma_{11}^0 = \sigma_{22}^0 = 0$ and $\sigma_{11}^0 = 3.74 \cdot 10^8\,\mathrm{cm^2 s^{-2}}$, $\sigma_{22}^0 \simeq 0.487 \cdot \sigma_{11}^0$, the discrepancies being divided by the respective values of the histogram for $n_{\varphi}(\varphi_2, \varphi_1)$ at $\sigma_{11}^0 = \sigma_{22}^0 = 0$. The values of the angle of nutation (φ) are expressed in degrees.

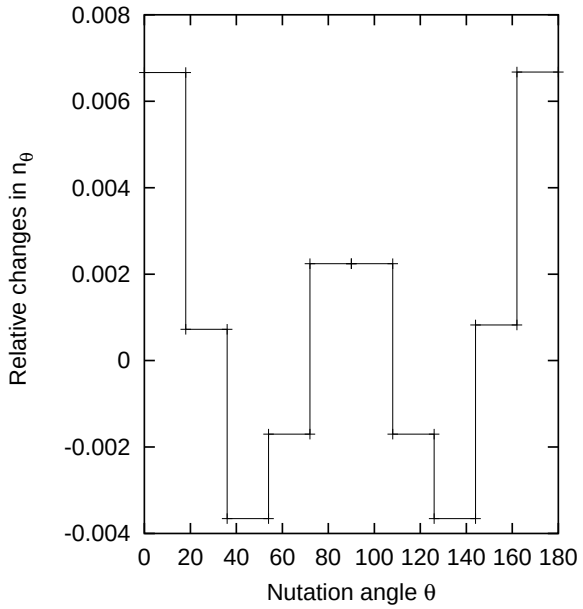

Fig. 9. The relative discrepancies between two histograms drawn for $n_{\theta}(\theta_2, \theta_1)$ at the limiting stresses: $\sigma_{11}^0 = \sigma_{22}^0 = 0$ and $\sigma_{11}^0 = 3.74 \cdot 10^8\,\mathrm{cm^2 s^{-2}}$, $\sigma_{22}^0 \simeq 0.487 \cdot \sigma_{11}^0$, the discrepancies being divided by the respective values of the histogram for $n_{\theta}(\theta_2, \theta_1)$ at $\sigma_{11}^0 = \sigma_{22}^0 = 0$. The values of the angle of nutation (θ) are expressed in degrees.

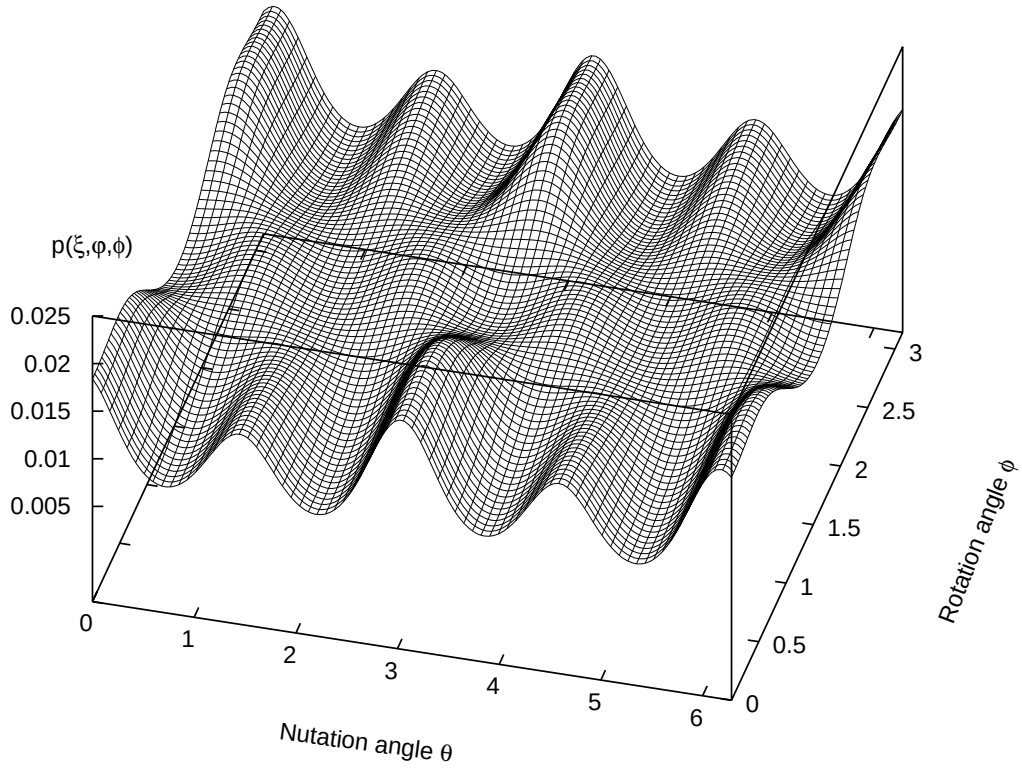

Fig. 10. Probability density function of the crystallite orientation, $p(\xi, \varphi, \phi)$, calculated together with c_{11}^{eff}, c_{12}^{eff}, and c_{44}^{eff} for the precession angle $\varphi = 0.3 \cdot \pi$ rad. The values of the angle of nutation (θ) and proper rotation (ϕ) are also expressed in radians.

where

$$
\begin{aligned}
G_{\alpha\beta} &= \text{DABS}\left[\left(H_{\alpha\beta}^{(\text{input})} - H_{\alpha\beta}^{(\text{deduced})}\right) / \text{DABS}\left(H_{\alpha\beta}^{(\text{input})}\right)\right], \quad \alpha\beta = 11, 12, 22, \\
G_{\gamma\delta} &= \text{DABS}\left[\left(H_{\gamma\delta}^{(\text{input})} - H_{\gamma\delta}^{(\text{deduced})}\right) / \text{DABS}\left(H_{\gamma\delta}^{(\text{input})}\right)\right], \\
H_{\gamma\delta}^{(\ldots)} &= \left(V_{\gamma\delta}^{(\ldots)}\right)^2, \qquad \gamma\delta = 31, 32, 33.
\end{aligned}
\tag{30}
$$

The superscripts (input) refers to the values of the quantities $H_{\alpha\beta}$, $H_{\gamma\delta}$ and $V_{\gamma\delta}^2$, which are given in the respective row of Table 2. As was mentioned, these values, which are the basis for determining (in the approximation of maximum Shannon entropy) the unknowns Z, L_1, L_3, L_5 (i.e., the function $p(\xi, \varphi, \phi)$) as well as $\overline{c}_{11}$, $\overline{c}_{12}$, $\overline{c}_{44}$, are regarded as experimental data (observables) obtained for the sample subjected to the initial plane stress σ_{ij}^0. Similarly, the superscripts (deduced) refer to the values of the quantities $H_{\alpha\beta}$ and $H_{\gamma\delta}$ which are deduced from Eqs. (23) – (28), (20), after inserting both the probability density function $p(\xi, \varphi, \phi)$ and the parameters $\overline{c}_{11}$, $\overline{c}_{12}$, $\overline{c}_{44}$ calculated from the observables in the former step. DMAX1 is the FORTRAN 77 intrisinc function, which

returns the maximum value in the argument list. The values of Gm for every set of input data, at which the respective iteration has been ended, are denoted by $q_{\min}$ and are listed in the sixth column of Table 3.

As was mentioned, each of the nine tasks of finding the unknowns Z, L_1, L_3, L_5, $\overline{c}_{11}$, $\overline{c}_{12}$ and $\overline{c}_{44}$ from Eqs. (23) – (28), (20) has more than one solution. This raises the need to provide a constructive criterion for making choice between numerous sets $\{Z, L_1, L_3, L_5, \overline{c}_{11}, \overline{c}_{12}, \overline{c}_{44}\}$ satisfying Eqs. (23) – (28), (20). Following Ref. [9], we make use herein of the criterion of the minimum value of the difference Q_c

$$Q_c = \mathrm{DMAX1}(Gc_{11}, Gc_{12}, Gc_{44}), \tag{31}$$

where

$$\begin{aligned} Gc_{ij} &= \mathrm{DABS}\left[\left(\overline{c}_{ij} - \overline{c}^0_{ij}\right)/\overline{c}^0_{ij}\right], \\ \overline{c}^0_{ij} &= c^0_{ij}/\rho^0, \qquad ij = 11, 12, 44. \end{aligned} \tag{32}$$

The values of the elastic stiffness moduli c^0_{11}, c^0_{12}, c^0_{44} and density ρ^0 of a single cubic crystal of the polycrystalline material (or a material as similar to that as possible) in the natural state (before deformation) are assumed to be known. Similarly as in Ref. [9], it is assumed that such a natural material for the rolled steel may be approximated by BCC Fe, which is characterized by the following values of $\overline{c}^0_{11}$, $\overline{c}^0_{12}$, and $\overline{c}^0_{44}$:

$$\begin{aligned} c^0_{11} &= 2.5982d + 07(m/s)^2, \\ c^0_{12} &= 1.6857d + 07(m/s)^2, \\ c^0_{44} &= 1.5843d + 07(m/s)^2. \end{aligned} \tag{33}$$

Now we formulate the criterion of minimum difference as the proposal of choosing this set of the values of Z, L_1, L_3, L_5, $\overline{c}_{11}$, $\overline{c}_{12}$, and $\overline{c}_{44}$ satisfying Eqs. (23) – (28), (20), which contains such values of the material parameters $\overline{c}_{11}$, $\overline{c}_{12}$, and $\overline{c}_{44}$ that lead to the minimum value of the difference parameter Q_c and simultaneously contains such values of Z, L_1, L_3, L_5 that lead to the probability density function $p(\xi, \varphi, \phi)$ achieving the maximum value of Shannon entropy. In each of the nine rows of the fifth column of Table 3, there is presented the value of the minimum difference Q_c corresponding to the solution $\{Z, L_1, L_3, L_5, \overline{c}_{11}, \overline{c}_{12}, \overline{c}_{44}\}$ of one of the nine examples under consideration. The first example concerns the situation where the material is not prestressed ($\sigma^0_{ij} = 0$). The full set $\{Z, L_1, L_3, L_5, \overline{c}_{11}, \overline{c}_{12}, \overline{c}_{44}\}$ for each of the nine examples (rows of Table 1) can be read in the following way: L_1, L_3, L_5 can be found in the respective row of the first column of Table 3, $\overline{c}_{11}$, $\overline{c}_{12}$, and $\overline{c}_{44}$ can be read out of Fig. 3 for each of the eight (No $= 2, 3, \ldots, 9$) prestressed states ($\sigma^0_{ij} \neq 0$) of the material. Since log scaling is set on the horizontal (normalized initial stress σ^0_{ij}/ρ) axis of each of Figs. 1 – 3, then the predicted values of material parameters $\overline{C}_{11}$, $\overline{C}_{22}$, $\overline{C}_{33}$, $\overline{C}_{44}$, $\overline{C}_{55}$, $\overline{C}_{66}$, $\overline{c}_{11}$, $\overline{c}_{12}$ and $\overline{c}_{44}$ of the non-prestressed body can not be indicated in Figs. 1 – 3. These values, expressed in $[10^{11}\,\mathrm{cm^2 s^{-2}}]$ units are as follows: 3.52304, 3.50293, 3.45607, 1.06056, 1.04044, 0.993586, 2.65267, 1.82618, 1.45220.

5. Discussion and conclusions

The data presented in the first column of Table 3 show the predicted changes in the values of the Lagrangian multipliers L_1, L_3 and L_5 with increasing stress components $\sigma_{11}^0 \geq 0$, $\sigma_{22}^0 \geq 0$ in the case when $\sigma_{22}^0/\sigma_{11}^0 \simeq 0.487$. For given L_1, L_3 and L_5, the partition function Z and, consequently, the function $p(\xi, \varphi, \phi)$ can also be regarded as a known quantity, since Z can be calculated immediately from the normalization condition (20). Therefore, the data presented in the first column of Table 3 enable us to estimate the influence of the increasing initial plane stress $\{\sigma_{11}^0, \sigma_{22}^0\}$ on the predicted texture of the polycrystalline aggregate under consideration. In order to visualize this effect, the quantities

$$n_\phi(\phi_2, \phi_1) \doteq \int_{\phi_1}^{\phi_2} \int_0^{2\pi} \int_{-1}^{1} p(\xi, \varphi, \phi)\, d\xi\, d\varphi\, d\phi, \tag{34}$$

$$n_\varphi(\varphi_2, \varphi_1) \doteq \int_0^{2\pi} \int_{\varphi_1}^{\varphi_2} \int_{-1}^{1} p(\xi, \varphi, \phi)\, d\xi\, d\varphi\, d\phi, \tag{35}$$

$$n_\theta(\theta_1, \theta_2) \doteq \int_0^{2\pi} \int_0^{2\pi} \int_{\xi_2}^{\xi_1} p(\xi, \varphi, \phi)\, d\xi\, d\varphi\, d\phi,$$

$$\theta_1 = \arccos \xi_1, \quad \theta_2 = \arccos \xi_2, \quad 0 \leq \theta_1 \leq \theta_2 \leq \pi \tag{36}$$

were calculated successively for L_1, L_3 and L_5 corresponding to the first and ninth sets $\{L_1, L_2, L_3\}$, which are written in the first and ninth rows of the first column of Table 3. The abbreviations, $n_\phi(\phi_2, \phi_1)$, $n_\varphi(\varphi_2, \varphi_1)$, and $n_\theta(\theta_2, \theta_1)$ denote the fractions of the total number of crystallites

(i) with the angle of proper rotation, ϕ, lying in the interval $\phi_1 \leq \phi \leq \phi_2$;

(ii) with the angle of precession, φ, lying in the interval $\varphi_1 \leq \phi \leq \varphi_2$, and

(iii) with the angle of nutation, θ, lying in the interval $\theta_1 \leq \theta \leq \theta_2$, respectively.

In Figs. 4 and 5, examples of numerical calculations of $n_\phi(\phi_2, \phi_1)$ and $n_\varphi(\varphi_2, \varphi_1)$, respectively, are presented for the case $\sigma_{11}^0 = \sigma_{22}^0$ with the whole domains $[0°, 360°]$ of the rotation angle ϕ and precession angle φ being divided into parts (subdomains) of equal size, 18°, with centres at $\phi = (\phi_1 - \phi_2)/2 = 9°, 27°, 45°, ..., 351°$ (Fig. 4) and at $\varphi = (\varphi_1 + \varphi_2)/2 = 9°, 27°, 45°, ..., 351°$ (Fig. 5). Similarly, in Fig. 6, an example of numerical calculations of $n_\theta(\theta_2, \theta_1)$ is presented for the same case $\sigma_{11}^0 = \sigma_{22}^0$ with the whole domain $[0°, 180°]$ of the nutation angle θ being divided into parts (subdomains) of equal size, 18°, with centres at $\theta = (\theta_1 + \theta_2)/2 = 9°, 27°, 45°, ..., 171°$. The crystallite fractions $n_\phi(\phi_2, \phi_1)$, $n_\varphi(\varphi_2, \varphi_1)$, and $n_\theta(\theta_2, \theta_1)$ were calculated separately for each subdomain and the results of these calculations are presented in the form of bar graphs (histograms) in Figs. 4–6. Results of numerical analysis show that the absolute values of the discrepancies between the elements of the histogram pairs, which correspond to the same subdomain of the same orientational angle ϕ, φ or θ but concern different initial stresses $\sigma_{11}^0 = \sigma_{22}^0 = 0$ or $\sigma_{11}^0 \neq 0$, $\sigma_{22}^0/\sigma_{11}^0 \simeq 0.487$, increases with increasing σ_{11}^0 (and σ_{22}^0). In this analysis,

$\overline{\sigma}^0_{11} = 3.74 \cdot 10^8\,\mathrm{cm^2 s^{-2}}$ and $\overline{\sigma}^0_{22} \simeq 0.487 \cdot \overline{\sigma}^0_{11}$ were the maximum values of the normalized plane stress $\{\overline{\sigma}^0_{11}, \overline{\sigma}^0_{22}\}$ under consideration. In Figs. 7–9, the values are presented of the relative discrepancies between elements of each of the three pairs of histograms $n_\phi(\phi_2, \phi_1)$, $n_\varphi(\varphi_2, \varphi_1)$, and $n_\theta(\theta_2, \theta_1)$, respectively, each of the histogram pairs being composed of two histograms for the same orientation angle ϕ, φ or θ and for the two limiting stresses: $\{\sigma^0_{11} = \sigma^0_{22} = 0\}$ and $\{\overline{\sigma}^0_{11} = 3.74 \cdot 10^8\,\mathrm{cm^2 s^{-2}}, \overline{\sigma}^0_{22} \simeq 0.487 \cdot \overline{\sigma}^0_{11}\}$. The relative discrepancy is defined for an angle subdomain as the ratio of the discrepancy in the subdomain between two histograms of the considered pair to the value of the histogram belonging to the same pair and concerning the case $\{\sigma^0_{11} = \sigma^0_{22} = 0\}$. The values of the relative discrepancies may be regarded as a measure of the effect of initial plane stress on the texture predicted by using the approach proposed in this paper. From Figs. 7–9 it can easily be seen that this effect for stress non greater than $\{\overline{\sigma}^0_{11} = 3.74 \cdot 10^8\,\mathrm{cm^2 s^{-2}}$, $\overline{\sigma}^0_{22} \simeq 0.487 \cdot \overline{\sigma}^0_{11}\}$ is revealed by the relative discrepancies smaller than 0.007 and therefore is negligibly small.

The increase of $\sigma^0_{ij} = \{\sigma^0_{11}, \sigma^0_{22}\} \neq 0$ also induces changes in the predicted normalized moduli $\overline{C}_{11}$, $\overline{C}_{22}$, $\overline{C}_{33}$, $\overline{C}_{44}$, $\overline{C}_{55}$, $\overline{C}_{66}$, $\overline{c}_{11}$, $\overline{c}_{12}$ and $\overline{c}_{44}$, which can be seen from Figs. 1–3. The maximum value of the relative changes in all the moduli (i.e., the changes in all the moduli divided by the values of the respective moduli of non-prestressed material) are smaller than 0.02, if $\overline{\sigma}^0_{11}$ increases from zero to about $374 \cdot 10^6\,\mathrm{cm^2 s^{-2}}$. For the steel of the density $\rho = 7.819\,\mathrm{g\,cm^{-3}}$, it denotes the changes in the value of σ^0_{11} lying in the interval from zero to about 292 MPa. This value is a typical one of residual stress in steel being plastically deformed (e.g., rolled). Hence we can conclude that for rolled steel the changes in the predicted values of the considered moduli, which are induced by the considered residual stress, are negligibly small.

References

[1] Tatsuo Tokuoka and Yukio Iwashimizu, *Acoustical birefringence of ultrasonic waves in deformed isotropic elastic materials*, Int. J. Solids Structures, **4**, 383–389 (1968).

[2] C.S. Man and W.Y. Lu, *Towards an acoustoelastic theory for measurement of residual stress*, Journal of Elasticity, **17**, 159–182 (1987).

[3] C.M. Sayers, *Ultrasonic velocities in anisotropic polycrystalline aggregates*, J. Phys.D: Appl. Phys., **15**, 2157–2167 (1982).

[4] R.B. Thomson, S.S. Lee and J.F. Smith, *Angular dependence of ultrasonic wave propagation in a stressed, orthorhombic continuum: Theory and application to the measurement of stress and texture*, J. Acoust. Soc. Am., **80**, 3, 921–931 (1986).

[5] A.D. Degtyar and S.I. Rokhlin, *Absolute stress determination in orthotropic materials from angular dependences of ultrasonic velocities*, J. Appl. Phys., **78**, 3, 1547–1556 (1995).

[6] W. Voigt, *Lehrbuch der Krystall Physik*, Teubner, Leipzig 1928.

[7] E.T. Jaynes, *Information theory and statistical mechanics*, Phys. Rev., **106**, 620–630 (1957).

[8] J. Lewandowski, *Maximum-entropy estimate of the orthorhombic texture from ultrasonic measurements*, Ultrasonics, 229–238 (1995).

[9] J. Lewandowski, *Determination of material parameters and texture of a polycrystalline aggregate from ultrasonic measurements*, NDT&E International, **32**, 383–396 (1999).

[10] E. Kroner, *Statistical continuum mechanics*, Lecture Notes, Springer, Berlin 1971.

[11] I. Ignberg, *Residual macrostresses in thin strip production*, [in:] Swedish Symposium on Residual Stresses, T. Ericsson, J. Bergstrom, I. Nyman [Eds.], March 30-April 2, 1987, 33–55.

[12] A. Reuss, Z. Angew: Math. Mech., **9**, 49, (1924).

[13] R.J. Hill, Mech. Phys. Solids, 5, 229 (1957).

ARCHIVES OF ACOUSTICS
26, 4, 331–349 (2001)

ESTIMATION OF LOCAL MATERIAL AND STRUCTURE PARAMETERS OF A POLYCRYSTALLINE AGGREGATE FROM ULTRASONIC MEASUREMENTS

J. LEWANDOWSKI, M. ADAMSKI and J. DEPUTAT

Polish Academy of Sciences
Institute of Fundamental Technological Research
(00-049 Warszawa, Świętokrzyska 21, Poland)

The propagation velocities of four ultrasonic waves in a steel plate are measured in twelve equally spaced observation points lying in a rolling plane on a straight line perpendicular to the rolling direction. The plate material was rolled plastically and uniaxially in the situation where the edges parallel to the rolling direction were free. The plate is considered to be a bulk sample with orthorhombic symmetry of bulk mechanical properties made of cubic crystals of the highest symmetry. The local probability density function of the crystallite orientation and the local effective stiffness moduli of a single grain (crystallite) are found from four ultrasonic velocities and the rules of orthorhombic symmetry and Jaynes' principle of maximum Shannon entropy. These results, which have been obtained for twelve mesodomains centered at each of the twelve observation points, show the effect of the distance between an observation point and a free plate edge on the local effective stiffness moduli and on the local probability density function of the crystallite orientation.

1. Introduction

In an isotropic polycrystalline material the ultrasonic velocities are independent of the direction of the ultrasonics' propagation through a macroscopic sample of the material. Most polycrystalline materials (e.g. metals) were acted on by forming forces, which caused plastic deformation, subjected the body to a state of stress or deformation and left the crystallites (basic units, grains) in certain preferred orientations. Consequently, the forces of the forming process caused anisotropy of the overall (effective) mechanical (amongst them acoustical) properties of the material. The non-random distribution of the crystallite orientation, which is caused by plastic deformation, is called the texture. Therefore, most polycrystalline materials exhibit texture resulting from their forming processes. The acoustical anisotropy is revealed by the variations in speeds at which ultrasonic waves propagate through the sample, the variations being dependent on the directions of the wave propagation and polarization. In numerous situations, the texture considerably contributes to the mechanical and acoustical anisotropy of the material.

Among the problems of forming the texture in metals during plastic deformation, there are mainly two fields of interest for both a fundamental and an applied researcher. The first is directed to the effect of roll forces, their geometry as well as another rolling

parameters and conditions on the texture. The second is concerned with the influence of the texture on the mechanical properties of rolled metal (e.g. steel). For example, for the application of structural steels in various fields of engineering, high strength, sufficient ductility and a good weldability as well as formability are often highly desired. Therefore, the changes in these steel properties during a plastic forming process (e.g. rolling) may be more exactly predicted as our knowledge of the problems belonging to these two fields becomes better.

In the paper, the considerations are confined to ultrasonic plane and linearly polarized waves which propagate in macroscopic pollycrystalline aggregates with orthorhombic symmetry of the bulk (effective) elastic properties, the aggregates being composed of a large number of cubic crystallites of the highest symmetry. The macroscopic orthorhombic symmetry is of considerable practical interest since the rolling process in one direction only of a polycrystalline aggregate with virgin (before deformation) isotropic symmetry always results in the transformation of the isotropic symmetry (or another one) into the othorhombic symmetry.

In the paper, there is presented a nondestructive ultrasonic method of the estimation of some local material parameters and the local texture of a steel plate which was rolled uniaxially in the situation where the edges parallel to the rolling direction were free. Thus in this paper, only such orientation statistics of the crystallites is considered which contributes to the orthorhombic symmetry of the dynamic properties of a bulk specimen of a polycrystalline aggregate made of cubic crystals of the highest symmetry. Using the approach proposed by LEWANDOWSKI in [2], we do not neglect the effect of other causes on the effective mechanical and ultrasonic propagation properties of the polycrystalline aggregate as well as on the macroscopic symmetry of these properties, since this approach is based on taking into account the fact that the values of measured velocities of the ultrasonic waves are determined not only by the structure and physical properties of the acoustical medium under examination but also by all these physical phenomena occurring in the medium which influence on the propagation. In other words, the measured velocities of ultrasonics, which are the basis for all calculations presented in the subsequent text, contain information on the structure and properties of the material, among other on the values of the dynamic single-crystal material parameters influenced on by the defects and imperfections of crystal microstructure, residual stress, scattering and the phenomena of mechanical energy dissipation.

2. Formulation of the problem

Although numerous ultrasonic investigations have been carried out in connection with the rolling process, quantitative information on the complete distributions both of some local mechanical properties of the plate material and the local texture in a plate undergoing rolling seems to be little. Among others here arises the question how strongly are the local mechanical properties and texture influenced on by the distance x between an observation point determined by the position vector $\mathbf{r}$ and one of the two plate edges parallel to the rolling direction, in the situation where these edges are free.

It should perhaps be emphasized that in this paper the term *local* concerns the use of three measuring scales, the smallest of which refers to a structural grain or crystallite of the material. For simplification of the analysis, an assumption is used as the first approximation of the internal contribution to the material response on an external (ultrasonic transducer) loading. In accordance with this assumption, the constitutive internal relations of a microelement (grain or crystallite) are describable by continuum laws, whilst the stress and displacement fields are described either in terms of random variables or stochastic processes depending on the loading and the material under investigation. All parameters concerned with the smallest region are prefixed by *micro*. Next an intermediary scale is introduced referred to as a *mesodomain* that contains a statistical ensemble of crystallites. A mesodomain is interpreted to be much smaller than the *macroscopic domain* of the entire material body (macroscopic sample), but is much larger than the domain of a microelement as containing a statistical ensemble of crystallites. In the subsequent text, the term *local* texture (properties) does not mean the texture (properties) in a point in the plate under study, which is determined by a position vector $\mathbf{r}$, but means the texture (properties) of the plate material filling a mesodomain geometrically centered at the point determined by the position vector $\mathbf{r}$. This point is called in the subsequent text the observation point.

In the paper, we are interested in some mechanical properties and the local texture of a steel plate of dimensions of $0.38\,\mathrm{m} \times 0.26\,\mathrm{m} \times 0.02\,\mathrm{m}$ which was rolled uniaxially in the situation where the edges parallel to the rolling direction were free. We are interested first in showing that it is possible to estimate from ultrasonic measurements the distribution of the local propagation (mechanical) properties and texture of the steel plate. Secondly, we are going to reveal the influence of the distance x between an observation point and the reference free edge on the the local values of effective material parameters and the local texture. For this reason, we are interested in deducing from the ultrasonics measurements the local values of effective material parameters of a crystallite as well as the distributions of the local texture in the plate in twelve equally spaced points (0.02 m apart) lying in rolling plane on a straight line perpendicular to the rolling direction. In this way, the measurements of the propagation velocities, V_{ij}, where $i, j = 1, 2, 3$, of ultrasonic plane waves propagating and polarized in the directions of the Cartesian reference axes $0x_i$ and $0x_j$, respectively, are the only experimental tools for texture investigations discussed in this paper. The Cartesian coordinate system $0x_1x_2x_3$ with the axes $0x_1$, $0x_2$ and $0x_3$ is defined below.

Among the reasonable choices of the reference system for analysing this problem is the Cartesian coordinate system $0x_1x_2x_3$ with the axes $0x_1$, $0x_2$ and $0x_3$ chosen as the rolling R, transverse (perpendicular to R in the rolling plane) T and normal (to the rolling plane) N directions, respectively. Let the abbreviations $\mathbf{e}_1$, $\mathbf{e}_2$ and $\mathbf{e}_3$ denote the unit vectors along the directions of the axes $0x_1$, $0x_2$ and $0x_3$, respectively. The Cartesian coordinate system $0x_1x_2x_3$ will be called the macroscopic reference system. To define the texture precisely, we also make use of a local Cartesian coordinate system $0X_1X_2X_3$ called the microscopic reference system. This reference system is defined, similarly as in Refs. [1, 2], for each single cubic crystallite. Its reference $0X_1$ axes, $0X_2$ and $0X_3$ are chosen in the crystallographic directions [100], [010] and [001], respectively. Let the

abbreviations $\mathbf{E}_1$, $\mathbf{E}_2$ and $\mathbf{E}_3$ denote the unit vectors along the directions of the axes $0X_1$, $0X_2$ and $0X_3$, respectively. In the subsequent considerations, the orientation of a crystallite in the polycrystalline sample is described by giving the values of three Eulerian angles θ, φ and ϕ where θ, φ and ϕ denote the Eulerian angles defined in this paper in the same way as in Ref. [3], i.e. θ is the angle of nutation, φ is the angle of precession and ϕ is the angle of proper rotation. In the paper, the texture is described by using the probability density function of the crystallite orientation, $p(\xi, \varphi, \phi)$, defined in such a way that $p(\xi, \varphi, \phi)\, d\xi\, d\varphi\, d\phi$ expresses the probability of a crystallite having an orientation described by the Euler angles $\theta = \cos^{-1}\xi$, φ and ϕ, lying in the intervals $\langle \cos^{-1}\xi, \cos^{-1}(\xi + d\xi)\rangle$, $\langle \varphi, \varphi + d\varphi\rangle$ and $\langle \phi, \phi + d\phi\rangle$, respectively.

Using the approach proposed by LEWANDOWSKI [2], we utilize the fact that the propagation properties of the polycrystal under examination, which are revealed by the results of ultrasonic measurements, contain information on the structure and properties of the components of the medium as well as on the phenomena occurring in the polycrystal and influencing on the propagation (e.g., scattering). It means that the dynamic mechanical and propagation properties (the values of the components of the effective stiffness tensor) of a single grain in the approach proposed in Ref. [2] and applied in this paper are taken to be "as they are" by letting the experimental data (ultrasonics wave velocities and the rules of orthorhombic symmetry) to determine the single-grain *effective* elastic properties and texture of the bulk sample under consideration. The respective numerical calculations are performed by using the equations which are derived and listed in Ref. [2, Eqs. (5), (7), (9), (15), (21) - (23)]. Starting from these equations, we find the function $p(\xi, \varphi, \phi)$ and obtain values of the components of the so-called *effective* stiffness tensor, $c_{ij}^{(\mathrm{eff})}$, $(i, j = 1, 2, 3)$, of a single grain of the polycrystalline aggregate under examination. The reasoning leading us to such results may be presented shortly as follows:

We start from the hypothesis that the propagation properties of the bulk specimen under examination are defined by the macroscopic tensor of the *effective* elastic stiffness, $C_{i,j}^{(\mathrm{eff})}$, of the sample (or, equivalently, elastic compliance tensor) and the effective density, ρ, the last being assumed in this paper to be equal to the density averaged over the volume of a single bulk sample. Let us remind that the symmetry of the effective elastic stiffness tensor of the bulk sample of the polycrystalline aggregate under examination, which is called in the subsequent text the macroscopic symmetry of the bulk sample, is orthorhombic in the situation where the material was plastically rolled in one direction. More strictly speaking, the term *effective properties* of the bulk sample is used to describe the physical properties of the so-called equivalent homogeneous medium [4] that exhibits the same macroscopic symmetry as the bulk sample under study, and the displacement response of the equivalent medium to the transducer loading is the same as the averaged displacement response of the polycrystalline material to the same loading, the averaging being carried out over a statistical ensemble of bulk samples, i.e. over all crystallites through the function $p(\xi, \varphi, \phi)$. Similar to the effective density, the effective elastic moduli are also independent of the position vector (space coordinates), but they are dependent on the frequency of the loading transducer. In contrast, the average displacement field resulting from the dynamic load is dependent on the position vector, $\mathbf{r}$, time, t, and

load (angular) frequency, ω, and, consequently, is called the effective displacement field or effective wave — especially, if is harmonically dependent on the position vector and time.

Knowing the effective properties of the sample under examination, we are able to estimate the dynamic response of the sample being acted on by ultrasonic transducer. In the case, when the response is of the form of ultrasonic plane waves propagating and polarized in the directions of the macroscopic Cartesian reference axes $0x_i$ and $0x_j$ $(i,j = 1,2,3)$, respectively, the propagation velocities, V_{ij}, of these waves can be calculated from the Christoffel equation [5]

$$\det\left(\Gamma^{ik} - \rho V_{gh}^2 \delta_{ik}\right) = 0, \qquad g,h,i,k = 1,2,3 \tag{1}$$

in which

$$\Gamma^{ik} = C_{ijkl}^{(\mathrm{eff})} \eta_j \eta_l \tag{2}$$

is the so-called "Christoffel-Kelvin stiffness", ρ stands for the mass density, and δ_{ik} is the Kronecker delta. In Eq. (2) the definition of Γ^{ik}, the components $C_{ijkl}^{(\mathrm{eff})}$ (effective sample stiffness moduli) of the stiffness tensor of the macroscopic sample are related to $C_{ij}^{(\mathrm{eff})}$ by using the reduced subscript notation. The abbreviations η_j and η_l denote the components of the unit vector in the direction of the wave propagation.

On the other hand, by using a suitable averaging procedure the effective sample stiffness moduli, $C_{ij}^{(\mathrm{eff})}$, can be calculated from the values of the dynamic stiffness moduli c_{11}, c_{12}, c_{44} of a single cubic grain (crystal), its density ρ, and from the probability density function of the crystallite orientation, $p(\xi,\varphi,\phi)$. There are numerous procedures to approximating the effective elastic constants, proposed by such authors as VOIGT [6], REUS [7] and HILL [8]. The solutions of the Christoffel equations (1) for an orthorhombically textured solid, which are obtained with applying the Voigt approximation (averaging procedure) to the calculation of the effective sample stiffness moduli, $C_{ij}^{(\mathrm{eff})}$, are listed in Ref. [9] as formulae (10) – (21). It should perhaps be emphasized that the values of the moduli c_{11}, c_{12}, c_{44} of a single cubic grain (crystal) were considered in Refs. [9, 1] for a deformed and textured steel as being equal to the values of c_{11}, c_{12}, c_{44} and ρ, which had been determined for a single-crystal of pure BCC Fe with using a statical method. It is not to be expected that such an approximation, which can be called the long-wavelength and ideal Fe crystal approximation, would be always acceptable for rolled steel, which is a polycrystalline aggregate of Fe with impurities and structure defects. For this reason, herein is used a modified approach proposed by LEWANDOWSKI in Ref. [2], in which the values of c_{11}, c_{12}, c_{44} are replaced by the so-called effective dynamic stiffness moduli of a single grain in deformed steel, $c_{11}^{(\mathrm{eff})}$, $c_{12}^{(\mathrm{eff})}$ and $c_{44}^{(\mathrm{eff})}$, the last being determined also from measured values of ultrasonic velocities. Using the SAYERS' solutions [9, formulae (10) – (21)], LEWANDOWSKI [2] arrived at the following equations, after a little algebra and manipulation

$$\begin{aligned} \langle r_1(\xi,\varphi,\phi)\rangle &= \frac{1}{2\overline{c}}\left(\overline{c}_{11} - V_{11}^2\right), \qquad \overline{c}_{11} = \frac{c_{11}^{(\mathrm{eff})}}{\rho}, \\ \overline{c} &= \frac{1}{\rho}\left(c_{11}^{(\mathrm{eff})} - c_{12}^{(\mathrm{eff})} - 2c_{44}^{(\mathrm{eff})}\right) \doteq \overline{c}_{11} - \overline{c}_{12} - 2\overline{c}_{44}\,; \end{aligned} \tag{3}$$

$$\langle r_2(\xi,\varphi,\phi)\rangle = \frac{1}{2\overline{c}}\left(\overline{c}_{11} - V_{22}^2\right), \tag{4}$$

$$\langle r_3(\xi,\varphi,\phi)\rangle = \frac{1}{2\overline{c}}\left(\overline{c}_{11} - V_{33}^2\right), \tag{5}$$

$$\langle r_4(\xi,\varphi,\phi)\rangle = \frac{1}{\overline{c}}\left(V_{23}^2 - \overline{c}_{44}\right), \qquad \overline{c}_{44} = \frac{c_{44}^{(\mathrm{eff})}}{\rho}, \tag{6}$$

$$\langle r_5(\xi,\varphi,\phi)\rangle = \frac{1}{\overline{c}}\left(V_{13}^2 - \overline{c}_{44}\right), \tag{7}$$

$$\langle r_6(\xi,\varphi,\phi)\rangle = \frac{1}{\overline{c}}\left(V_{12}^2 - \overline{c}_{44}\right), \tag{8}$$

where

$$\begin{aligned} V_{ij} &= V_{ji}\,, \\ V_{i1}^2 + V_{i2}^2 + V_{i3}^3 &= V_{1j}^2 + V_{2j}^2 + V_{3j}^2 = \overline{c}_a\,, \\ \overline{c}_a &= \frac{1}{\rho}\left(c_{11}^{(\mathrm{eff})} + 2c_{44}^{(\mathrm{eff})}\right), \end{aligned} \tag{9}$$

$$r_4 = r_3 + r_2 - r_1\,, \qquad r_5 = 2(r_1 - r_2) + r_4\,, \qquad r_6 = 2r_1 - r_5\,, \tag{10}$$

$$\begin{aligned} r_1 &= l_1^2 l_2^2 + l_1^2 l_3^2 + l_2^2 l_3^2\,, \\ r_2 &= m_1^2 m_2^2 + m_1^2 m_3^2 + m_2^2 m_3^2\,, \\ r_3 &= n_1^2 n_2^2 + n_1^2 n_3^2 + n_2^2 n_3^2\,, \end{aligned} \tag{11}$$

$$l_i = E_i e_1\,, \qquad m_i = E_i e_2\,, \qquad n_i = E_i e_3. \tag{12}$$

The abbreviations $\langle r_q\rangle$, $q = 1, 2, ..., 6$, in Eqs. (3) – (8) denote averaging the above defined functions of a single-crystal orientation, $r_q(\theta,\varphi,\phi)$, over all the crystallites in the sample, i.e. $\langle r_q(\theta,\varphi,\phi)\rangle$ is $r_q(\theta,\varphi,\phi)$ weighted by $p(\theta,\varphi,\phi)$:

$$\langle r_q(\xi,\varphi,\phi)\rangle = \int_0^{2\pi}\int_0^{2\pi}\int_{-1}^{1} r_q(\xi,\varphi,\phi)p(\xi,\varphi,\phi)\,d\xi\,d\varphi\,d\phi. \tag{13}$$

Let us remind that $p(\xi,\varphi,\phi)d\xi\,d\varphi\,d\phi$ stands for the probability of a crystallite having an orientation described by the Euler angles θ $(= \cos^{-1}\xi)$, φ and ϕ, lying in the intervals $\langle \cos^{-1}\xi, \cos^{-1}(\xi + d\xi)\rangle$, $\langle \varphi, \varphi + d\varphi\rangle$ and $\langle \phi, \phi + d\phi\rangle$, respectively. The probability density function $p(\xi,\varphi,\phi)$ fulfils the normalization condition

$$\langle p(\xi,\varphi,\phi)\rangle = \int_0^{2\pi}\int_0^{2\pi}\int_{-1}^{1} p(\xi,\varphi,\phi)\,d\xi\,d\varphi\,d\phi = 1. \tag{14}$$

It should perhaps be emphasized that each left-hand side of the six equations (3) – (8) is of the form of an expectation value of one of known six functions, $r_q(\xi,\varphi,\phi)$, of a single-

crystal orientation. As it follows from Eqs. (9) – (12), only three functions $r_q(\xi, \varphi, \phi)$ are linearly independent of each other. Each right-hand side of the six equations (3) – (8) is of the form of a known function of an ultrasonic velocity, V_{ij}, the effective single-crystal stiffness moduli $c_{11}^{(\mathrm{eff})}$, $c_{12}^{(\mathrm{eff})}$, $c_{44}^{(\mathrm{eff})}$, and density ρ. In Ref. [1], where the polycrystalline aggregate was approximated by the respective ideal polycrystalline solid, the values of all the quantities appearing on the right-hand side of each of the six equations (5) – (10) are regarded to be known and are to be equal to the respective single-crystal stiffness moduli c_{11}, c_{12}, c_{44} and density ρ.

As it was shown in Ref. [1], in the situation, where the left-hand sides of Eqs. (3) – (8) are the expectation values of $r_q(\xi, \varphi, \phi)$ weighted with $p(\xi, \varphi, \phi)$ and the right-hand sides of these equations are functions of the observables V_{ij}, and when $\bar{c}_{11}$, $\bar{c}_{12}$, $\bar{c}_{44}$ are known, the information theory approach can be used successfully for determining the probability density function $p(\xi, \varphi, \phi)$ in the long-wavelength and ideal polycrystal approximation. It can be done for uniaxially rolled material from three of Eqs. (5) – (10) with such three functions $r_q(\xi, \varphi, \phi)$, which are linearly independent on each other. This requirement is fulfilled by three equations under testing, if each of the numbers 1, 2, and 3 appears as subscripts i or/and j at no more than two velocities involved in the equations [1]. Such a system of three equations was called in the Ref. [2] the *basic system of three equations*. From results of Refs. [1, 2] it follows that the measurements of three propagation velocities involved in the basic system of three equations, e.g. V_{11}, V_{33} and V_{13}, are sufficient for the probability function $p(\xi, \varphi, \phi)$ to be fully determined for aggregates with orthorhombic macroscopic symmetry and when $\bar{c}_{11}$, $\bar{c}_{12}$ $\bar{c}_{44}$ are known. Then the probability density function $p(\xi, \varphi, \phi)$ implied by the JAYNES' [10] principle of maximum Shannon entropy is given in terms used in [2, Appendix] by the following expression

$$p(\xi, \varphi, \phi) = \frac{1}{Z} \exp\left[-L_1 r_1(\xi, \varphi, \phi) - L_3 r_3(\xi, \varphi, \phi) - L_5 r_5(\xi, \varphi, \phi)\right], \tag{15}$$

where the partition function Z and the Lagrangian multipliers L_1, L_3 and L_5 may be determined from Eqs. (3), (5), (7) and the normalization condition (14).

The method proposed in Ref. [1] has been improved in Ref. [2] by avoiding the limiting assumptions concerning the length of ultrasonic waves (long-wavelength approximation) and the absence of imperfections (e.g. voids, imperfect adhesion of neighbouring grains, residual stress, impurities) of the material of the polycrystalline aggregate and its microstructure. In Ref. [2], a theoretical approach has been proposed utilizing the same as in Ref. [2] information theory method to determine the probability density function $p(\xi, \varphi, \phi)$ and the material parameters $\bar{c}_{11} \doteq c_{11}^{(\mathrm{eff})}/\rho$, $\bar{c}_{12} \doteq c_{12}^{(\mathrm{eff})}/\rho$, $\bar{c}_{44} \doteq c_{44}^{(\mathrm{eff})}/\rho$ from the rules of macroscopic orthorhombic symmetry and the results of the measurements of four respectively chosen ultrasonic velocities, V_{ij}, three of them being involved in the basic system of equations.

In the remainder of this paper, the procedure proposed in Ref. [2] will be utilized for solving the problem of determination the function $p(\xi, \varphi, \phi)$ and the single-crystal

material parameters $\overline{c}_{11}$, $\overline{c}_{12}$, and $\overline{c}_{44}$ in the case when the same three ultrasonic velocities Ve_{11}, Ve_{33}, Ve_{13} and additionally one of the velocities Ve_{22}, Ve_{33} and Ve_{12}, namely Ve_{23}, are known. Similarly as in Ref. [2], henceforth, a value of V_{ij}, which will be regarded to be obtained experimentally, will be denoted Ve_{ij}. The ultrasonic measurements were performed in the twelve observation points on the real material under examination. Hence, the values of measured velocities, Ve_{ij}, contain information on the structure and properties of the material as well as on the phenomena influencing on the propagation and occurring in the polycrystal under examination. Therefore, it may be expected that the values of Ve_{ij} together with the symmetry rules allow us to determine the function $p(\xi, \varphi, \phi)$ as well as the material parameters $\overline{c}_{11}$, $\overline{c}_{12}$, and $\overline{c}_{44}$. In this case, assuming that the probability density function $p(\xi, \varphi, \phi)$ is implied by the JAYNES' [10] principle of maximum Shannon entropy, $p(\xi, \varphi, \phi)$ is also of the form given by Eq. (15). Contrary to Ref. [1], now the partition function Z and the Lagrangian multipliers L_1, L_3 and L_5 are to be determined together with the material parameters $\overline{c}_{11}$, $\overline{c}_{12}$ and $\overline{c}_{44}$ from the seven Eqs. (3) – (8), (14), after setting the results of the measurements of the ultrasonic velocities Ve_{11}, Ve_{33}, Ve_{13}, and Ve_{23}. Therefore, from the four velocities Ve_{ij}, the maximum-entropy estimate of the probability density function, $p(\xi, \varphi, \phi)$, will be determined together with the material parameters $\overline{c}_{11}$, $\overline{c}_{12}$ and $\overline{c}_{44}$, after enlarging the approach presented in paper [1] by including a self-consistent computational procedure proposed in Ref. [2]. In using such a procedure the dynamic parameters of the ideal single-crystal material, $\overline{c}_{11}^{(0)} = c_{11}^{(0)}/\rho$, $\overline{c}_{12}^{(0)} = c_{12}^{(0)}/\rho$, $\overline{c}_{44}^{(0)} = c_{44}^{(0)}/\rho$, should be replaced by the effective ones, $\overline{c}_{11}$, $\overline{c}_{12}$, $\overline{c}_{44}$, of the crystallite in the real bulk specimen, the effective moduli being calculated also from the four ultrasonic velocities and symmetry rules given by Eqs. (9). Contrary to the problem defined Ref. [1], the problem of finding the maximum-entropy estimate of the function $p(\xi, \varphi, \phi)$ and the values of material parameters, $\overline{c}_{11}$, $\overline{c}_{12}$, $\overline{c}_{44}$, from the results of the measurements of four propagation velocities Ve_{ij} of ultrasonic waves and from the rules of macroscopic orthorhombic symmetry is not unambiguous. To make a choice between numerous solutions to the problem, LEWANDOWSKI [2] proposed the *criterion of the minimum relative difference* between the values of the material parameters, $\overline{c}_{11}$, $\overline{c}_{12}$, $\overline{c}_{44}$, obtained in the procedure of the maximum-entropy estimate, and their analogues, $\overline{c}_{11}^{(0)}$, $\overline{c}_{12}^{(0)}$, $\overline{c}_{44}^{(0)}$, referring to the same (or the most similar) ideal material in the virgin (before deformation) state. Obviously, a great difficulty of the analysis is encountered when one wishes to find the solution to such a problem of great complexity. In considering this problem, only the concepts and equations required in this study are reiterated herein after [2].

In the present paper, the method proposed in Ref. [2] is utilized for the estimation of the local texture and local basic material parameters of a steel plate which was rolled uniaxially in the situation where the edges parallel to the rolling direction were free. In this way, we seek the answer on the question how strongly are some local material parameters and the local texture influenced on by the distance x between an observation point $\mathbf{r}$ on a plate and one of the two plate edges, which are parallel to the rolling direction.

3. Measurements and numerical analysis

The measurements have been confined to measuring only the ultrasonic velocities Ve_{11}, Ve_{33}, Ve_{13}, which are involved in the so-called basic system of three equations, and additionally the velocity Ve_{32}. The twelve equally spaced *observation* (measurement) *points* have been chosen as lying on a straight line in the rolling plane, the straight line being perpendicular to the $0x_1$ (rolling) direction. The measurement points have been chosen at the distances $x = (0.02, 0.04, 0.06, ..., 0.24)$ m from the reference $0x_1$-edge of the plate.

The volume of a macroscopic sample is regarded as large enough to include a large number of crystallites with each of the occurring orientations. Then, it is reasonable to assume that the measured velocities of ultrasonic pulses propagating through such a macroscopic sample (the pulses being generated by a transducer oscillating normally or transversely to the coupling surface) are equal to the propagation velocities of the respective ultrasonic waves.

The propagation velocities of waves propagating normally to the rolling plane (Ve_{33}, Ve_{32}) have been measured by using commercially available wide-band ultrasonic transducers having a maximum middle frequency of 2.5 MHz. By making use of reflection, a single transducer served as both a transmitter (source) and a receiver (detector). The longitudinal and shear waves propagating parallel to the rolling plane, i.e. Ve_{11} and Ve_{13}, respectively, have been generated and detected by using transducers mounted on Plexiglas wedges and inclined at such angles to the plate surface that ensure the values of the refraction angles of the waves to be nearly critical (equal to 90°). These pieces of equipment allow the transit time of acoustic waves to be measured for all desired directions. The transit distance is to be regarded for the first pair of waves (Ve_{33}, Ve_{32}) as the double plate thickness at the region of the coupling of the transducer and plate, the plate thickness being equal to 0.02 m. Similarly, the transit distances are to be regarded for the second pair of waves, Ve_{11} and Ve_{13}, as the distances between the geometrical centres of the regions of coupling of the plate with the transmitter and receiver, the distances being equal to 0.182 m and 0.0985 m, respectively. The propagation velocities of the second pair of waves deduced from the transit times are regarded to be the velocities at the distances x from the reference $0x_1$-edge, x being determined by the middles of the respective distances between the geometrical centres of the regions of coupling of the plate with the transmitter and receiver. The transit time was measured with an error equal to $5 \cdot 10^{-10}$ s. The final results of the determination of the ultrasonic velocities for the twelve values of x from the transit time are presented in Figs. 1 – 2.

In the subsequent numerical analysis, we examine the texture in the twelve equally spaced observation points by utilizing for each observation point separately the results of the measurements of the ultrasonic velocities Ve_{11}, Ve_{33}, Ve_{13}, which are involved in the basic system of three equations, and additionally the velocity Ve_{32}. It means that first we find for each observation point separately the analytical form of the maximum-entropy probability density function $p(\xi, \varphi, \phi)$, which is that given by Eq. (15). On evaluating the material parameter $\overline{c}_a$ for each observation point from Eq. (9), after substituting $V_{ij} = Ve_{ij}$, $j = 1, 2, 3$, the second step was to calculate the two missing velocities Ve_{12}

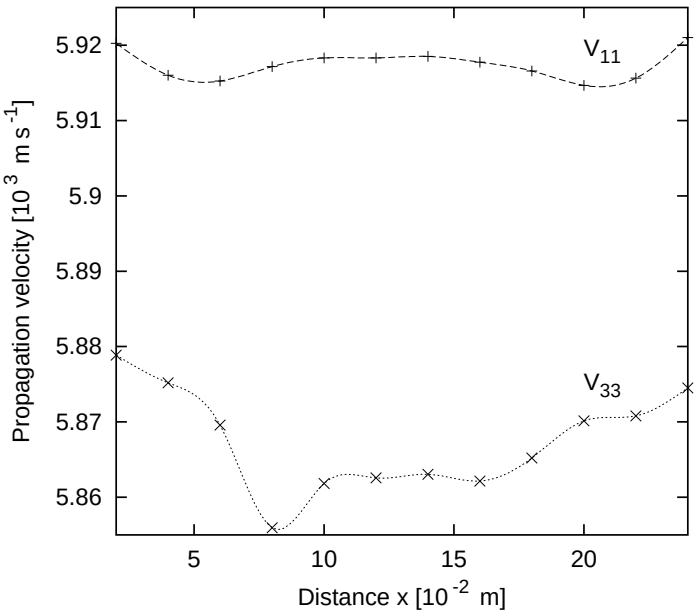

Fig. 1. Velocities Ve_{11} and Ve_{33} of longitudinal waves plotted against the distance x between an observation point on the steel plate and one of the two plate edges parallel to the rolling direction.

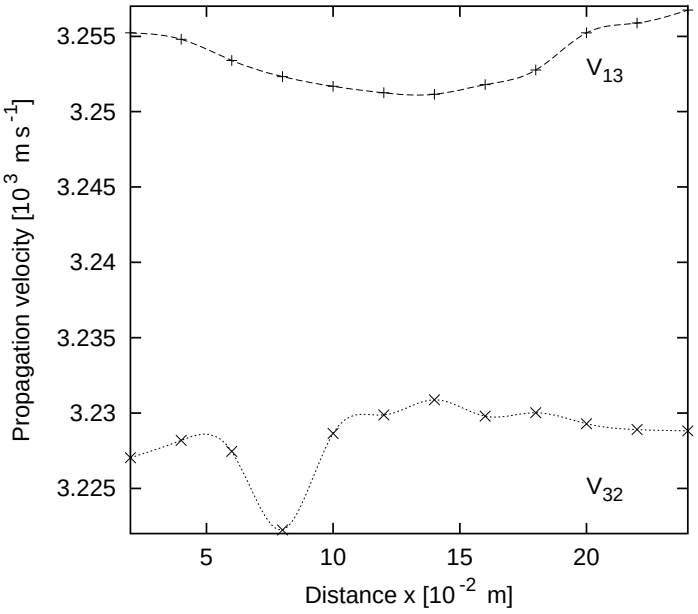

Fig. 2. Velocities Ve_{13} and Ve_{32} of shear waves plotted against the distance x between an observation point on the steel plate and one of the two plate edges parallel to the rolling direction.

and Ve_{22} (for each observation point as well) from the following equations:

$$\begin{aligned} Ve_{12} &= \sqrt{C_a - Ve_{11}^2 - Ve_{31}^2}\,, \\ Ve_{22} &= \sqrt{C_a - Ve_{12}^2 - Ve_{23}^2} \end{aligned} \tag{16}$$

which are deduced from the macroscopic othorhombic symmetry, i.e. are derived also from Eq. (9). In this way for each observation point we have arrived at the following set $\{Ve_{ij}\}$ of the values of the six velocities

$$\{Ve_{ij}\} = \{Ve_{11},\, Ve_{22},\, Ve_{33},\, Ve_{12},\, Ve_{23},\, Ve_{31}\}. \tag{17}$$

As it will be pointed out below, the knowledge of the set (17) enable us to make some check of the actual accuracy of calculating digitally the partition function Z, Lagrangian multipliers L_1, L_3, L_5 and material parameters $\bar{c}_{11}$, $\bar{c}_{12}$, $\bar{c}_{44}$. In the situation where the material parameters $\bar{c}_{11}$, $\bar{c}_{12}$ and $\bar{c}_{44}$ are unknown, the task consists of finding Z, L_1, L_3, L_5, $\bar{c}_{11}$, $\bar{c}_{12}$ and $\bar{c}_{44}$ for each observation point separately from Eqs. (3) – (8), (14). Seeking the texture for each of the twelve observation points, we utilize the numerical procedure proposed in Ref. [2] for each such a point separately. Any full description of the numerical method will be omitted from this paper for the sake of brevity.

As was mentioned above, the partition function Z, Lagrangian multipliers L_1, L_3, L_5 and single-crystallite (grain) material parameters $\bar{c}_{11}$, $\bar{c}_{12}$, $\bar{c}_{44}$ are to be determined from Eqs. (3) – (8), (14). However, these equations present so complicated nonlinear dependencies of the quantities Z, L_1, L_3, L_5, $\bar{c}_{11}$, $\bar{c}_{12}$ and $\bar{c}_{44}$ on each other that the problem of

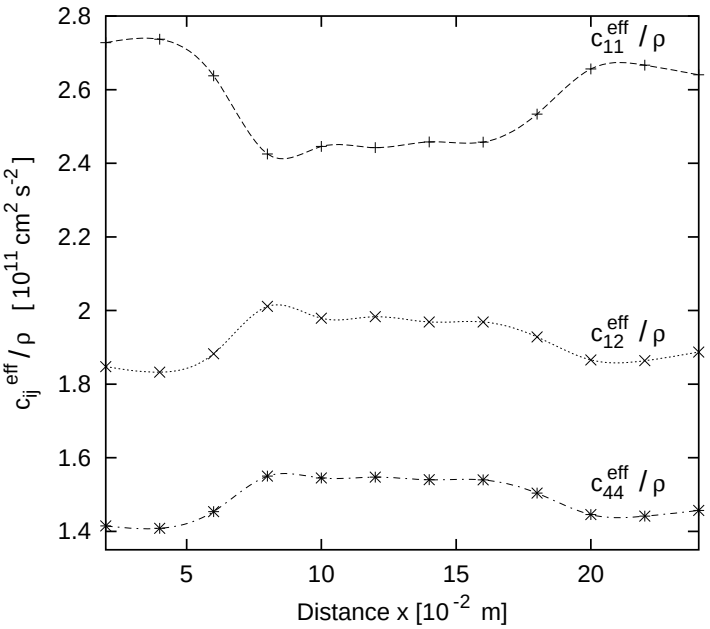

Fig. 3. Effective single-crystallite material parameters $\bar{c}_{11}$, $\bar{c}_{12}$, and $\bar{c}_{44}$ calculated from ultrasonic measurements plotted against the distance x between an observation point on the steel plate and one of the two plate edges parallel to the rolling direction.

evaluating these quantities from Eqs. (3) – (8), (14) is not unambiguous. This raises the need to make a choice between numerous solutions of the problem. In this way arises the need to provide a constructive criterion for choosing one set of Z, L_1, L_3, L_5, $\overline{c}_{11}$, $\overline{c}_{12}$ and $\overline{c}_{44}$ from all such sets satisfying Eqs. (3) – (8), (14). Following Ref. [2], in the subsequent text we confine ourselves only to present numerical results obtained in the situation where the criterion of the minimum value of a difference is used, the proposal of the criterion of the minimum difference being described after Ref. [2] below.

First we suppose that the rolled polycrystalline material (steel) we are dealing with herein is such that, on one hand, all the values of the effective material parameters, $\overline{c}_{11}$, $\overline{c}_{12}$ and $\overline{c}_{44}$, of a single cubic crystal in the bulk sample of the rolled material are unknown and, on the other hand, all the parameter values, $\overline{c}_{11}^{(0)}$, $\overline{c}_{12}^{(0)}$ and $\overline{c}_{44}^{(0)}$, of a single cubic crystal of the polycrystal material (or a material as similar to that as possible) in the virgin state (before deformation) are known from measurements. In accordance with the criterion of the minimum difference, $\overline{c}_{11}$, $\overline{c}_{12}$ and $\overline{c}_{44}$, are as close to $\overline{c}_{11}^{(0)}$, $\overline{c}_{12}^{(0)}$ and $\overline{c}_{44}^{(0)}$, respectively, as it is allowed by Eqs. (3) – (8), (14). Moreover, if we are interesting in rolled steel, similarly as in Refs. [1, 2], and its parameters' values $\overline{c}_{11}^{(0)}$, $\overline{c}_{12}^{(0)}$ and $\overline{c}_{44}^{(0)}$ are unknown, it is supposed that such a virgin material for the rolled steel may be approximated by BCC Fe, which is characterized by the following values of $C_{11}^{(0)}$, $C_{12}^{(0)}$, $C_{44}^{(0)}$:

$$\begin{aligned} \overline{c}_{11}^{(0)} &= 2.5982d + 07 \left(\frac{\mathrm{m}}{\mathrm{s}}\right)^2, \\ \overline{c}_{12}^{(0)} &= 1.6857d + 07 \left(\frac{\mathrm{m}}{\mathrm{s}}\right)^2, \\ \overline{c}_{44}^{(0)} &= 1.5843d + 07 \left(\frac{\mathrm{m}}{\mathrm{s}}\right)^2. \end{aligned} \tag{18}$$

Now we define the difference parameter Qc by the following formula, using the FORTRAN 77 intrisinc functions DMAX1 and DABS

$$Qc = \mathrm{DMAX1}\,(Gc_{11},\, Gc_{12},\, Gc_{44}). \tag{19}$$

The nomenclature introduced in Eq. (17) is as follows:

$$Gc_{ij} = \mathrm{DABS}\left[(\overline{c}_{ij} - \overline{c}_{ij}^{(0)})/\overline{c}_{ij}^{(0)}\right]. \tag{20}$$

According to the choice rule applied herein after Ref. [2], we use this set of the values of Z, L_1, L_3, L_5, $\overline{c}_{11}$, $\overline{c}_{12}$ and $\overline{c}_{44}$ satisfying Eqs. (3) – (8), (14), *which contains such values of the material parameters* $\overline{c}_{11}$, $\overline{c}_{12}$ and $\overline{c}_{44}$ *that lead to the minimum value of the difference parameter* Qc *and simultaneously contains such values of* Z, L_1, L_3, L_5 *that lead to the probability density function* $p(\xi, \varphi, \phi)$ *achieving the maximum value of Shannon entropy*. In this way, we formulate the criterion of the minimum difference.

On finding for each of the twelve observation points the partition function Z and Lagrangian multipliers L_1, L_3, L_5, the maximum-entropy probability density functions, $p(\xi, \varphi, \phi)$, are known for all the observation points. Then the next step was to make the

use of the functions $p(\xi, \varphi, \phi)$, and the material parameters $\bar{c}_{11}$, $\bar{c}_{12}$ and $\bar{c}_{44}$ for calculating the ultrasonic velocities Vm_{11}, Vm_{22}, Vm_{33}, Vm_{12}, Vm_{23}, Vm_{31} for each of the twelve observation points. In the remainder of this paper, the value of a velocity V_{ij} will be denoted by Vm_{ij}, if it is calculated in the maximum-entropy approximation. Thus on the basis of the previously determined maximum-entropy estimate of the probability density function $p(\xi, \varphi, \phi)$ and the material parameters $\bar{c}_{11}$, $\bar{c}_{12}$ and $\bar{c}_{44}$, all the six ultrasonic velocities Vm_{11}, Vm_{22}, Vm_{33}, Vm_{12}, Vm_{23}, Vm_{31} were calculated from Eqs. (3) – (8) for each observation point. By comparing in pairs the values of velocities Vm_{11}, Vm_{22}, Vm_{33}, Vm_{12}, Vm_{23}, Vm_{31} with their analogues defined by Eqs. (17), it was possible to have some check of the actual accuracy of calculating digitally the partition function Z, Lagrangian multipliers L_1, L_3, L_5 and material parameters $\bar{c}_{11}$, $\bar{c}_{12}$ and $\bar{c}_{44}$ by employing a numerical method, which consists of a succession of iterations with increasing accuracy of calculation. To have some estimation of the actual accuracy of calculation, the error parameter Q_m has been used. Q_m had been defined in Ref. [2] using the FORTRAN 77 intrisinc function, DMAX1, which returns the maximum value in the argument list. Q_m had been defined by the following formula:

$$Q_m = \mathrm{DMAX1}(Gm_{11}, Gm_{22}, Gm_{33}, Gm_{12}, Gm_{23}, Gm_{31}). \tag{21}$$

The nomenclature introduced in Eq. (21) is as follows

$$Gm_{ij} = \mathrm{DABS}\left[(Vm_{ij} - Ve_{ij})/Ve_{ij}\right], \tag{22}$$

where the FORTRAN 77 intrisinc function DABS returns the absolute value of its argument.

In solving numerically the system of Eqs. (3) – (8), (14) with respect to Z, L_1, L_3, L_5, $\bar{c}_{11}$, $\bar{c}_{12}$ and $\bar{c}_{44}$ for each of the twelve observation points, the succession of iterations with increasing accuracy of calculation was continued as long as the error parameter Q_m became less than 1.0×10^{-6}. In this way we obtained the numerical results given in Table 1.

In each of the twelve columns of Table 1, there is presented a numerical solution of the system of Eqs. (3) – (8), (14) with respect to Z, L_1, L_3, L_5, $\bar{c}_{11}$, $\bar{c}_{12}$ and $\bar{c}_{44}$, which are calculated with an exactness characterized by the values of the parameters of error, Q_m, and difference, Q_c. The values of Q_m and Q_c are given in each column in the before last row and in the last one, respectively. In all columns, the error parameters Q_m are less than 1.1×10^{-8}. The x-th column ($x = 2, 4, 6, \ldots, 24$ cm) is the set of the values of Z, L_1, L_3, L_5, $\bar{c}_{11}$, $\bar{c}_{12}$ and $\bar{c}_{44}$ which satisfies Eqs. (3) – (8), (14), after inserting the results of the measurements the observables V_{11}, V_{33}, V_{13}, and V_{32} performed in the x-th observation point and employing the symmetry rules given by Eqs. (9). Moreover, one can say that the x-th column contains such values of the material parameters $\bar{c}_{11}$, $\bar{c}_{12}$ and $\bar{c}_{44}$ that lead to the minimum value of the difference parameter, Q_c, and simultaneously contains such values of Z, L_1, L_3, L_5 that lead to the maximum-entropy estimate of the function $p(\xi, \varphi, \phi)$ for the observables V_{11}, V_{33}, V_{13}, (and V_{32}). For these reasons, the values of Z, L_1, L_3, L_5, $\bar{c}_{11}$, $\bar{c}_{12}$ and $\bar{c}_{44}$, which are given in each column, should be regarded in the paper as the solution to the problem under consideration for the respective observation point.

Table 1. Results of numerical calculations of Lagrangian multipliers and material parameters from ultrasonic measurements for twelve observation points.

x [cm]	2	4	6	8
Z	6.98979	7.01548	7.12077	7.07534
L_1	−1.51127138407	−1.52080828560	−1.52376497056	−1.59628175935
L_3	0.839757785471	0.90380655508	0.89713214274	1.00258928214
L_5	1.30840170534	1.292058967	1.22100600410	1.2274019498
$\bar{c}_{11}$ [m^{2}s^{-2}]	2.72759×10^7	2.73678×10^7	2.63767×10^7	2.42525×10^7
$\bar{c}_{12}$ [m^{2}s^{-2}]	1.84753×10^7	1.83255×10^{-1}	1.88247×10^7	2.01129×10^7
$\bar{c}_{44}$ [m^{2}s^{-2}]	1.41477×10^7	1.40824×10^7	1.45381×10^7	1.55000×10^7
$\bar{c}$ [m^{2}s^{-2}]	-1.37794×10^7	-1.16776×10^7	-0.896665×10^7	-0.894442×10^7
$\bar{c}_a$ [m^{2}s^{-2}]	5.55712×10^7	5.55326×10^7	5.54530×10^7	5.52525×10^7
Q_m	9.85135×10^{-7}	9.22084×10^{-7}	8.68158×10^{-7}	1.54281×10^{-7}
Q_c	1.29988×10^{-1}	1.35226×10^{-1}	0.99639×10^{-1}	0.98409×10^{-1}

x [cm]	10	12	14	16
Z	7.41466	7.30817	7.43995	7.44211
L_1	−1.61829511744	−1.52896286792	−1.60507903061	−1.61990847820
L_3	0.85983673731	0.911152470345	0.87014804885	0.85225414589
L_5	1.14268717833	1.07185579723	1.09977675460	1.13241671318
$\bar{c}_{11}$ [m^{2}s^{-2}]	2.44562×10^7	2.44249×10^7	2.45795×10^7	2.45747×10^7
$\bar{c}_{12}$ [m^{2}s^{-2}]	1.97888×10^7	1.98309×10^7	1.96878×10^7	1.96895×10^7
$\bar{c}_{44}$ [m^{2}s^{-2}]	1.54512×10^7	1.54737×10^7	1.54021×10^7	1.53979×10^7
$\bar{c}$ [m^{2}s^{-2}]	-2.62351×10^7	-2.63534×10^7	-2.59126×10^7	-2.59106×10^7
$\bar{c}_a$ [m^{2}s^{-2}]	5.53586×10^7	5.53723×10^7	5.53838×10^7	5.53705×10^7
Q_m	9.69190×10^{-7}	9.77151×10^{-7}	8.52790×10^{-7}	9.45054×10^{-7}
Q_c	1.40431×10^{-1}	1.42255×10^{-1}	1.36023×10^{-1}	1.36097×10^{-1}

x [cm]	18	20	22	24
Z	7.38138	7.21346	7.18267	7.19703
L_1	−1.61571682028	−1.55860866956	−1.60577916205	−1.60124022736
L_3	0.85416318209	0.86426789517	0.85955105606	0.85111195804
L_5	1.16982116073	1.22217644441	1.30172316513	1.29450264631
$\bar{c}_{11}$ [m^{2}s^{-2}]	2.53361×10^7	2.65628×10^7	2.66659×10^7	2.64029×10^7
$\bar{c}_{12}$ [m^{2}s^{-2}]	1.92828×10^7	1.86581×10^7	1.86364×10^7	1.88732×10^7
$\bar{c}_{44}$ [m^{2}s^{-2}]	1.50390×10^7	1.44553×10^7	1.44134×10^7	1.45692×10^7
c [m^{2}s^{-2}]	-2.40246×10^7	-2.10060×10^7	-2.07972×10^7	-2.16058×10^7
$\bar{c}_a$ [m^{2}s^{-2}]	5.54140×10^7	5.54734×10^7	5.54927×10^7	5.55414×10^7
Q_m	4.79940×10^{-7}	9.42212×10^{-7}	3.86125×10^{-7}	9.66848×10^{-7}
Q_c	1.17873×10^{-1}	1.05939×10^{-1}	1.09158×10^{-1}	0.98728×10^{-1}

The degree and type of the texture in each of the twelve observation points can be determined in the fullest detail by making use of the function $p(\xi, \varphi, \phi)$, which gives the probability density of a given crystallite having a specified orientation with respect to the axes of the Cartesian coordinate system of the sample (plate), the crystallite being placed in the region of the considered observation point in the sample. Following Refs. [2], we use the quantities

$$n_\varphi(\varphi_2, \varphi_1) = \int_0^{2\pi} \int_{\varphi_1}^{\varphi_2} \int_{-1}^{1} p(\xi, \varphi, \phi)\, d\xi\, d\varphi\, d\phi, \tag{23}$$

$$n_\theta(\theta_2, \theta_1) = \int_0^{2\pi} \int_0^{2\pi} \int_{\xi_2}^{\xi_1} p(\xi, \varphi, \phi)\, d\xi\, d\varphi\, d\phi, \tag{24}$$

as examples of such specifications. Here

$$\theta_1 = \arccos \xi_1\,, \qquad \theta_2 = \arccos \xi_2\,, \qquad 0 \le \theta_2 \le \pi \tag{25}$$

and $n_\varphi(\varphi_1, \varphi_2)$, $n_\theta(\theta_1, \theta_2)$ denote the fractions of the total number of crystallites (in the region of the considered observation point in the sample) with the angle of precession, φ, lying in the interval $\varphi_1 \le \varphi \le \varphi_2$ and with the angle of nutation, θ, lying in the interval $\theta_1 \le \theta \le \theta_2$, respectively. In Fig. 4, examples of numerical calculations of $n_\varphi(\varphi_1, \varphi_2)$ are

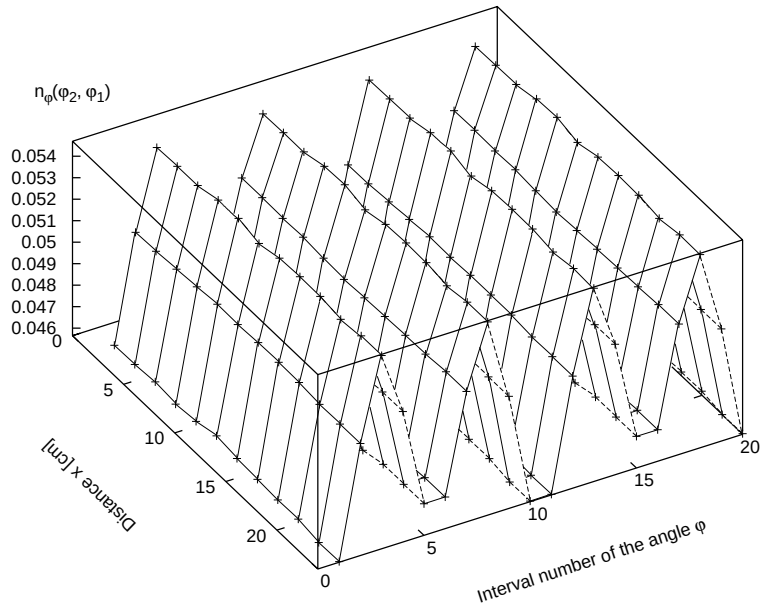

Fig. 4. $n_\varphi(\varphi_2, \varphi_1)$ defined by Eq. (23) and plotted against both the distance x between an observation point on the steel plate and one of the two plate edges parallel to the rolling direction as well as against the the number of each subdomain of the precession angle φ, the whole domain $[0°, 360°]$ of the precession angle φ being divided into parts (subdomains) of equal size, $18°$, numbered from 1 to 20, with centres at $\varphi_0 = (\varphi_1 + \varphi_2)/2 = 9°$, $27°$, $45°$, ..., $351°$.

presented (for each of the twelve observation points) with the whole domain $[0°, 360°]$ of the precession angle φ being divided into parts (subdomains) of equal size, $18°$, with centres at $\varphi_0 = (\varphi_1 + \varphi_2)/2 = 9°$, $27°$, $45°$, ..., $351°$. Similarly, in Fig. 5, examples of numerical calculations of $n_\theta(\theta_1, \theta_2)$ are presented (also for each of the twelve observation points) with the whole domain $[0°, 180°]$ of the nutation angle θ being divided into parts (subdomains) of equal size, $18°$, with centres at $\theta_0 = (\theta_1 + \theta_2)/2 = 9°$, $27°$, $36°$, ..., $171°$. For each region of the twelve observations points, the particle fractions $n_\varphi(\varphi_1, \varphi_2)$ and $n_\theta(\theta_1, \theta_2)$ were calculated separately for each subdomain and the results of these calculations are presented in Figs. 4 and 5.

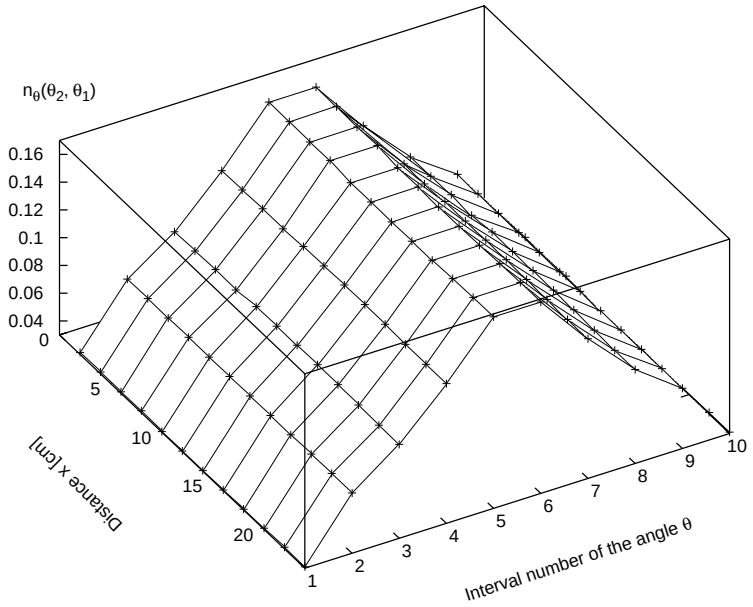

Fig. 5. $n_\theta(\theta_2, \theta_1)$ defined by Eq. (24) and plotted against both the distance x between an observation point on the steel plate and one of the two plate edges parallel to the rolling direction as well as against the number of each subdomain of the nutation angle θ, the whole domain $[0°, 180°]$ of the nutation angle θ being divided into parts (subdomains) of equal size, $18°$, numbered from 1 to 10, with centres at $\theta_0 = (\theta_1 + \theta_2)/2 = 9°$, $27°$, $36°$, ..., $171°$.

From Figs. 4 and 5 it can easily be seen that rolling, say, in the $0x_1$ direction, leaves the crystallites in some non-random orientations. The statistics of the forced non-random orientations leads to the occurrence of the most preferred intervals of the Euler angles, the preferred orientation being a periodic function of the Euler angles. Obviously, all the symmetry properties of $n_\varphi(\varphi_1, \varphi_2)$ and $n_\theta(\theta_1, \theta_2)$, which are shown in Figs. 4 and 5, result in the orthorhombic symmetry of the macroscopic mechanical properties of the polycrystalline aggregate (rolled steel). Similarly as in Ref. [2], the preference of the crystallite orientations, which is revealed by the numerical results presented in Figs. 4 and 5, can be defined in the crystallographic terms as follows: If a solid plate made of

cubic crystallites with the highest symmetry is uniaxially rolled, say, in the $0x_1$ direction, the rolling process leaves the crystallites in a non-random orientations with an orientation preference for the crystallographic plane $[1,1,0]$ to be parallel to the rolling plane x_1x_2 as well as for the crystallographic direction $\langle 1,1,0\rangle$ to be parallel to the rolling direction Ox_1.

4. Final remarks and conclusions

This paper is concerned with the nondestructive ultrasonic method of the estimation of the local texture and local basic material parameters of a steel plate which was rolled uniaxially in the situation where the edges parallel to the rolling direction were free. The aim of the paper was also to estimate how strongly are the local texture and mechanical properties influenced on by the distance x between an observation point determined by the position vector $\mathbf{r}$ and one of the two plate edges parallel to the rolling direction, in the situation where the edges parallel to the rolling direction were free during the rolling process. In the presented method, there is involved the inversion of the problem of calculating the ultrasonic velocities from texture with making use of the Voigt averaging procedure. The inversion, which has been performed with using the information theory approach, leads to the maximum-entropy estimate of the probability density function of the crystallite orientation, $p(\xi,\varphi,\phi)$. This function for each of the twelve observation points is of the form given by Eq. (15), this form being implied by Eqs. (3), (5), (7), (14) under the assumption that the ultrasonic velocities (observables) Ve_{11}, Ve_{33} and Ve_{13} in these regions are known from measurements. Next the same Eqs. (3), (5), (7), (14) together with Eqs. (4), (6), (8), (9) and the criterion of the minimum difference are used for determining, for each of the twelve observation points successively and separately, both the exact form of $p(\xi,\varphi,\phi)$ (by evaluating the three Lagrangian multipliers L_1, L_3, L_5 and normalization constant Z) and the values of three single-crystal material parameters ($\overline{c}_{11} \doteq c_{11}^{(\mathrm{eff})}/\rho$, $\overline{c}_{12} \doteq c_{12}^{(\mathrm{eff})}/\rho$, $\overline{c}_{44} \doteq c_{44}^{(\mathrm{eff})}/\rho$). These quantities and parameters are to be calculated from the values of four observables (Ve_{11}, Ve_{33}, Ve_{13} and Ve_{32}) and orthorhombic symmetry rules given by Eqs. (9).

The analysis presented in Ref. [2] leads to the relations between the probability density function of the crystallite orientation, $p(\xi,\varphi,\phi)$, as well as the values of single-crystal material parameters $\overline{c}_{ij}$, $ij = 11,\ 12,\ 44$, of the rolled material and ultrasonic velocities (Ve_{11}, Ve_{33}, Ve_{13} and Ve_{32}). The present study, moreover, leads to showing that the quantities and parameters involved in the analysis performed by using the method of Ref. [2] are considerably influenced on by the distance $x = (0.02,\ 0.04\,0.06, ...,\ 0.24)$ m between an observation point on the steel plate and one of the two plate edges parallel to the rolling direction, the edges being free during the rolling process. If along a straight line of distance x the rolling load and other forces acting in the rolling process were constant and the microstructure of the material in the virgin (before deformation) state had been statistically homogeneous, then the changes in the values of all the quantities and parameters (Ve_{11}, Ve_{33}, Ve_{13}, Ve_{32}; $p(\xi,\varphi,\phi)$, L_1, L_3, L_5, Z; $\overline{c}_{ij}$, $ij = 11,\ 12,\ 44$), which are observed in the material in a plane parallel to the rolling plane, would be both

constant along the straight line and symmetrical with respect to the axis of geometrical symmetry of the plate, the symmetry axis being parallel to the rolling direction. From Table 1 and Figs. 1 – 3 it can immediately be seen that the deviations of the changes from the axial symmetry are considerable in the case of the material under examination. These deviations contain information on the local inhomogeneity of the material under investigation.

In the presented method, there is involved the inversion of the problem of the relations between the probability density function of the crystallite orientation, $p(\xi, \varphi, \phi)$, and the values of the effective single-crystal material parameters, $\overline{c}_{ij}$, $ij = 11, 12, 44$, of the rolled material as well as of the measured ultrasonic velocities (Ve_{11}, Ve_{33}, Ve_{13} and Ve_{32}). This analysis has been performed for the polycrystalline aggregate with orthorhombic macroscopic symmetry, the aggregate being composed of cubic crystals. In every heterogeneous elastic body, the ultrasonic velocities depend on the effective density and components of the so-called effective dynamic tensor of stiffness of the bulk sample as well as on the frequency of the ultrasonic waves. In turn, the components of the effective dynamic tensor of stiffness of the bulk sample are determined by the probability density function of the crystallite orientation, $p(\xi, \varphi, \phi)$, as well as by the values of the effective single-crystal material parameters, $\overline{c}_{ij}$, $ij = 11, 12, 44$. In the limit, as the wavelength increases to infinity (or the frequency diminishes to zero), the dynamic effective moduli in these relations may be replaced by the static effective moduli, if the polycrystal under consideration may be regarded as an ideal polycrystalline aggregate. In accordance with the long-wavelength approximation and in view of the common opinion that plastic deformation does not induce any considerable changes in the static values of single-crystal material parameters, c_{ij}/ρ, $ij = 11, 12, 44$, it seems to be reasonable to replace the effective dynamic values of these material parameters, which are involved in problems of ultrasonic testing of plastically deformed materials, by their static values measured before deformation. However, from the the twelve examples, which has been considered above and in which $9.84\% < Q_c < 14.23\%$, it can easily be seen that such assumptions may lead to considerable errors in analysing problems concerning the application of ultrasonic methods in material science, because observed changes in acoustic (ultrasonic) anisotropy may be accompanied by considerable changes in the values of c_{ij}/ρ, $ij = 11, 12, 44$.

In this context, it can easily be seen the advantage of the approach applied above and proposed by LEWANDOWSKI in [2] over that which are based on the long-wavelength and ideal polycrystal approximations. By contrast, one might claim that the approach proposed in this paper is more free because it allows us to determine completely the effective single-grain dynamic properties and the texture of the bulk sample under examination from experimentally observed data (velocities Ve_{11}, Ve_{33}, Ve_{13}, Ve_{32}) and Eqs. (3) – (8), (9), (14). In this way we avoid neglecting the effects of the changes in the grain shape (morphological texture) as well as the influence of the distributions of such material defects as voids, impurities, residual stress, etc. on the mechanical and propagation properties of the polycrystalline aggregate made of steel. In this approach we also avoid neglecting the influence of the scattering and mechanical energy dissipation on the propagation of ultrasonic waves.

References

[1] J. Lewandowski, *Maximum-entropy estimate of the orthorhombic texture from ultrasonic measurements*, Ultrasonics, 229–238 (1995).

[2] J. Lewandowski, *Determination of material parameters and texture of a polycrystalline aggregate from ultrasonic measurements*, NDT&E International, **32**, 383–396 (1999).

[3] R.J. Roe, *Inversion of pole figures for materials having cubic crystal symmetry*, J. Appl. Phys., **37**, 2069–2072 (1966).

[4] E. Kroner, *Statistical continuum mechanics*, Lecture Notes, Springer, Berlin 1971.

[5] M.J.P. Musgrave, *Crystal acoustics*, Holden Day, San Francisco 1970.

[6] W. Voigt, *Lehrbuch der Krystall Physik*, Teubner, Leipzig 1928.

[7] A. Reuss, Z Angew: Math Mech, **9**, 49 (1924).

[8] R.J. Hill, Mech. Phys. Solids, **5**, 229 (1957).

[9] C.M. Sayers, *Ultrasonic velocities in anisotropic polycrystalline aggregates*, J. Phys D: Appl. Phys., **15**, 2157–2167 (1982).

[10] E.T. Jaynes, *Information theory and statistical mechanics*, Phys. Rev., **106**, 620–630 (1957).

ARCHIVES OF ACOUSTICS
26, 4, 351–360 (2001)

NONLINEAR EVOLUTION OF THE ACOUSTIC WAVE IN A SEMI-IDEAL GAS

A. PERELOMOVA, S. LEBLE and M. KUŚMIREK-OCHRYMIUK

Technical University of Gdańsk
(80-952 Gdańsk, ul. G. Narutowicza 11/12, Poland)
e-mail: anpe@mifgate.pg.gda.pl,
leble@mif.pg.gda.pl,
ochrymiuk@mif.pg.gda.pl

The method of deriving the evolution equation, based on projecting is applied for the evaluation of the sound velocity and the parameters of nonlinearity for real gases and liquids. The method yields in a coupled system of interacting modes: leftwards and rightwards acoustic and heat modes in the one-dimensional flow problem. The general form of the caloric equation of state allows to get the coefficients of nonlinear equations in the general form. As an example, the sound velocity and the nonlinear parameter B/A for a variety of semi-ideal gases were calculated and the results compared with experimental data.

Notations

x – space coordinate [m],
t – time [s],
ρ – density [kg/m^3],
p – pressure [N/m^2],
v – velocity [m/s],
T – absolute temperature [K],
e – internal energy per unit mass [J/kg],
$\rho_0, p_0, v_0, e_0, T_0$ – unperturbed values,
$\acute{\rho}, \acute{p}, \acute{v}, \acute{e}, \acute{T}$ – perturbations,
$x_*, t_*, \rho_*, p_*, v_*$ – dimensionless variables,
λ – characteristic scale of disturbance,
α – coefficient responsible for amplitude of acoustic wave,
$D_1..D_5$ – dimensionless coefficients in evolution equations,
$E_1..E_5$ – coefficients in caloric equation of state,
c – linear sound velocity [m/s],
B/A, C/A – acoustic parameters of nonlinearity,
$c_{v(p)}$ – heat capacity under constant (volume) pressure per unit mass [J/kg·K],
R – the universal gas constant [J/mol·K],
μ – molar mass [kg/mol],
$f_{\rm osc}$ – number of oscillation degrees of freedom of a gas molecule,
θ_i – characteristic temperature of oscillation [K],
γ – adiabatic gas constant (c_p/c_v).

1. Introduction

The projecting method serves for deriving nonlinear evolution equations for the interacting modes. Modes as basic types of motion of the concrete problem, to be defined by this method as eigenvectors of the corresponding linear problem. The main physical idea hence is to fix relations between the perturbations of wave variables. For linear flows, the modes are independent and may be extracted from the overall perturbation by operators projecting to the eigenspaces. The operators may be constructed by means of the eigenvectors and are applied when either linear or nonlinear dynamics is considered. Acting projectors on the full nonlinear system of gas dynamic equations leads to coupled nonlinear evolution equations which may be related with known evolution equations.

Examples of acoustic-gravity waves in the atmosphere and electromagnetic waves are studied in [1]. Nonlinear evolution equations for the bubbly liquid dynamics are derived in [2], and the acoustics in the exponentially stratified atmosphere is investigated in [3]. In the present paper, we apply the projecting technique for deriving the nonlinear evolution equation for one progressive acoustic mode. The caloric and thermal equations of state are incorporated in their general forms which allow to treat an arbitrary fluid. We, however, go to the representation of the equations as multivariable Taylor series: these formulas are convenient for practical purposes. Therefore the sound velocity, the nonlinear parameter B/A and some nonlinear parameters of higher order (C/A, ...) depend on the coefficients of the Taylor series of the equations of state. A similar approach is developed in [4 – 6] on a different theoretical basis and applications. Beginning from the results in [4], the theory allows to study the direct links of the acoustic parameters with the thermodynamic ones and in turn the modeling of the intermolecular forces. Let also mention the developing techniques and quality of the measurements of the nonlinear constants (see e.g. [7, 8]). The results give hope of a progress in this difficult problem of the condensed matter physics.

Though a wide variety of gases and fluids may be treated in this way, we start from the examples of semi-ideal gases which account for oscillatory degrees of freedom. The motivation is simplicity, that help to explain the main ideas, as well as the existence of explicit formulae for the state equations. One arrives at the sound velocity and the nonlinear parameter B/A in an explicit form and it is easy to calculate both these values over a wide range of equilibrium states of a gas. The important thing is the existence of available experimental data with which the results of calculations could be compared.

2. Basic equations

Let us repeat briefly the ideas and results of the projecting method. We consider an one-dimensional fluid flow without thermal conduction and internal friction. A basic

system thus represents conservation laws of momentum, energy and mass:

$$\begin{aligned} \frac{\partial v}{\partial t} + v\frac{\partial v}{\partial x} + \frac{1}{\rho}\frac{\partial p}{\partial x} &= 0, \\ \rho\frac{\partial e}{\partial t} + \rho v\frac{\partial e}{\partial x} + p\frac{\partial v}{\partial x} &= 0, \\ \frac{\partial \rho}{\partial t} + \frac{\partial(\rho v)}{\partial x} &= 0. \end{aligned} \tag{2.1}$$

We should complete (2.1) with the caloric equation of state $e(p,\rho)$. Let $\acute{e}$ has the form of the Taylor series of two variables:

$$\begin{aligned} \rho_0\acute{e} = E_1\acute{p} + \frac{E_2 p_0}{\rho_0}\acute{\rho} + \frac{E_3}{p_0}\acute{p}^2 + \frac{E_4 p_0}{\rho_0^2}\acute{\rho}^2 + \frac{E_5}{\rho_0}\acute{p}\acute{\rho} \\ + \frac{E_6}{p_0\rho_0}\acute{p}^2\acute{\rho} + \frac{E_7}{\rho_0^2}\acute{p}\acute{\rho}^2 + \frac{E_8}{p_0^2}\acute{p}^3 + \frac{E_9}{\rho_0^3}p_0\acute{\rho}^3 + \dots, \end{aligned} \tag{2.2}$$

E_1, ..., E_9 are dimensionless coefficients. The system (2.1), (2.2) is valid for a wide variety of fluids and we are not restricted to any special cases of internal energy on pressure and density since we use the caloric $e = e(p,\rho)$ equation of state in a general form.

The equivalent system $(v_*, \acute{p}_*, \acute{\rho}_*, \acute{r}_*, \acute{t}_*)$ in dimensionless variables:

$$v = \alpha c v_*, \qquad \acute{p} = \alpha c^2\rho_0\acute{p}_*, \qquad \acute{\rho} = \alpha\rho_0\acute{\rho}_*, \quad x = \lambda x_*, \qquad t = t_*\lambda/c, \tag{2.3}$$

where c is the linear sound velocity, as follows from (2.1), (2.2)

$$c = \sqrt{\frac{p_0(1-E_2)}{\rho_0 E_1}},$$

λ means the characteristic scale of disturbance along x and α is the coefficient responsible to the amplitude of the acoustic wave, may be written in the matrix form (asterisks for dimensionless variables will be later omitted):

$$\frac{\partial}{\partial t}\Psi + L\Psi = \widetilde{\Psi} + \widetilde{\widetilde{\Psi}} + O(\alpha^3), \qquad \Psi = \begin{pmatrix} v \\ \acute{p} \\ \acute{\rho} \end{pmatrix}, \tag{2.4}$$

where

$$L = \begin{pmatrix} 0 & \dfrac{\partial}{\partial x} & 0 \\ \dfrac{\partial}{\partial x} & 0 & 0 \\ \dfrac{\partial}{\partial x} & 0 & 0 \end{pmatrix}, \qquad \widetilde{\Psi} = \alpha \begin{pmatrix} -v\dfrac{\partial v}{\partial x} + \acute{\rho}\dfrac{\partial \acute{p}}{\partial x} \\ -v\dfrac{\partial \acute{p}}{\partial x} + \dfrac{\partial v}{\partial x}\left(\acute{p}D_1 + \acute{\rho}D_2\right) \\ -v\dfrac{\partial \acute{\rho}}{\partial x} - \acute{\rho}\dfrac{\partial v}{\partial x} \end{pmatrix}, \tag{2.5}$$

$$\widetilde{\widetilde{\Psi}} = \alpha^2 \begin{pmatrix} -\acute{\rho}^2\dfrac{\partial \acute{p}}{\partial x} \\ \dfrac{\partial v}{\partial x}\left(\acute{\rho}^2 D_3 + \acute{p}^2 D_4 + \acute{\rho}\acute{p}D_5\right) \\ 0 \end{pmatrix},$$

where the symbols $D_1..D_5$ denote dimensionless coefficients in following forms:

$$
\begin{aligned}
D_1 &= \frac{1}{E_1}\left(-1+2\frac{1-E_2}{E_1}E_3+E_5\right),\\
D_2 &= \frac{1}{1-E_2}\left(1+E_2+2E_4+\frac{1-E_2}{E_1}E_5\right),\\
D_3 &= \frac{1}{1-E_2}\left(1-3E_9-2E_4-\frac{E_7(1-E_2)}{E_1}+\frac{E_5}{E_1}(1+E_2+2E_4)+\frac{E_5^2(1-E_2)}{E_1^2}\right),\\
D_4 &= \frac{(1-E_2)}{E_1^3}\left(\frac{4E_3^2(1-E_2)}{E_1}-E_6E_1+2E_3E_5-3E_8(1-E_2)-2E_3\right),\\
D_5 &= \frac{1}{E_1^2}\left(\frac{4E_5E_3(1-E_2)}{E_1}+2E_3(1+E_2)-2E_6(1-E_2)-2E_1E_7-E_1E_5\right.\\
&\qquad\left.+E_5^2+4E_3E_4-E_1-E_5\right).
\end{aligned}
$$

The second-order nonlinearity column $\widetilde{\Psi}$ will contribute to the B/A parameter, and the third-order one $\widetilde{\widetilde{\Psi}}$ will yield in C/A.

3. Projecting technique

For a linear flow, we may find a solution as the sum of plane waves, every plane wave being a solution of the linearized system (2.1), (2.2). Let us introduce plane waves $\sim \exp(i\omega t - ikx)$ with amplitudes V_k, P_k and R_k. The eigenvalues of the corresponding system of equations for Fourier transformed components in the linear problem, are determined from the equation:

$$
\begin{vmatrix} i\omega & -ik & 0\\ -ik & i\omega & 0\\ -ik & 0 & i\omega \end{vmatrix} = 0.
$$

The solution of this equation serve as dispersion relations for the right- and left-progressive and stationary components. Eigenvectors in the k-presentation look as:

$$
\Psi_{1,2} = \begin{pmatrix} \pm 1\\ 1\\ 1 \end{pmatrix} R_{k_{1,2}}, \qquad \Psi_3 = \begin{pmatrix} 0\\ 0\\ 1 \end{pmatrix} R_{k_3}\,.
$$

Therefore, returning to the (x,t) representation connections for the specific variables appear and we write it down as:

$$
v_{1,2} = \pm\rho_{1,2}, \qquad p_{1,2} = \rho_{1,2}, \qquad v_3 = 0, \qquad p_3 = 0. \tag{3.6}
$$

In this way we defined the components of the right, left and stationary modes of a wave in the linear model. From these relations (3.6) the projectors follow immediately:

$$
P_1 = \frac{1}{2}\begin{pmatrix} 1 & 1 & 0\\ 1 & 1 & 0\\ 1 & 1 & 0 \end{pmatrix}, \quad P_2 = \frac{1}{2}\begin{pmatrix} 1 & -1 & 0\\ -1 & 1 & 0\\ -1 & 1 & 0 \end{pmatrix}, \quad P_3 = \begin{pmatrix} 0 & 0 & 0\\ 0 & 0 & 0\\ 0 & -1 & 1 \end{pmatrix}. \tag{3.7}
$$

The matrices (3.7) have general properties of orthogonal projectors:

$$P_1 + P_2 + P_3 = \widetilde{I},$$

$$P_1P_2 = P_2P_3 = P_3P_1 = \widetilde{0}, \qquad P_1P_1 = P_1, \quad \text{etc.},$$

where the $\tilde{I}$ and $\tilde{0}$ projectors separate the chosen mode from the overall field in a unique way: $\Psi_1\colon\ P_1\Psi = \Psi_1$, $P_2\Psi = \Psi_2$, $P_3\Psi = \Psi_3$. Projectors P_1, P_2, P_3 do commute both with L and $\partial/\partial t$, that allows to generate the equations of modes interaction acting by P_i on the basic system (2.4).

4. Nonlinear coupled evolution equations

In the nonlinear problem we preserve the same notations for the modes. We consider (now approximately defined) rightwards, leftwards and stationary modes of the nonlinear problem with the eigenvectors Ψ_1, Ψ_2 and Ψ_3 as it was accepted in the linear model and assume that the relation equations (3.6) also holds. Thus, the defined modes are strictly directed and stationary in the linear limit and form a system of coupled nonlinear equations when the projectors act on both sides of (2.4). Marking these modes by indices 1, 2, 3 correspondingly for the quasi-rightwards, leftwards and stationary one, we get finally the system:

$$P_n\frac{\partial}{\partial t}\Psi + P_nL\Psi - P_n\widetilde{\Psi} - P_n\widetilde{\widetilde{\Psi}} + O(\alpha^3) = 0, \tag{4.8}$$

or another one (for density only):

$$\frac{\partial\rho_n}{\partial t} + c_n\frac{\partial\rho_n}{\partial x} + \frac{\alpha}{2}\sum_{i,m=1}^{3} Y^n_{im}\rho_i\frac{\partial\rho_m}{\partial x} + \frac{\alpha^2}{2}\sum_{i,m=1}^{3} {T^I}^n_{im}\rho_i\rho_m\frac{\partial\rho_1}{\partial x} + \frac{\alpha^2}{2}\sum_{i,m=1}^{3} {T^{II}}^n_{im}\rho_i\rho_m\frac{\partial\rho_2}{\partial x} + O(\alpha^3) = 0, \tag{4.9}$$

where

$$c_n = \left\{\begin{array}{ll} 1 & \text{for } n=1 \\ -1 & \text{for } n=2 \\ 0 & \text{for } n=3 \end{array}\right\}$$

and the matrices of constants the Y, T^I and T^{II} for the first mode are:

$$\left|\begin{array}{cccc} Y^1_{i,m} & m=1 & m=2 & m=3 \\ i=1 & -D_1-D_2+1 & D_1+D_2-1 & 0 \\ i=2 & -D_1-D_2-3 & D_1+D_2-1 & 0 \\ i=3 & -D_2-1 & D_2-1 & 0 \end{array}\right|$$

$$\left|\begin{array}{cccc} {T^I}^1_{i,m} & m=1 & m=2 & m=3 \\ i=1 & -D_3-D_4-D_5+1 & -D_3-D_4-D_5+1 & -D_3+1 \\ i=2 & -D_3-D_4-D_5+1 & -D_3-D_4-D_5+1 & -D_3+1 \\ i=3 & -D_3-D_5+1 & -D_3-D_5+1 & -D_3+1 \end{array}\right|$$

$$\left| \begin{array}{cccc} {T^{II}}^1_{i,m} & m=1 & m=2 & m=3 \\ i=1 & D_3+D_4+D_5+1 & D_3+D_4+D_5+1 & D_3+1 \\ i=2 & D_3+D_4+D_5+1 & D_3+D_4+D_5+1 & D_3+1 \\ i=3 & D_3+D_5+1 & D_3+D_5+1 & D_3+1 \end{array} \right|$$

The other matrices look similarly. There are also equivalent equations for pressure and velocity.

The system (4.9) allows to calculate all possible interactions of modes. One may specify a class of initial (boundary) conditions, define the dominant modes and later solve the system approximately. Here we are interested in the evolution equation for one progressive (say, rightwards) mode. Physically it means, that this mode is dominant initially: $\rho_1 \gg \rho_2$, $\rho_1 \gg \rho_3$, and we account self-interaction only in the evolution equation for this mode:

$$\frac{\partial \rho_1}{\partial t} + c_1 \frac{\partial \rho_1}{\partial x} + \varepsilon \rho_1 \frac{\partial \rho_1}{\partial x} + \delta \rho_1^2 \frac{\partial \rho_1}{\partial x} = 0, \tag{4.10}$$

where $\varepsilon = \frac{\alpha}{2}(-D_1 - D_2 + 1)$, and $\delta = \frac{\alpha^2}{2}(-D_3 - D_4 - D_5 + 1)$. The parameters B/A, C/A are well known nonlinear parameters of the nonlinear acoustics equation:

$$p = p_0 + A\frac{\rho - \rho_0}{\rho_0} + \frac{B}{2}\frac{(\rho-\rho_0)^2}{\rho_0^2} + \frac{C}{6}\frac{(\rho-\rho_0)^3}{\rho_0^3} + \left(\frac{\partial p}{\partial s}\right)\Big|_{\rho, s=s_0} (s - s_0) + \dots$$

where s is entropy. For our accounting the last expression is neglected — we assume an adiabatic process. The coefficients A, B, C can be expressed as:

$$\begin{aligned} A &= \frac{1-E_2}{E_1} p_0, \qquad B = -(D_1 + D_2 + 1)\frac{1-E_2}{E_1} p_0\,, \\ C &= ((D_1 + D_2 + 1)(D_1 + 2) - 2(D_3 + D_4 + D_5))\frac{1-E_2}{E_1} p_0\,. \end{aligned}$$

5. Semi-ideal gases: theory and experiment

We stress once more that the system (2.1) + (2.2) and the subsequent formula for the operators are suitable for gases and liquids treated by the general caloric equation of state. The case of ideal gas is considered with coefficients:

$$E_1 = E_4 = E_7 = \frac{1}{\gamma - 1}\,, \qquad E_2 = E_5 = E_9 = -\frac{1}{\gamma - 1}\,, \qquad E_3 = E_6 = E_8 = 0.$$

and: $B/A = \gamma - 1$, $C/A = (\gamma - 1)(\gamma - 2)$. To find some corresponding coefficients for the semi-ideal gas, we have to accept the energy of oscillation in the molecules([1]) [9]:

$$c_{v,\mathrm{sid}} = c_{v,\mathrm{id}} + c_{\mathrm{osc}} + \Delta c_{\mathrm{rot}} + \Delta c_{\mathrm{el}}\,. \tag{5.11}$$

We use the Einstein–Planck formula for the vibrational specific heat:

$$c_{\mathrm{osc}} = R \sum_{i=1}^{f_{\mathrm{osc}}} \left(\frac{\theta_i}{T}\right)^2 \frac{e^{\theta_i/T}}{\left(e^{\theta_i/T} - 1\right)^2}. \tag{5.12}$$

[1] We neglect electron excitations energy because it concerns very high temperatures, and we omit the energy of rotation — it is significant for very low temperatures and light gases only.

Using the above formula, we get the equation for the internal energy for semi-ideal gases [9]:

$$e = e_{\rm id} + \frac{R}{\mu}\sum_{i=1}^{f_{\rm osc}} \frac{\theta_i}{e^{\theta_i/T}-1}\,, \qquad e_{\rm id} = \frac{p}{\rho}\,\frac{1}{(\gamma-1)}\,, \tag{5.13}$$

where c, e, μ, $f_{\rm osc}$ mean respectively: molar heat, internal energy per unit mass, molar mass and number of oscillation degrees of freedom of a gas molecule. θ_i it is characteristic temperature of oscillation (T — absolute temperature) and γ — adiabatic gas constant (c_p/c_v, in classical theory we take $\gamma = 5/3$ for a monoatomic ideal gas, 1.4 for a diatomic one and $4/3$ for other gases).

Below, we present a comparison of the values founded for a few gases treated first as ideal ones and then as semi-ideal ones. To calculate the sound velocity c and B/A values we use the following formulas:

$$c = \sqrt{RT_0\frac{(1-E_2)}{E_1}}, \qquad \frac{B}{A} = -D_1 - D_2 - 1, \tag{5.14}$$

where the coefficients $E_1..E_5$, which have been used (see (2.2)), have the general forms:

$$\begin{aligned} E_1 = \left.\frac{\partial e}{\partial p}\right|_{p_0,\rho_0}\rho_0, \qquad E_2 = \left.\frac{\partial e}{\partial \rho}\right|_{p_0,\rho_0}\frac{\rho_0^2}{p_0}\,, \qquad E_3 = \frac{1}{2}\left.\frac{\partial^2 e}{\partial p^2}\right|_{p_0,\rho_0}\rho_0 p_0, \\ E_4 = \frac{1}{2}\left.\frac{\partial^2 e}{\partial \rho^2}\right|_{p_0,\rho_0}\frac{\rho_0^3}{p_0}\,, \qquad E_5 = \left.\frac{\partial^2 e}{\partial \rho p}\right|_{p_0\rho_0}\rho_0^2 \end{aligned} \tag{5.15}$$

and for the concrete semi-ideal gas model with account of oscillation degrees of freedom (the model described above):

$$\begin{aligned} E_1 &= -E_2 = \frac{1}{\gamma-1} + \sum_{i=1}^{f_{\rm osc}}\left(\frac{\theta_i}{T_0}\right)^2 e^{\theta_i/T_0}\left(e^{\theta_i/T_0}-1\right)^{-2}, \\ E_3 &= \frac{1}{2}\sum_{i}^{f_{\rm osc}}\left(\frac{\theta_i}{T_0}\right)^2 e^{\theta_i/T_0}\left(e^{\theta_i/T_0}-1\right)^{-2}\left(-2-\frac{\theta_i}{T_0}+2\frac{\theta_i}{T_0}e^{\theta_i/T_0}\left(e^{\theta_i/T_0}-1\right)^{-1}\right), \\ E_4 &= \frac{1}{\gamma-1} - \frac{1}{2}\sum_{i}^{f_{\rm osc}}\left(\frac{\theta_i}{T_0}\right)^3 e^{\theta_i/T_0}\left(e^{\theta_i/T_0}-1\right)^{-2}\left(1-2e^{\theta_i/T_0}\left(e^{\theta_i/T_0}-1\right)^{-1}\right), \\ E_5 &= -\frac{1}{\gamma-1} + \sum_{i}^{f_{\rm osc}}\left(\frac{\theta_i}{T_0}\right)^2 e^{\theta_i/T_0}\left(e^{\theta_i/T_0}-1\right)^{-2}\left(1+\frac{\theta_i}{T_0}+\frac{\theta_i}{T_0}\left(e^{\theta_i/T_0}-1\right)^{-1}\right). \end{aligned}$$

For calculating C/A we need the next coefficients: $E_6, ..., E_9$, which are higher order derrivatives of e.

The results of calculations are presented in Table 1.

Now, we can notice that for any monoatomic gases (for example He) we have the ideal gas model without oscillations, and for the diatomic ones (N_2, CO) there is a very small difference in the sound velocities (about 10^{-2} m/s). Next, for some poliatomic gases (CO_2, CH_4) the difference is noticeable, especially for CO_2, even for the low temperatures.

Table 1. (2)

Gas	Model of ideal gas		Model of semi-ideal gas		Experimental data	
	B/A	c [m/s]	B/A	c [m/s]	B/A^a	c [m/s]^b
He	0.67	972.9	0.67	972.9	0.66	971^c
N_2	0.40	336.9	0.40	336.9	0.40	334.0
CO	0.40	337.0	0.40	337.0	0.40	336^d (338)
CO_2	0.33	262.2	0.24	255.0	0.31	256.7
CH_4	0.33	434.7	0.29	431.3	0.30	430

[a] All values are taken as $\gamma - 1$ from [9].
[b] All values are taken from [10].
[c] The experimental value is taken from [11].
[d] The first value is taken from [9].

It is necessary to add that the experimental data are taken from various sources, so we are sure of the temperature measurements only (273 K), but data on pressure are often not available and we often do not know the other measurement parameters. (For example: c value in the case of the gas CO.)

For an ideal gas $B/A \equiv \gamma - 1$ [12], but it must be stressed that for a semi-ideal gas and real gases c_v is a function of temperature and a new γ' has a new thermodynamic sense. The experimental data of γ for monoatomic gases are almost the same as the theoretical values, but for poliatomic gases the experimental values are lower than theoretical ones, which results from the classical approach to the ideal gas [13]. Some experimental data of γ, taken from other sources, for example [14], would be more close to our theoretical values:

$$B/A_{CO_2} = 0.28, \qquad B/A_{CH_4} = 0.26,$$

but they describe some gases under somewhat different measurement conditions. However, finding various experimental data, we can notice the temperature and pressure sensibility of the γ parameter.

Below we present also diagrams of the temperature dependence of c and B/A for some gases:

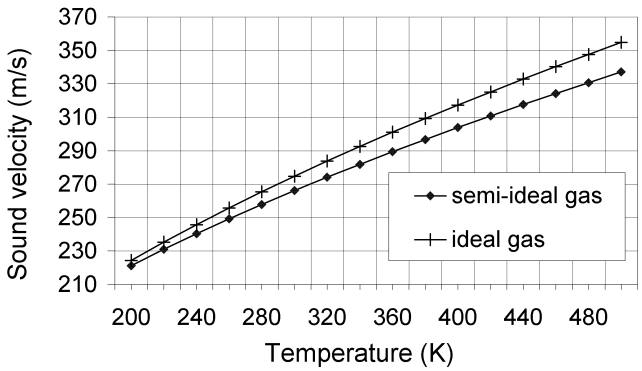

Fig. 1. Comparison of theoretical values of sound velocities for CO_2 gas.

(2) All values in Table 1 are obtained for $T = 273.15$ K.

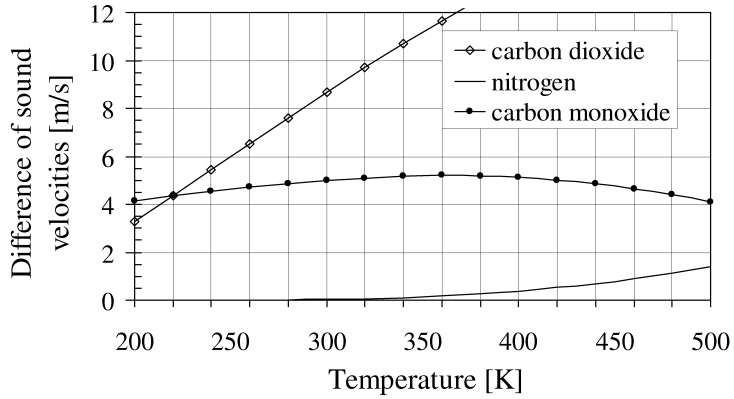

Fig. 2. Difference of theoretical sound velocities: $c_{\mathrm{id}} - c_{\mathrm{sid}}$ for N_2, CO and CO_2 gases.

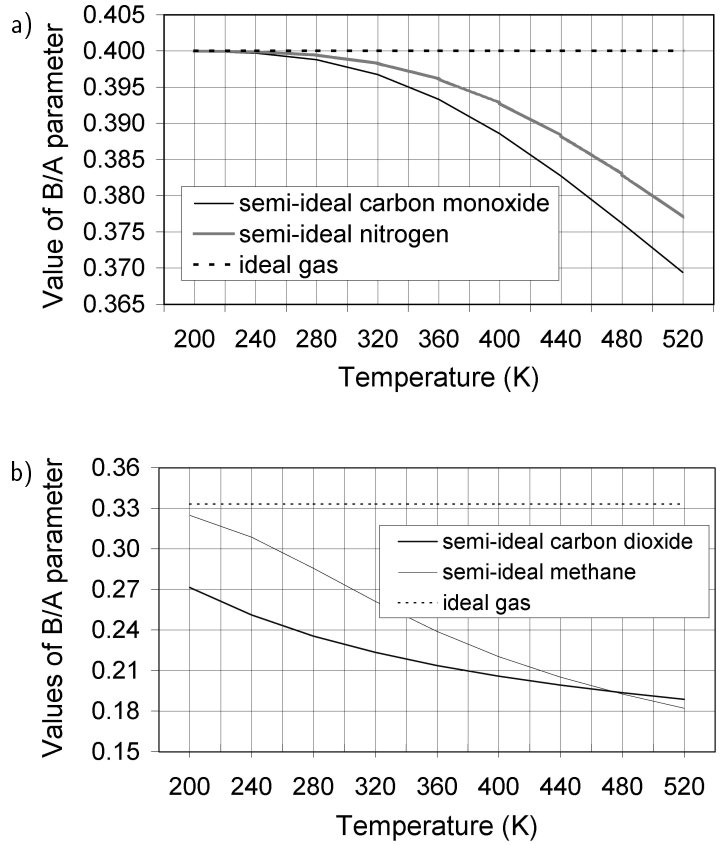

Fig. 3. Temperature dependence of theoretical values of B/A for: a) diatomic gases CO and N_2 and b) polyatomic ones: CO_2 and CH_4.

6. Conclusions

A comparison of the theoretical values of the sound velocity and the nonlinear parameter B/A for an ideal and semi-ideal gas demonstrate that both of the approaches give different results for the considered gases. For some polyatomic gases (CO_2, CH_4) the theoretical values of c at 0°C, are in the semi-ideal model of gas closer to the experimental ones. In the case of the B/A parameter, we have a less clear situation, but one can notice that for the mentioned polyatomic gases the ideal gas model is valid.

The method presented in this paper was applied for deriving the evolution equation for one progressive acoustic mode only, though its application is considerably extensive. After adding some thermoconducting and viscous expressions to the basic system of equations, and adding a thermic equation of state, we could get some new projectors for a thermoviscous flow. Also the formula of the equation of state written in the general form allows to apply the method to different liquids.

References

[1] S.B. Leble, *Nonlinear waves in waveguides with stratification*, Springer-Verlag, Berlin 1990.

[2] A.A. Perelomova, *Projectors in nonlinear evolution problem: Acoustic solitons of bubbly liquid*, Applied Mathematics Letters, **13** (2000).

[3] A.A. Perelomova, *Nonlinear dynamics of vertically propagating acoustic waves in a stratified atmosphere*, Acta Acustica, **84**, 6, 1002–1006 (1998).

[4] B. Hartmann, Journal of the Acoustical Society of America, **65**, 6, 1392–1396 (1979).

[5] B. Sharma, Journal of the Acoustical Society of India, **17**, 3-4, 172–175 (1989).

[6] B. Sharma, Pramana–Journal of Physics, **37**, 6, 489–496 (1991).

[7] S. Takahashi, Japanese Journal of Applied Physics, **34**, 2790–2792 (1995).

[8] K. Zakhariasz, *The acoustic method for measurement of the nonlinearity parameter B/A of the liquid using parabolic model* [in Polish], Proceedings of the XV Symposium on Hydroacoustics, R. Salamon, L. Kilian [Eds.], Politechnika Gdańska, 1998.

[9] J. Szargut, *Thermodynamics* [in Polish], PWN, Warsaw 1976.

[10] A.P. Babichev, N.A. Babushkina, A.M. Bratkovski *et al.*, *Physical values* [in Russian], Energoatomizdat, Moscow 1991.

[11] S. Szczeniowski, *Experimental physics* [in Polish], PWN, Warsaw 1972.

[12] S. Makarov and M. Ochmann, *Nonlinear and thermoviscous phenomena in acoustics*, Part I. *Acustica*, Acta Acustica, **82**, 579–606 (1996).

[13] A.I. Anselm, *Foundations of statistical physics and thermodynamics* [in Russian], Nauka, Moscow 1973.

[14] *Handbook of fluid dynamics*, Mc Graw–Hill Book Company Inc., London 1961.

ARCHIVES OF ACOUSTICS
26, 4, 361–369 (2001)

CORRELATION BETWEEN SOME PHYSICAL PROPERTIES FOR TRI-COMPONENT TELLURITE GLASSES AND LOW TEMPERATURE ULTRASONIC RELAXATION

M.A. SIDKEY, N.S. ABD EL AAL, L. ABD EL LATIF

National Institute for Standards
El Haram – Egypt

A. ABD EL MONEIM

Physics Department Faculty of Science
Zagazig University Egypt

Theoretical analysis of ultrasonic wave absorption and elastic moduli for TeO_2-V_2O_5-Sm_2O_3 glass system is presented. A correlation between low temperature ultrasonic relaxation parameters and other physical (elastic) properties for this glass system was achieved according to a model presented by Bridge and Patel. Correlation coefficients greater than 96% were obtained indicating that correlations between ultrasonic attenuation and activation energy at low temperatures and the bulk modulus of this glass system at room — temperature (through the two crucial structural parameters, number of anions and anion-cation force) exist.

1. Introduction

Based on the great deal of experimental information about the physical properties of tellurite glasses (which have been obtained from ultrasonic investigations) it is generally accepted that in almost all binary and ternary tellurite glass systems, the composition is a decisive factor [1–8]. The elastic constants (bulk modulus), experimental ring size, and the mean stretching force constant, calculated at room temperature, are strongly compositional dependent. The change in these parameters with the increase of the modifier mol percent content is mainly due to progressive strengthening of the network with more crosslinks between the units of the structure introduced by the increase of the modifier. On the other hand, the position and overall shape of the loss peaks (peaks of the temperature dependence of ultrasonic absorption occuring at low temperature), number of loss centers per oxygen atom, and activation energies of the relaxation process are also strongly composition sensitive. The relaxation spectra have been attributed to loss mechanisms of the standard linear solid type, and a broad distribution of Arrhenius-type relaxation times. This is caused by thermal motion of particles in two-well potentials of

atomic dimensions, with a distribution of barrier heights, [2, 5, 7]. The number of loss centers per oxygen atom (vibrating particles in thermal motion) control the loss occured in double-well potential which is a property of the vitreous network. The activation energy of the relaxation process (activation energy of the anion atoms in the double-well system) depends on the value of the cation-anion forces.

Bridge and Patel [9] proposed a model of correlation between low temperature ultrasonic relaxation parameters and other physical properties for oxide glasses. Their study was carried out with gradual and wide ranging changes in the glass composition in order to understand the microscopic origin of the relaxation mechanisms of the vitreous system Mo-P-O. The model assumed that, in almost all glass systems, there is a distribution of the thermally averaged cation-anion-cation spacings about the equilibrium values, and correspondingly a distribution of cation-anion-cation angles because straight bond angles are rare and not necessarily equal to 180°. It follows that there will exist two-well systems with a distribution of barrier heights, for both longitudinal and transverse motions of the anions with all kinds of bonds. The longitudinal and transverse double-well potentials are associated with elongated and contracted cation-anion-cation angles. In another article [10], Bridge and Patel tried to apply the model developed from the study of the MoO_3-P_2O_5 system to explain the differences in the low temperature acoustic loss behaviour in different oxide glass systems. A theoretical analysis of ultrasonic wave attenuation and the elastic moduli of tellurite glasses was reported by El Mallawany [11]. His treatment of the peak loss (maximum absorption coefficient of ultrasonic waves) and the bulk modulus for TeO_2-MoO_3 networks is based on the fact that the total number of two-well systems per unit volume (number of loss centers) is proportional to the oxygen density, and the average activation energy is proportional to the mean first-order stretching force constant. He reported correlations between the ultrasonic absorption coefficients and the activation energy at low temperatures, on the one handside, and the bulk modulus of the glasses at room temperature, on the other side. The correlations were achieved through two crucial structural parameters: the number of anions and the anion-cation force.

The work under report aims to apply the model presented by Bridge and Patel [9] to the ternary glass system TeO_2-V_2O_5-Sm_2O_3 in order to examine its validity for this glass system.

2. Model

Bridge and Patel [9] noted that there is a distribution in thermally averaged cation-anion-cation spacings about the equilibrium values, and correspondingly a distribution of cation-anion-cation angles. Furthermore, the authors noted that, the longitudinal and transverse double-well potentials are associated with a spread of bond length and spread of cation-cation spacings. Therefore, there exist double-well systems with a distribution of barrier heights for all kinds of bonds. They also reported that the total number of loss centers (n) is proportional to oxygen density [O], and it increases with the mean atomic ring size (ℓ). The activation energy (E_p) increases with the average stretching force

constant (F), and it also increases with the mean atomic ring size (ℓ). Quantitatively, they proposed the following empirical equations:

$$n = c_1[\mathrm{O}]\,\ell^m, \tag{1}$$

$$E_p = c_2 F \ell^m, \tag{2}$$

where [O] is the oxygen density that can be calculated from the chemical composition of the glass according to the following relation [11]:

$$[\mathrm{O}] = (c/D)(N_\mathrm{A}/16), \tag{3}$$

where c is the total amount of oxygen in 100 g of the glass, D is the volume of 100 g of the glass, N_A is Avogadro's number, c_1 and c_2 are constants, and m is a high positive power.

The total number of two-well systems per unit volume (n) is also given by:

$$n = \frac{\rho V_\ell^2 E_p}{2D} \int_0^\infty C(E)\,dE, \tag{4}$$

where ρ is the density of the glass, V_ℓ is the longitudinal ultrasonic velocity, E_p is the activation energy of the relaxation process, D is the deformation potential (energy shift of the two-well states in a strain field of unit strength), and the integral $C(E)\,dE$ is the area under the curve relating between absorption and temperature. The average stretching force constant $\overline{F}$ for a network is calculated from the relation given by Higazy and Bridge [12] as

$$F = \frac{\sum(x n_f f)_i}{\sum(x n_f)_i}, \tag{5}$$

where x is the mole fraction of component oxide, n_f is the coordination number of cations (number of network bonds per formula unit), and f is the first order stretching force constant of the oxide (values of stretching force of each cation-anion pair, or mean force constant for respective types of the network bond).

Bridge *et al.* [13] argued that the average ring sizes could be obtained for the oxide network by

$$K = c_3 F/\ell^n, \tag{6}$$

where K is the bulk modulus, and n is a high positive power. Taking $c_3 = 0.0106$, $n = 3.84$, F is in Nm^{-1}, ℓ in nm, and K in GPa, they obtained a correlation factor of 99%. Then by eliminating (ℓ) between equations (1), (2), and (6) Bridge and Patel found

$$N = c_4 (F/K)^{m/n}, \tag{7}$$

$$E_p = c_5 F (F/K)^{m/n}, \tag{8}$$

where N is the number of two-well systems per unit volume expressed as a percentage of the number of oxygen atoms. From inspection of Eqs. (7) and (8), Bridge and Patel observed that (F) can in fact be eliminated to yield the relation

$$E_p = c_6 N^{(1+n/m)} K. \tag{9}$$

They tested their model on the Mo-P-O glass system and after performing linear regression on $Ln(N)$ and F/K, they obtained the relationship

$$N = 0.589(F/K)^{0.576} \tag{10}$$

with a correlation coefficient of 80%. A linear regression performed on E_p and $F(F/K)$ yielded the relation

$$E_p = 6.92 \times 10^{-5} F(F/K)^{0.576} \tag{11}$$

with a correlation coefficient of 98%. However, apart from the correlation coefficient, the most important feature of Eqs. (7) and (8) is the fact that they predict correctly the general character of the compositional dependence of (N) and (E_p).

3. Results and discussion

In previous published articles by the authors [6, 7], the results of studies on low-temperature ultrasonic relaxation and physical properties for ternary tellurite glass system TeO_2-V_2O_5-Sm_2O_3 were reported. The authors observed that, the calculated bulk modulus (K) increases from 28.87 GPa to 32.47 GPa with increasing Sm_2O_3 from 0.1 to 5.0 mol %. Both the atomic ring size (ℓ) and average stretching force constant (F) decrease from 0.532 to 0.509 nm, and from 240.3 to 228.0 N/m respectively, as the Sm_2O_3 content increases indicating a change in the glass structure given in Table 1. On the other hand, as Sm_2O_3 mol % increases, both the activation energy (E_p) and total number of loss centers $(N\,\%)$, decrease from 0.197 to 0.106 eV and from 5.88 to 3.54, respectively, as given in Table 1. It was also observed that, the total number of loss centers $(N\,\%)$ decreases with the decrease in the atomic ring size (ℓ). The activation energy (E_p) also decreases with the decrease of the stretching force constant (F), Table 1. Moreover, the total number of two-well systems per unit volume per oxygen atoms $(N\,\%)$ was found [7] to be proportional to the oxygen density (i.e. to the reciprocal of the volume per gram atom of oxygen). Moreover, the average activation energy (E_p) was found [7] to be proportional to the mean atomic ring size (ℓ) and the average stretching force constant (F). These observations show clearly the strong composition dependence of both the physical properties at room temperature, and of the acoustic loss parameters at low-temperature for the studied tellurite glass system TeO_2-V_2O_5-Sm_2O_3.

Table 1. Values of the experimental bulk modulus (K), average stretching force constant (F), ring diameter (ℓ), and the oxygen density (O).

Glass Composition			K	F	ℓ	$O \times 10^{28}$
TeO_2	V_2O_5	Sm_2O_3	(GPa)	(N/m)	(nm)	(m^{-3})
65	34.99	0.1	28.87	240.3	0.532	4.79
65	34.95	0.5	29.04	239.3	0.531	4.78
65	34.00	1.0	29.45	238.0	0.528	4.788
65	33.00	2.0	30.30	235.5	0.523	4.79
65	32.00	3.0	30.66	233.0	0.520	4.73
65	31.00	4.0	31.83	230.6	0.513	4.79
65	30.00	5.0	32.47	228.0	0.509	4.74

Table 2. Values of the experimental number of loss centers ($N_{\mathrm{exp}}\,\%$), theoretically calculated number of loss centers ($N_{\mathrm{th}}\,\%$), experimental activation energy (E_{exp}), and theoretically calculated activation energy (E_{th}).

Glass Composition			$N_{\mathrm{exp}}\,\%$	$N_{\mathrm{th}}\,\%$	E_{exp} (eV)	E_{th} (eV)
TeO_2	V_2O_5	Sm_2O_3				
65	34.99	0.1	5.88	1.363	0.197	0.197
65	34.95	0.5	5.63	1.355	0.172	0.195
65	34.00	1.0	5.37	1.340	0.153	0.192
65	33.00	2.0	4.72	1.310	0.144	0.186
65	32.00	3.0	4.33	1.294	0.139	0.181
65	31.00	4.0	3.72	1.259	0.115	0.175
65	30.00	5.0	3.54	1.236	0.106	0.169

Taking the values of $n = 3.84$ and $c_3 = 0.0106$ [13] and the value of $m = 2.21$, as obtained from a close fit of equation (2) to the data given in Table 1, and performing a linear regression on $Ln(N)$ and (F/K) we obtained

$$N = 0.402(F/K)^{0.576}, \tag{12}$$

with a correlation factor of 99.8%.

The linear regression was performed on E_p and $F(F/K)$ fitting equation (8) to the experimental values of average activation energy for our glass system; we obtained

$$E_p = 2.42 \times 10^4 F(F/K)^{0.576} \tag{13}$$

with the correlation factor of 95.8%.

The linear regression was also performed on $Ln(E_p/K)$ and $Ln(N)$. It results in

$$E_p = 6.7 \times 10^4 N^{1.374} \cdot K \tag{14}$$

with a correlation factor of 98%.

Apart from the correlation coefficients, the important feature of equations (12) and (13) is the fact that they predict correctly the general character of the compositional dependence of N and E_p, Table 1. Thus, as the Sm_2O_3 mol% increases from 0.01 to 5.0 mol%, the number of loss centers expressed as a function of the number of oxygen atoms per m^3, ($N_{\mathrm{th}}\,\%$), which was predicted from Eq. (12), decreases from 1.363 to 1.236 showing the same trend as found from the experimental data ($N_{\mathrm{exp}}\,\%$) which decreases from 5.88 to 3.54. This is shown in Fig. 1. In the case of the average activation energy (E_p), the values of the theoretically calculated data (E_{th}) predicted from equation (13) decrease from 0.197 to 0.106 eV, Fig. 2.

The decrease in both the activation energy (E_p), stretching force constant (F) and the increase in the bulk modulus (K) fulfill equation (13). The relations are shown in Figs. 3 and 4.

From an inspection of the ring size values (ℓ) given in Table 1, it can be observed that the decrease in the average ring size (ℓ) with decreasing activation energy (E_p) obeys the first principal given in Eq. (2) and shown in Fig. 5.

The decrease of the oxygen density [O] from 4.79 to $4.74 \times 10^{28}\,m^{-3}$ with increasing modifier content means that the number of loss centers decreases at a high Sm_2O_3

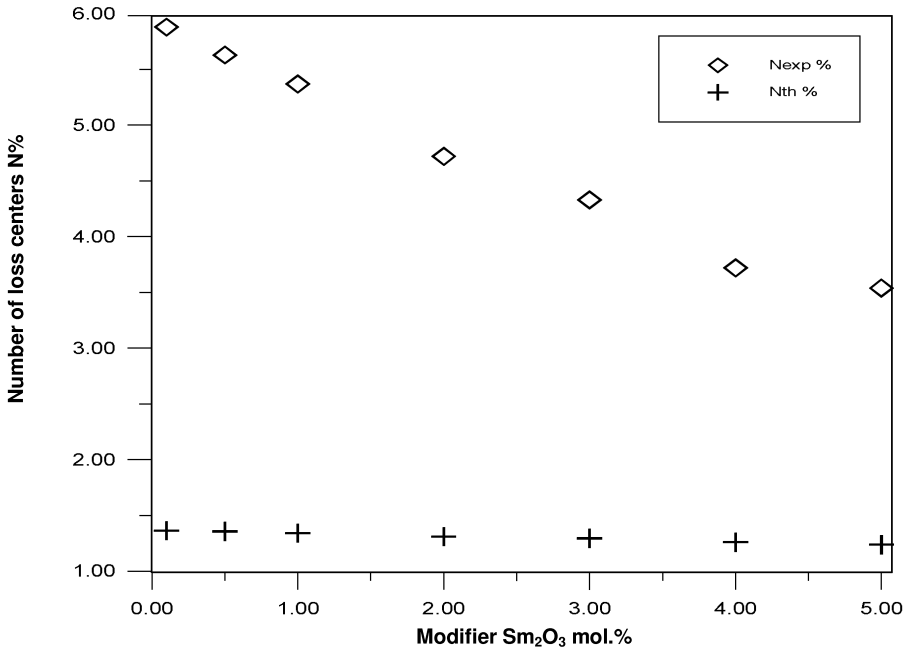

Fig. 1. Compositional dependence of the number of loss center N expressed as a function of oxygen atoms per cm^3 (TeO_2-V_2O_5-Sm_2O_3 glasses). N_{exp} and N_{th} (predicted theoretically by Eq. (12)).

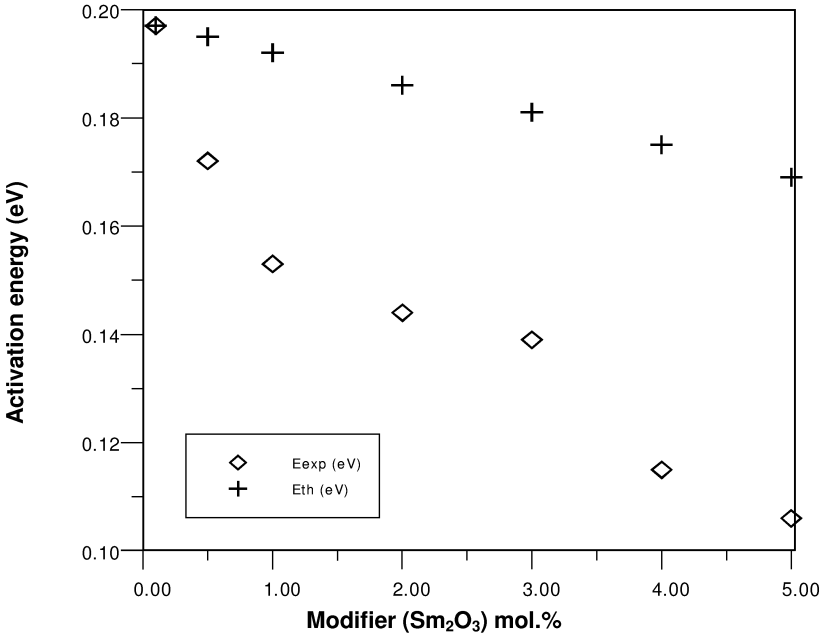

Fig. 2. Compositional dependence of the average activation energy E_{exp} (experimental) and E_{th} (theoretically predicted by Eq. (13)).

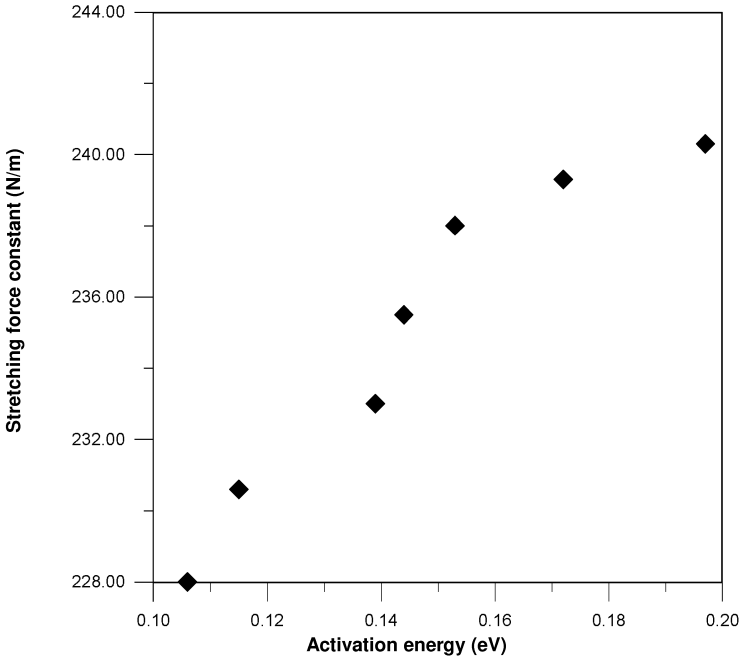

Fig. 3. Variation of the average stretching force constant with activation energy.

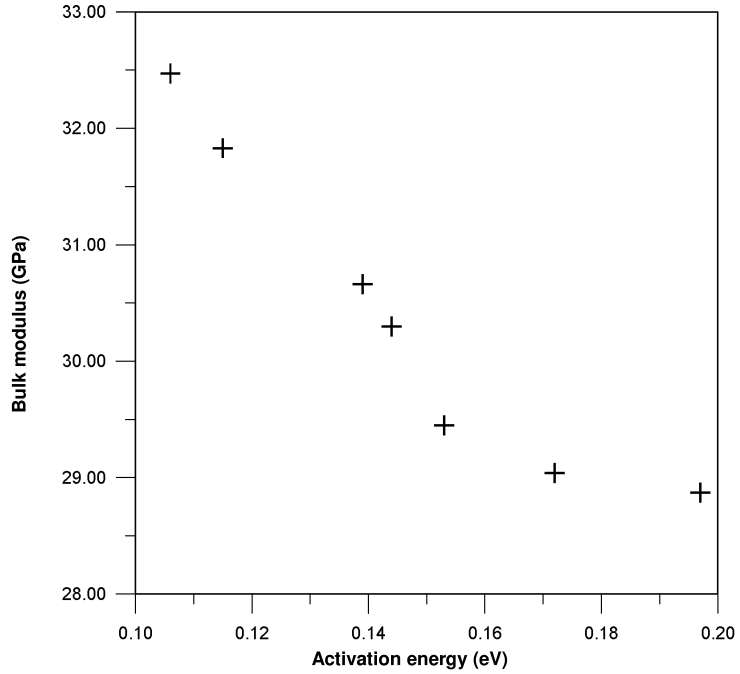

Fig. 4. Variation of experimental bulk modulus with activation energy.

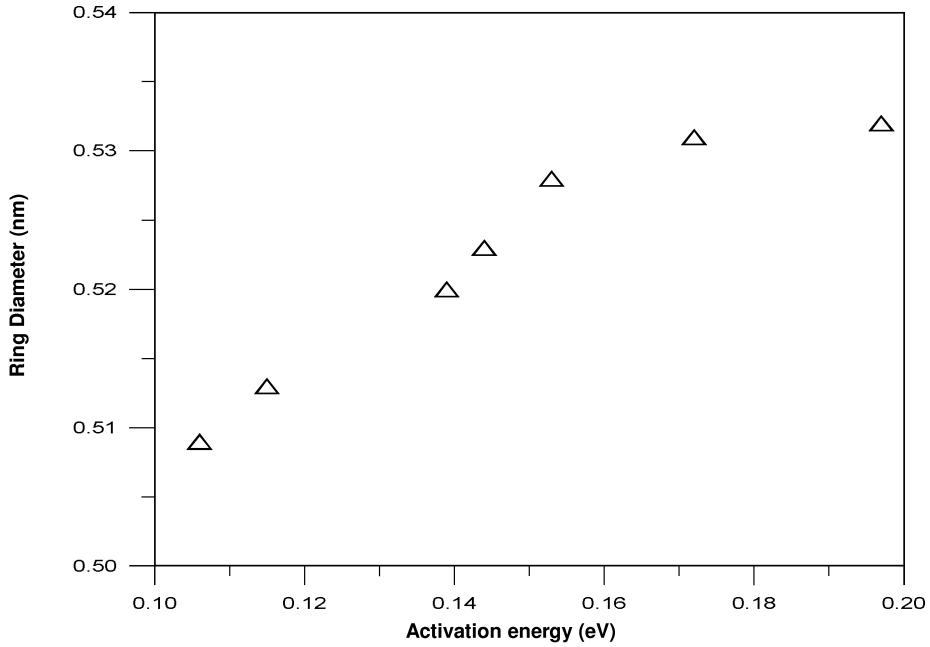

Fig. 5. Variation of the ring diameter with the activation energy.

content, that is added on the expense of V_2O_5. Since the number of loss centers is a fraction of the oxygen density. Therefore, this decrease will cause a decrease in the average activation energy and this fits Eq. (9).

The discussion, under report explains the role of Sm_2O_3 on tellurium-vanadium glasses. The behaviour of Sm_2O_3 in these glasses can be explained as follows; the activation energy (E_p) of the ternary TeO_2-V_2O_5-Sm_2O_3 glass system decreases due to the decrease of both the average stretching force constant (F), and the number of loss centers $(N\,\%)$ (oxygen atoms per unit volume) on one hand side and the increase in bulk modulus (K) on the other side.

4. Conclusion

The correlation between some physical properties for tri-component tellurite glasses (bulk modulus K measured at room temperature and low temperature ultrasonic relaxation parameter, i.e. the activation energy E_p) was achieved through the two structural parameters: the number of anions (N) and the anion-cation stretching forces (F).

References

[1] R. El Mallawany, M.A. Sidkey, A. Khafagy and H. Afifi, *Elastic constants of semiconducting tellurite glasses*, Mat. Chem. and Phys., **37**, 295 (1994).

[2] R. El Mallawany, M.A. Sidkey, A. Khafagy and H. Afifi, *Ultrasonic attenuation of tellurite glasses*, Mat. Chem. and Phys., **37**, 197 (1994).

[3] R. El Mallawany, M.A. Sidkey and H. Afifi, *Elastic moduli of ternary tellurite glasses at room temperature*, Glastech. Ber. Glass Sci. Technol., **73**, 61 (2000).

[4] M.A. Sidkey, R. El Mallawany, R.I. Nakhla and A. Abd El Moneim, *Ultrasonic studies of* $(TeO_2)_{1-x}$-$(V_2O_5)_x$ *glasses*, J. Non-Crystalline Solids, **215**, 75, (1997).

[5] M.A. Sidkey, R. El Mallawany, R.I. Nakhla and A. Abd El Moneim, *Ultrasonic attenuation at low temperature of* TeO_2-V_2O_5 *glasses*, Phys. Stat. Sol., **159**, 397 (1997).

[6] M.A. Sidkey, A. Abd El Moneim and L. Abd El Latif, *Ultrasonic studies on ternary* TeO_2-V_2O_5-Sm_2O_3 *glasses*, Mat. Chem. and Phys., **61**, 103 (1999).

[7] M.A. Sidkey, N.S. Abd El Aal and L. Abd El Latif, *Relaxation of ultrasonic waves in ternary* TeO_2-V_2O_5-Sm_2O_3 *glasses*, Glastech. Ber. Glass Sci. Technol., **73**, 1 (2000).

[8] R. El Mallawany and G.A. Saunders, *Elastic properties of binary, ternary and quaternary rare earth tellurite glasses*, J. Mat. Science Letters, **7**, 870 (1988).

[9] B. Bridge and N.D. Patel, *Ultrasonic relaxation studies of the vitreous system* Mo-P-O *in the temperature range 4 to* 300 K, J. Mat. Sci., **21**, 3783 (1986).

[10] B. Bridge and N.D. Patel, *Correlations between low-temperature ultrasonic relaxation parameters and other physical properties for the oxide glasses*, J. Mat. Sci. Lett., **5**, 1255 (1986).

[11] R. El Mallawany, *Theoretical analysis of ultrasonic wave attenuation and elastic moduli of tellurite glasses*, Mat. Chem. and Phys., **39**, 161 (1994).

[12] B. Bridge and A. Higazy, *A model of the compositional dependence of the elastic moduli of polycomponent oxide glasses*, Phys. Chem. Glasses, **27**, 1 (1986).

[13] B. Bridge, N.D. Patel and D.N. Waters, *On the elastic constants and structure of the pure inorganic oxide glasses*, Phys. Stat. Sol., **77**, 655 (1983).